J. M. Torralba, P. Alvaredo & Andrea García-Junceda (2019) High-entropy alloys fabricated via powder metallurgy. A critical review, Powder Metallurgy, 62:2, 84-114,

DOI: 10.1080/00325899.2019.1584454

High-entropy alloys fabricated via powder metallurgy. A critical review.

J.M. Torralba (1), P. Alvaredo (1) and Andrea García-Junceda (2)

(1) Department of Materials Science and Engineering, IAAB, Universidad Carlos III, Av. Universidad 30, 28911 Leganés, Madrid, Spain.

(2) IMDEA Materials Institute, Calle Eric Kandel 2, 28906 Getafe, Madrid, Spain.

Abstract

High-entropy alloys (HEAs) have attracted a great deal of interest over the last 14 years. One reason for this level of interest is related to these alloys breaking the alloying principles that have been applied for many centuries (i.e., they contain more than five alloying elements without a host principal element). Thus, HEAs usually possess a single phase (contrary to expectations according to the composition of the alloy) and exhibit a high level of performance in different properties related to many developing areas in industry (resistance to high temperature, corrosion, wear, etc.). Despite this significant interest, most HEAs have been developed via ingot metallurgy. More recently, powder metallurgy (PM) has appeared as an interesting alternative for further developing this family of alloys to possibly widen the field of nanostructures in HEAs and improve some capabilities of these alloys. In this paper, PM methods applied to HEAs are reviewed, and some possible ways to develop the use of powders as raw materials are introduced.

Keywords: high-entropy alloys, powder metallurgy, mechanical alloying, spark plasma sintering, high performance materials

Nomenclature	
HEAs	High-entropy alloys
PM	Powder metallurgy
PMHEA	HEAs manufactured by PM
FCC	Face-centered cubic
BCC	Body-centered cubic
HCA	Hierarchical cluster analysis
VEC	Valence electron concentration
MA	Mechanical alloying
HEAMA	HEA powders made by mechanical alloying
PCA	Process control agent
SPS	Spark plasma sintering
HP	Hot pressing
CIP	Cold isostatic pressing
HIP	Hot isostatic pressing
FAHP	Field-assisted hot pressing
LMD	Laser melting deposition
DMD	Direct melting deposition
DLF	Direct laser fabrication
SLM	Selective laser melting

SEBM	Selective electron beam melting
LPBF	Laser powder bed fusion
SAED	Selected-area electron diffraction
EDS	Energy dispersive X-ray spectroscopy
TEM	Transmission electron microscopy
SFE	Stacking fault energy
ODS	Oxide-dispersion-strengthened (alloys)
HFIHS	High-frequency induction-heated sintering
PPS	Pulse plasma sintering
XRD	X-ray diffraction
HRB	Brinell hardness
DSC	Differential scanning calorimetry
DTA	Differential thermal analsis
CCT	Continuous cooling temperature diagram
EBSD	Electron back-scattered diffraction
HEAMC	HEA matrix composite
TWIP	Twinning-Induced Plasticity steel
HEAMCs	Metal matrix composites based on HEAs
MMCs	Metal matrix composites
ID Layer	Inter-diffusion layer
HEAODS	Oxide dispersion strengthened high-entropy alloys

1. Introduction

For over 7000 years, since the first copper-based alloy was cast [1], metallurgy has been based on the development of alloys where one metal, the base alloy, was used as the host for other metals (alloying elements) to improve possible weaknesses of the base metal. Most metals are ductile materials, so the purpose of alloying elements is to improve, primarily, hardness and strength. As society became more sophisticated, it began to demand more of metallic materials, and other requirements were introduced such as resistance to corrosion, wear, high temperature, fatigue, impact, etc. These requirements forced physical metallurgists to develop new classes of materials and new heat treatments. The paradigm of a “base metal” to construct an alloy started to change in the 1970s, when a new class of materials was developed industrially: the intermetallics. Intermetallics play an important role as secondary components after heat treatments, due to their defined stoichiometry providing high hardness. Thus, the search for materials with improved strength at high temperatures and low densities opened an opportunity for some intermetallics such as γ-TiAl, with a stable face-centered cubic (FCC) structure at room temperature [2]. However, these new families of alloys with no defined base element were restricted to a few families of intermetallics, where usually two different metals together formed the main component of the alloy. Except for the intermetallic approach and “superalloys”, wherein the amount of alloying elements could reach half of the composition, the use of alloying elements has always been restricted. This restriction is linked to the risk of forming uncontrolled intermediate compounds, which usually introduce brittleness in the material.

However, this method of working in physical metallurgy started to change in 2004 when Cantor et al. [3] published a paper in which a multicomponent alloy, starting from five elements in equiatomic proportions ($Fe_{20}Cr_{20}Mn_{20}Ni_{20}Co_{20}$), was produced, reaching an FCC monophasic structure. At the same time, Yeh et al. [4] developed the same concept, defining

"high-entropy alloys" (HEAs) as those composed of five or more principal elements in equimolar ratios. According to Yeh et al., to extend the scope of the alloy design, HEAs may contain principal elements within an atomic concentration range between 35% and 5% for each element. In this paper, Yeh et al. explained that the reason why we can attain a single-phase solid solution with such a high amount of alloying elements is fully linked to controlling the configurational entropy of the system. In conventional metallurgy, there is a main element and the alloying elements are added in a small percentage. In HEA the alloy is composed by five or more alloying elements in similar atomic percentage. This is what we want to symbolize in Figure 1, where the size of the circles represents the contribution (in at. %) of the different alloying elements in the final alloy.

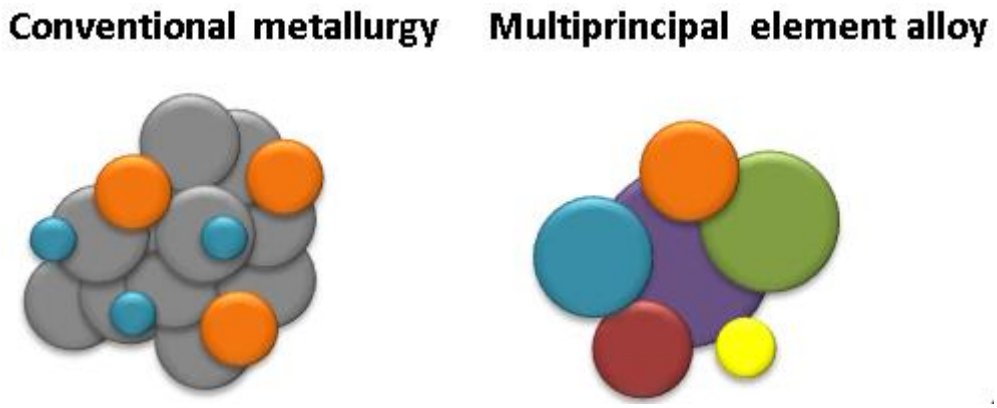

Figure 1. Alloying philosophy in conventional metallurgy and in HEAs.

Fourteen years have passed since these foundational papers. Today, HEAs have become a promising research field, with more than 5000 scientific papers published, according to the most extensive databases. Among those papers, we want to highlight some interesting reviews. Perhaps the most comprehensive review is the one by Miracle and Senkov[5] who established a full state of art regarding this topic. Their paper covers principles, fundamentals, families of alloys, microstructural discussions, properties (including a comparison with those of possible competing alloys), etc. This paper is critical for researchers who want an introduction to this field. Other general and critical reviews about the topic can be found in [6]–[10]. In addition, HEAs have been proven to be capable of demonstrating a wide variety of properties, so many works have collected arguments focusing on their value in different fields. References [11], [12] highlight the importance of HEAs in applications related to physical properties such as magnetic, electrical or thermal properties. HEAs can also be used under extremely corrosive conditions [13]–[15]. Moreover, HEAs are clearly a promising material for their introduction in the market due to their good mechanical performance [16]–[18] including at high [5] or cryogenic temperatures [19]. Other reviews on the mechanical behavior of HEAs deal with their fundamental deformation behavior [20] or fracture resistance [21]. Two books concerning this topic have also been written [22], [23].

Most of the works related to HEAs have developed processing methods based on ingot metallurgy. Arc melting has been confirmed to be a highly efficient technique when more than five metals, some of them with high melting points, must be melted and solidified with a good level of solubility while avoiding segregation. However, in cases where a complex composition must be achieved, ingot metallurgy presents some difficulties that can diminish its potential

for fabricating an emerging, promising family of alloys. In this context, powder metallurgy (PM) has shown high potential as a way to manufacture HEAs. PM, a forming technology that allows significant compositional accuracy can completely avoid segregation, achieve superior microstructural control (including the formation of nanocrystalline materials) and easily produce metal matrix composites.

Although the first works related to HEAs started to be published in 2004, some papers using PM started to appear a few years later [24]–[26]. Since the early days of this new family of structural alloys, the benefits of nanostructures and their potential use for many applications have been highlighted [4]. In this competitive environment, PM, similar to other forming techniques such as high-pressure torsion has many advantages [27]. PM also has two other advantages over other forming techniques: 1) it can be applied when metals with dissimilar densities must be used, which is the case when lightweight HEAs are developed[28]; and 2) it can be applied when many metals with extremely high melting points are involved in the development of the HEA, i.e., so-called refractory HEAs [29].

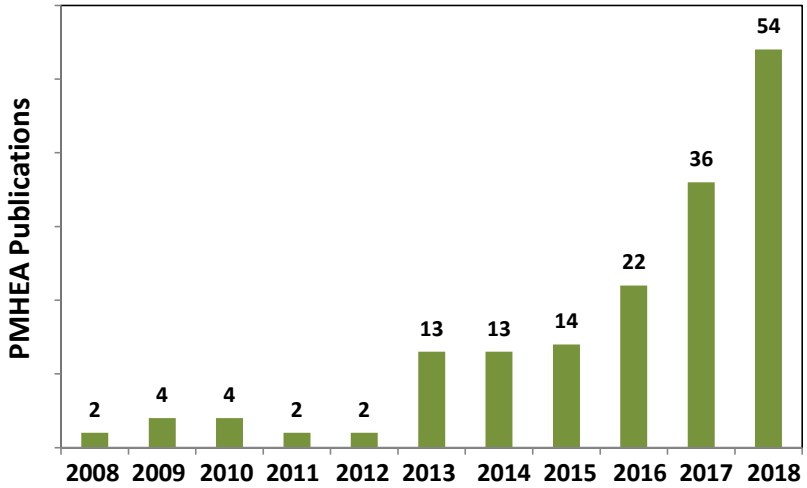

Figure 2. Papers published from 2008 on PM HEAs.

For this review, a selective search was performed in four databases (ISI Web of Science, Scopus, Science Direct and Google Scholar). Different combinations of keywords (high-entropy alloys, powder metallurgy, sintering, mechanical alloying (MA), gas atomizing, spark plasma sintering, among others) were used, and 166 papers that fulfill the requirements were found. Some papers were not included in the database of the review for some of the following reasons: a reliable citation system could not be reproduced, some steps in the experimental procedure were not clear, or PM was used as an alternative process to other production methods. As an example of this latter issue, many papers on “laser cladding” were found, where powders were used to produce coatings or surface modifications on substrates using a laser power source. In these cases, papers were included only when the powder development had a special role. Most of the papers aimed to consolidate a bulk material (after a sintering process), and only a few were devoted to the development of the powder technology and thus were included for special importance.

The relevance of the topic can be seen in the increasing number of papers published in the last 10 years (see Figure 2). The interest in PMHEAs has produce a geometrical increase in the papers published during this period.

2. Powder Metallurgy HEAs: chemical compositions.

HEAs were firstly developed by ingot metallurgy using at least five core elements alloyed in equimolar concentrations. The literature offers hundreds of different compositions, based mainly on the 3d transition metals. Such complex compositions (5 or more elements, all of them with an important role in the alloy) are needed to conform to a basic set of requirements established by Yeh et al. [6] to be considered a HEA. These requirements are 1) thermodynamics: high-entropy effects; 2) kinetics: sluggish diffusion; 3) structures: severe lattice distortion; and 4) properties: cocktail effects. These four core effects in HEAs have been widely discussed in many papers but are highlighted in [5], [18] and [30].

Reviewing the technical literature regarding ingot casting HEAs, these alloys can be divided in four families: 3d transition metals, lightweight materials, lanthanide and refractory HEAs (Figure 3).

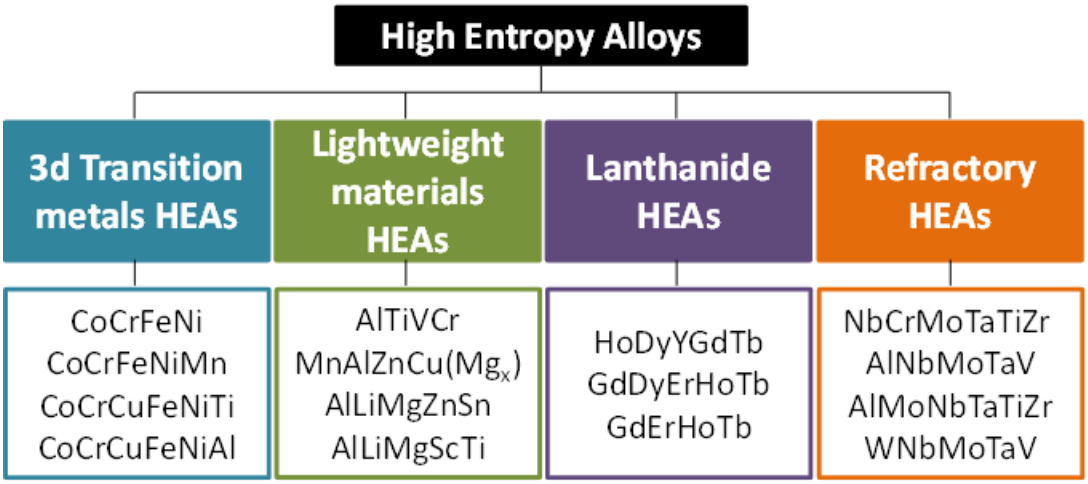

Figure 3. Classification of ingot metallurgy HEAs.

In the present review, nearly two hundred papers considering 166 PM alloys are included. The number of papers is higher than the number of alloys because many authors use the same alloys. If the frequency with which the different alloying elements have been used is analyze the frequency with which the different alloying elements were used (Figure 4), three main groups of elements arise, which are also represented in Figure 5.

The most commonly used elements are Fe, Ni, Cr and Co, all of which can be considered in the core group of transition metals. A second group of alloying elements is used less frequently, also belonging to the transition metals (except Al): Al, Ti, Cu and Mn. If we take into account the definition of HEA introduced by Yeh et al. [4] we would need at least five alloying elements. Considering the distribution shown in Figure 4, most of the alloys studied are composed of the 4 elements of the first group, and one or two elements of the second group. We can also find a third interesting group of elements used with less frequency: Mo, V, Zn, Zr, Ta, W, and Nb. Except for Zn, these elements are all refractory metals and play the leading role in the so-called refractory HEAs [29]. After the first booming of the HEAs mainly based on the 3d transition metals, later refractory HEAs were developed, possessing very specific and different properties that could cover another range of applications. Finally, there are some

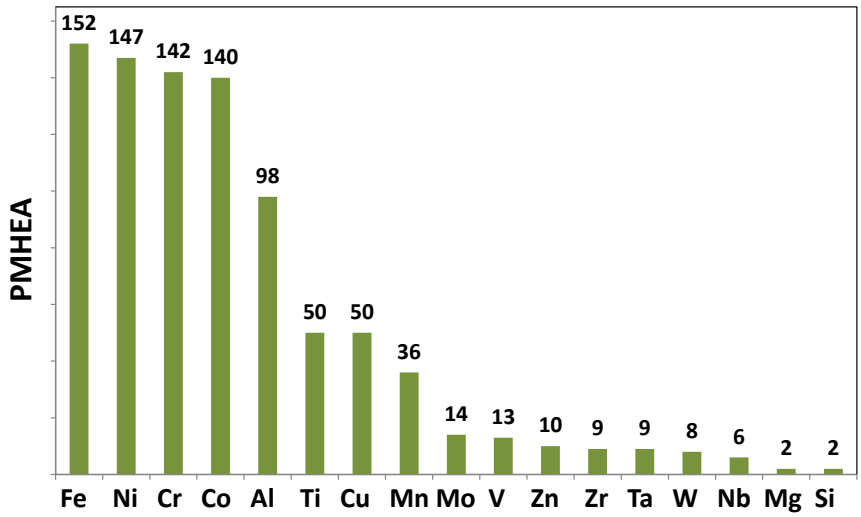

Figure 4. Distribution (frequency) of alloying elements in the studied PM HEAs (i.e. Fe is in 152 different alloys; Al in 98 of the studied alloys).

examples in which the use of elements such as Mg and Si is reported, so a fourth group can be seen in Figure 5.

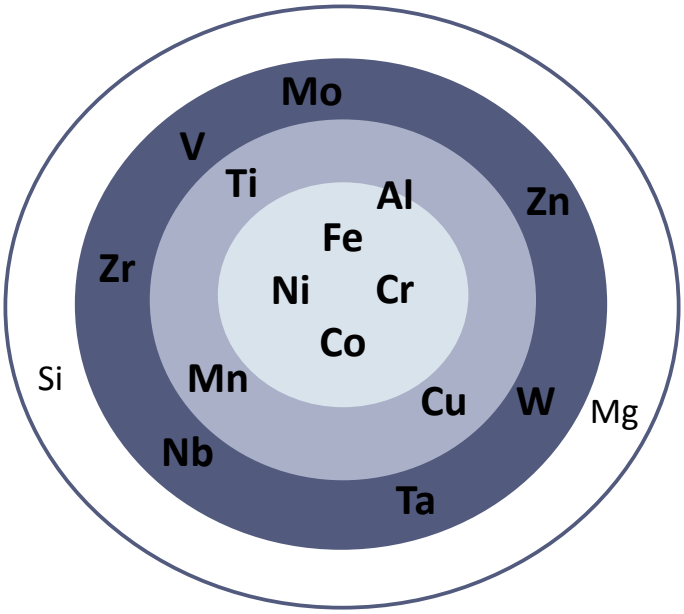

Figure 5. Main alloying elements in the HEAs studied.

To determine whether some combinations of elements tend to be used consistently, we performed a hierarchical cluster analysis (HCA) by means of the statistical Jaccard distance [31]. The clustering followed the complete linkage method based on dissimilarities between the different alloys' compositions. We used 166 PM HEAs from different papers in the study.

The HCA identified 9 different clusters of alloys based on their composition (Figure 6). Some of the clusters had a few members, and others were composed of a considerably higher number of members (Table 1). As could be expected, the clusters with more members are related to the HEAs based on the 3d transition metals.

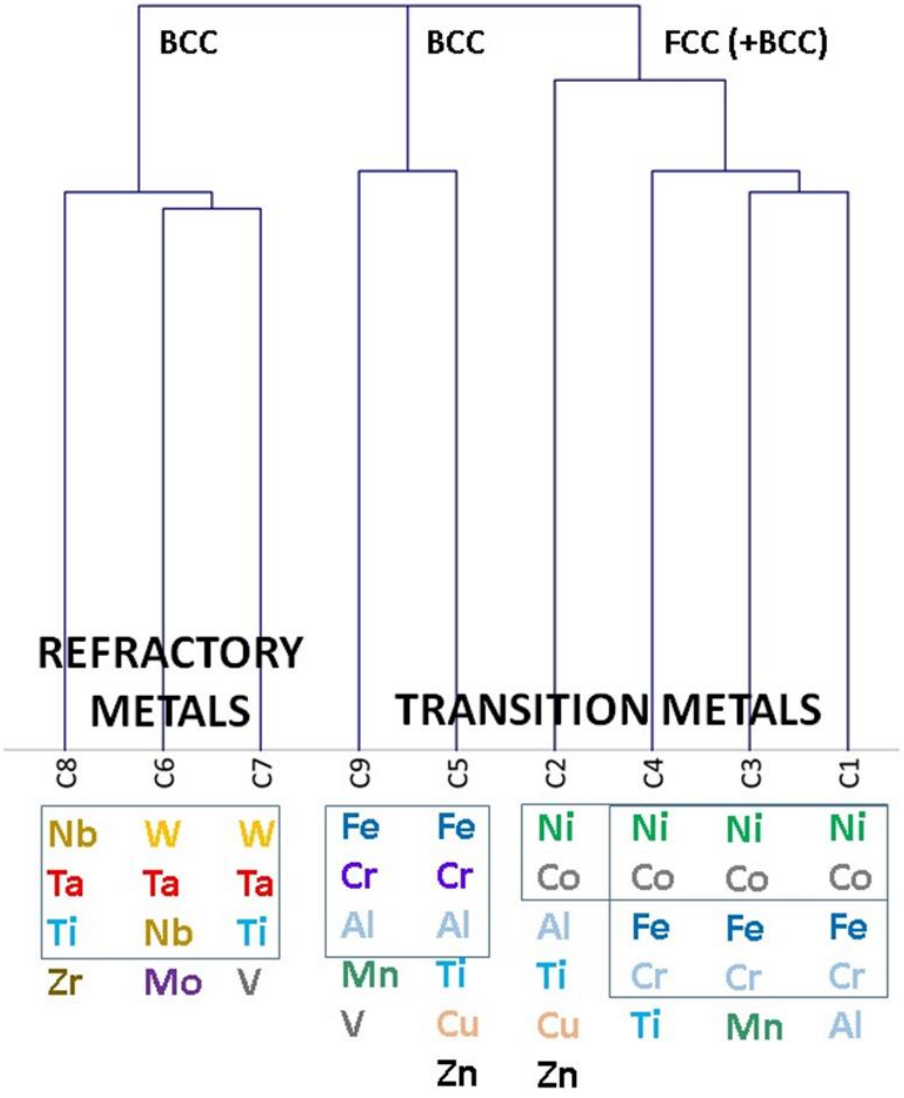

Figure 6. Dendrogram (“tree diagram”) showing the 9 types of HEA alloys derived from the HCA.

Cluster nº	Number of members in the cluster	Alloyig ellements	Comments	Some related papers
1	83	FeNiCrCoAl	Most of the alloys BCC after MA, FCC (or FCC-BCC) after consolidation	[25], [26], [32]–[100]
2	5	NiCoAlTiCuZn	Most of the alloys BCC after MA, FCC (or FCC-BCC) after consolidation	[101]–[105]
3	43	FeNiCrCoMn	Cantor Alloy [3], Most of the alloys BCC after MA, FCC (or FCC-BCC) after consolidation	[105]–[148]
4	11	FeNiCrCoTi	Most of the alloys BCC after MA, FCC (or FCC-BCC) after consolidation	[63], [149]–[158]
5	9	FeCrAlTiCuZn	Most of the alloys, BCC after MA, BCC after consolidation	[24], [159]–[168]
6	2	MoTaWNb	Most of the alloys BCC after consolidation	[169]–[171]
7	3	CrTiVTaW	Most of the alloys BCC after consolidation	[172]–[174]
8	3	TiZrTaNb	Most of the alloys BCC after consolidation	[37], [175], [176]
9	3	FeCrAlMnV	Most of the alloys, BCC after MA, BCC after consolidation	[165], [177], [178]

Table 1. Clusters compositions and some members in the cluster.

Table 1 describes the main alloying elements that characterize each cluster and some comments providing more information about the group.

On the right side of the dendrogram (Figure 6) we can see a bundle of papers among clusters 1-3 and 4, and these latter groups are related to cluster 2. These clusters are the most powerful in terms of membership. Interestingly, the core group (clusters 1 and 3) are composed of four transition metals (Fe, Ni, Cr and Co), the most common in HEAs (Figure 4), plus a fifth transition metal from the second most used elements (Al, Mn and Ti). Another interesting fact is that the core composition of cluster 3 is the so-called “Cantor alloy”[3] one of the most studied HEAs in the field. If we analyze the alloys included in these clusters in some detail, most of them exhibit an FCC structure after consolidation or, in some cases, FCC+body-centered cubic (BCC). The main composition of cluster 1 is a clear example of how Al is a critical element that can appreciably modify the crystal structure. Just by increasing the Al content in the HEA, the final crystal structure can be moved from FCC to FCC+BCC and BCC [6]. These four clusters are connected to cluster 2, which only has Ni and Co in common with all the other clusters, and some other elements depending on the cluster, i.e., Al and Ti but also Cu and Zn. Considering Ni, Co, Al and Ti, cluster 2 shares elements with all the other clusters on

this side of the dendrogram. These combinations of elements also produce a final structure of FCC+BCC in all the members of the cluster.

On the left side of the dendrogram are three clusters with all the refractory elements, including Ti. All of these elements have a BCC structure, so all the HEAs produced from different combinations of these elements should produce a BCC structure. These are also transition metals, mostly belonging to periods 5 and 6 of the periodic table. These HEAs are called “refractory high-entropy alloys”[29], [179], and were developed in the search for high-temperature load-bearing structures and thermal protection materials for the aerospace industry, among other applications.

In the center of the dendrogram are two clusters composed mainly of alloying elements from the 3d transition metals. Clusters 5 and 9 share Fe, Cr and Al and include Ti, Cu, Zn, Mn and V. These two clusters contain many elements with a preferential BCC structure, so these HEAs will preferably crystallize as BCC.

The formation of one single phase is a desired objective when producing HEAs. In a conventional alloy, where we could have one main component and some minor alloying elements, the prediction of possible solid solutions are governed by the Hume-Rothery rules. In HEAs, where we have a much more complex situation in terms of alloying elements, the enthalpy and entropy of mixing play the most relevant role. There are a couple of deep investigations [180]–[182] that have studied these key parameters on the phase formation, and they have proposed different empirical rules : the formation of solid solutions or intermetallics depends on the enthalpy of mixing (ΔH_{mix}), the entropy of mixing (ΔS_{mix}) and the atomic size (δ). There are some specific conditions related to the limits of these parameters that promote the formation of simple phases or intermetallics. In Figure 7 the different regions are mapped according these limits: ΔH_{mix} cannot be too large in value because large positive ΔH_{mix} leads to phase separation and large negative ΔHmix typically generates intermetallic phases. δ has to be small enough since large δ leads to excess strain energy and destabilizes simple structures.

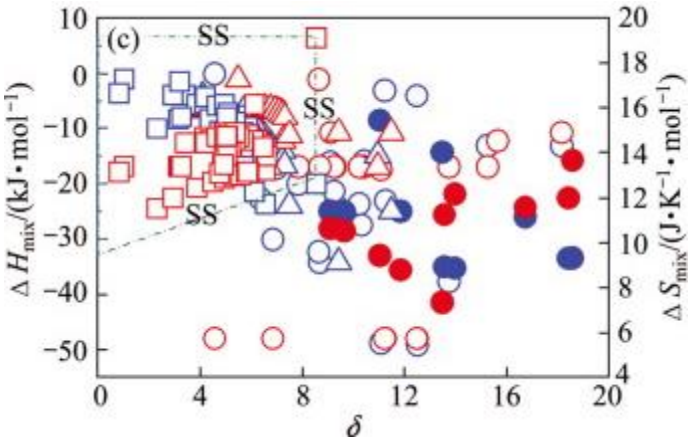

Figure 7 . Superimposed effect of ΔHmix, δ (atomic size) and ΔSmix on phase stability in equiatomic multi-component alloys and bulk metallic glasses. The symbol ○ represents equiatomic amorphous phase forming alloys; ● represents non-equiatomic amorphous phase forming alloys; □ represents solid solution phases and △ represents intermetallic phases. The region delineated by the dash-dotted lines indicates the requirements for solid solution phases to form, from [181].

This equilibrium among solid solution, intermetallics and amorphous phases was explored with more detail also by Guo et al. [183] and can be analysed in Figure *8*8.

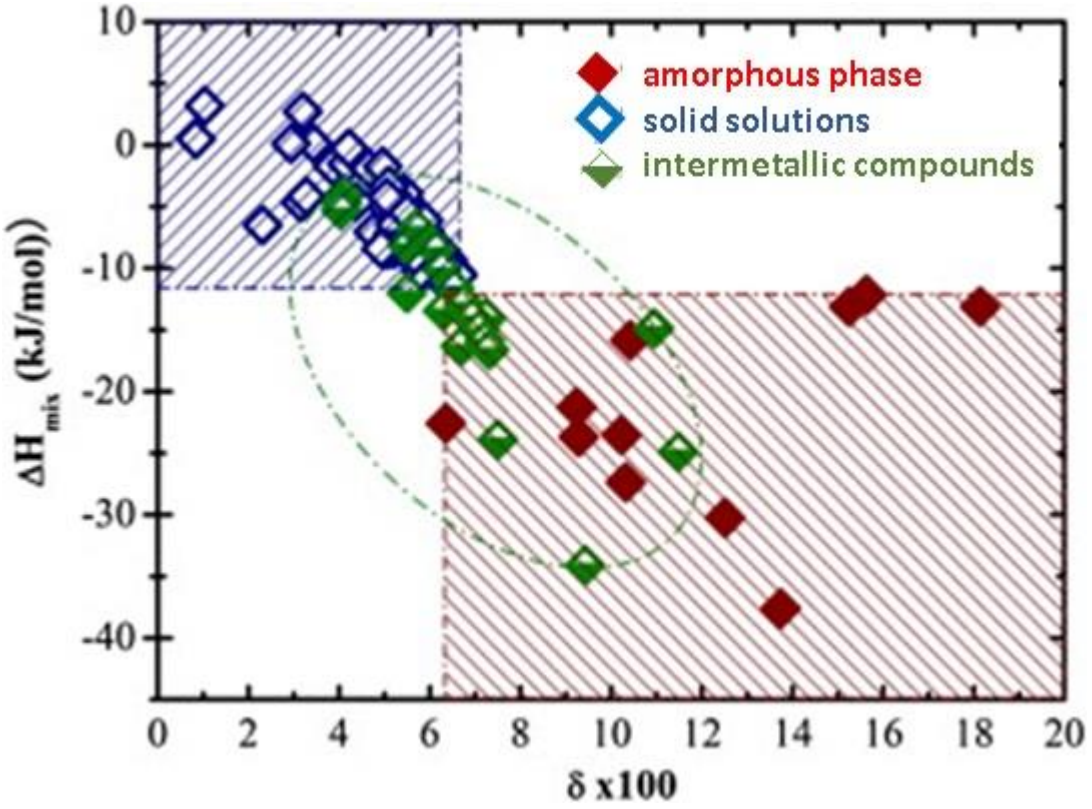

Figure 8. A *δ (*atomic size*)*-Δ*H*mix plot delineating the phase selection in high entropy alloys. The dash-dotted regions highlight the individual region to form solid solutions, intermetallic compounds and the amorphous phase. From [183]

Once the limits in terms of *Δ*H*mix,* Δ*Smix* and δ, have been stablished, the next interesting point to analyse is the nature of the possible single phase formed. In principle in HEAs it could be BCC, FCC or a mix of BCC and FCC. According to [184] the most critical factor that can predict if the alloy crystallizes into BCC or FCC is the valence electron concentration (VEC), which is calculated from the weighted average VEC of the constituent components. Guo et al. [184] summarized the relationship between VEC and structure of many HEAs in Figure 9.

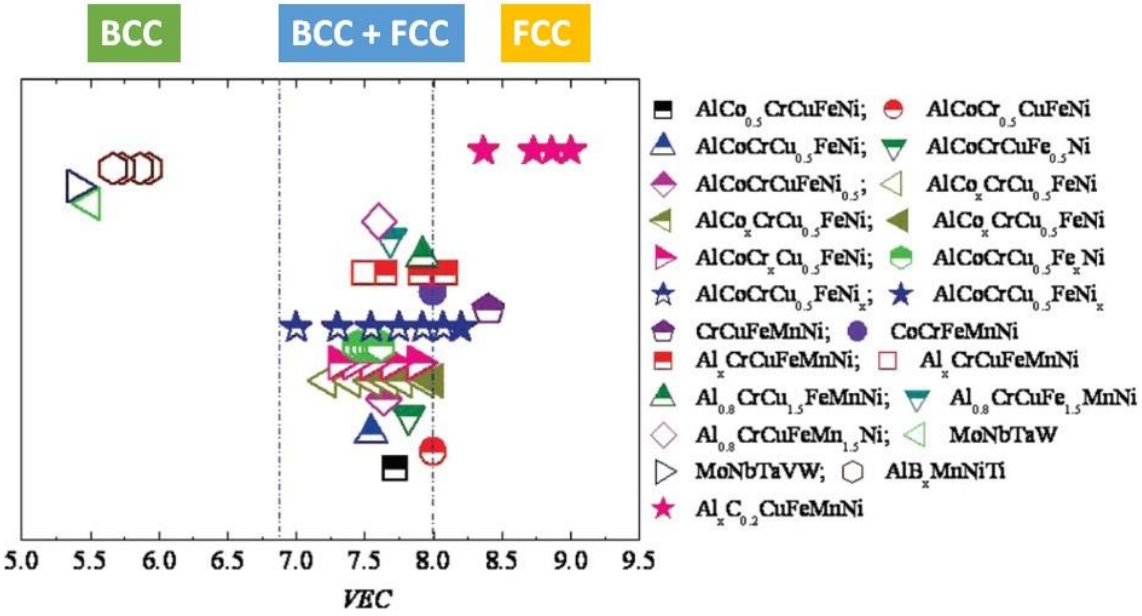

Figure 9. Relationship between VEC and the FCC, BCC phase stability for various HEA systems. Notes: Fully closed symbols for sole FCC phases; fully open symbols for sole BCC phase; top-half closed symbols for mixed FCC and BCC phases, from [184]

The VEC can also be used to predict the sigma phase formation in Cr and V containing HEAs [185]. These alloys with so high amount of Cr or V, can easily produce sigma phase that may affect strongly the properties.

Considering the predictions of phase formation that can be achieved from the VEC displayed in Figure 9 and the obtained phases in PMHEAs (Figure 6), two different facts should be taken into account: in the works used to obtain the Figure 9 most of alloys are included in a few of the clusters compositions presents in this work (mainly C1, C5 and C8) and PMHEAs considered to obtain the clusters compositions, were not heat treated to homogenize their final stages, being the measured phases obtained after sintering.

Summarizing what we can extract form the statistical analysis of the studied PMHEAs samples, there are five connected clusters, based mainly on Fe, Ni, Cr and Co, to which the majority of the studied alloys belong. These connected clusters preferably produce FCC HEAs or a mix of FCC and BCC. Three clusters contain refractory HEAs, crystallizing as BCC and opening new opportunities in the field of high-temperature applications. Finally, two small clusters are composed of transition metals but with a combination of alloying elements that promote BCC structures. Using PM, we can form any HEA that can be produced via ingot metallurgy and open new possibilities for alloying with very competitive performance, as we will see later.

3. Powder development

The first step in any PM process is to obtain suitable powders for the process. In this special family of alloys where at least 5 different metals contribute to the alloy, any PM route should be easier by using fully prealloyed powders as the starting material. However, we have found many papers in which the starting point is a conventional mix of powders, using pure metals in powder form[33], [49], [52], [69], [80], [83], [157], [172], [173], [186], [187]. In those works,

the powders were submitted to different shaping methods such as uniaxial pressing, cold isostatic pressing or spark plasma sintering.

In the different works where fully prealloyed powders were used, two different methods were selected to obtain the powders: MA and atomizing. The most common method to obtain HEA powders is MA. This method makes any possible composition feasible with enough time and energy to combine the optimal powder with the optimal composition. In Table S1 of the accompanying supplementary data, Appendix A shows the different conditions used to obtain different fully prealloyed powders by MA, as well as the phase obtained when the process is completed. The main records of this table are presented in Figure 10 and Figure 11. The main milling system used is a planetary ball mill, and the main grinding system is composed of stainless-steel vials and balls, although other combinations are suitable.

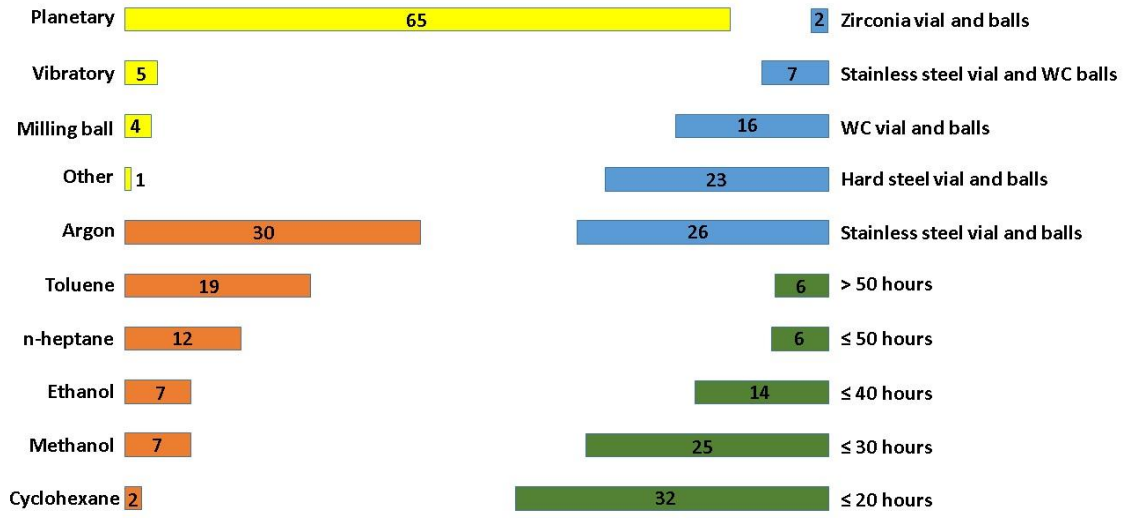

Figure 10. Mechanical alloying conditions. The length of the bars represent the number of times a certain procedure was used.

In all cases, a protective milling environment was used. Depending on the goal in terms of composition of the alloy, different authors have selected different ways to reach the optimum powder for the process. One interesting point is that in most works, a carbon-based process control agent (PCA) is used, but as is discussed in the next paragraph, only a few authors consider its possible contamination or influence in the final development of the HEA.

In all the analyzed papers, a monophasic HEA (BCC or FCC, depending on the starting metal powder) is obtained (see Figure 11) after a prudential time for the process, i.e., on the order of hours (Figure 10). In clusters C1 to C4, from the powder state and before any heat treatment, the departing phases are FCC and BCC, and in clusters C5 to C9, a BCC structure preferentially forms from the powder.

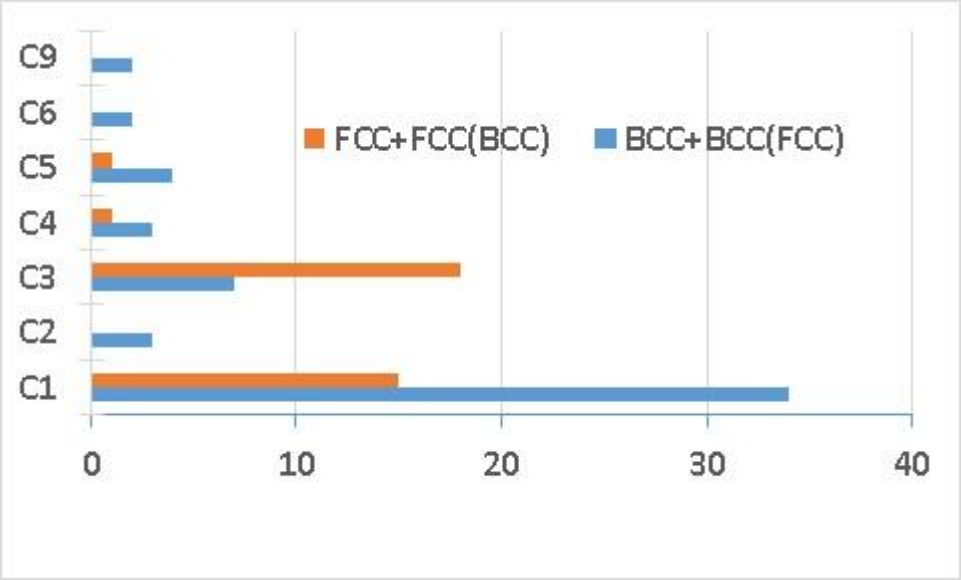

Figure 11. Frequency of the main phases associated to the clusters' compositions, obtained after the mechanical alloying step: BCC, FCC and BCC with some minor FCC and FCC with some minor BCC.

One weakness of MA to consider is the possible contamination of the powder from two different sources: the PCA and the grinding media. When the grinding media are stainless steel, and the target alloy contains Cr and/or Fe, the possible transfer of these elements may be controlled, in the same way that tungsten carbide is used to produce some refractory HEAs. Nevertheless, the effect of the PCA is not negligible and is not mentioned in most of the analyzed papers. Only two papers consider the effect of the PCA [144], [171], minimizing this effect because of the possible formation of undesirable carbides, which are produced during the formation process by spark plasma sintering (SPS). In contrast, in other works, the presence of extra carbon is desirable because the final goal of the process is to develop a hardmetal from the HEA [146], [174].

The second most commonly used method to obtain a full prealloyed HEA powder is atomizing. This PM method is especially suitable for most additive manufacturing methods. In this review, different atomizing methods are presented, all of them with successful results: gas atomizing in Ar [73], [107], [108], [121], [140], [147], [160], [188], [189], gas atomizing in N_2 [59] or even water atomizing.

An alternative to MA and atomizing to produce fully prealloyed HEA powders was followed in [61], [70]. In those works, alloys were obtained by melting, and the as-cast bulk part was then powdered via high-energy milling.

To conclude this chapter related to powder development, we must mention the work of Liu et al. [154]. In their work, a hardmetal based on the HEA binder was pursued. Instead of using pure elemental powders as the starting powders for the alloying elements of the binder and then mixing these powders with the reinforcing carbide (this time TiC), the authors mixed WC, Mo_2C, TaC, NbC and VC with pure Ti in a high-energy mill. The mixed powders were subsequent sintered at high temperature (1500 ºC) by SPS and considering the higher affinity of the Ti by the C and looking for the reduction of all the refractory carbides at the sintering

temperature. At the end of the process, a matrix of BCC HEA with TiC as the reinforcing agent was obtained.

4. Conventional consolidation methods

Once the alloy has been prepared by mixing powders in some way to obtain a fully prealloyed powder, we have to follow a PM processing method to obtain the bulk materials. Omitting the additive manufacturing methods, which will be treated in another section, Figure 12 analyzes the methods selected in the studied papers, including the percentage of works that use each technique. In this figure, we can see that MA is the preferred way to produce the fully prealloyed HEA powders and SPS is the preferred consolidation method. Therefore, the most common combination is MA+SPS.

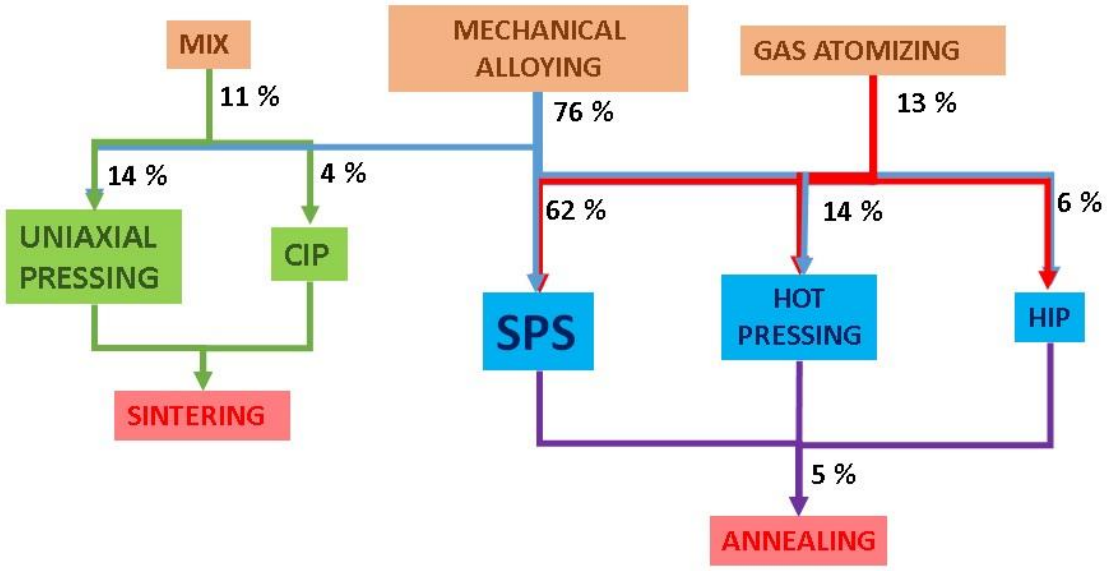

Figure 12. Different PM processing routes to obtain PMHEAs.

In many papers, the route followed to obtain the bulk material is SPS [190]. One of the main advantages of SPS is that the sintering temperature is reached rapidly, and the dwell time is usually short. Those conditions enable fully densifying the sintered material but avoiding excessive grain growth. Other methods that also combine pressure and temperature (such as other hot pressing (HP) methods or hot isostatic pressing (HIP) methods) can also attain full density, but these methods usually need higher temperatures and longer times, so grain growth is not fully avoided, and the mechanical properties can be affected.

Table S2 of the accompanying supplementary data, Appendix A, shows the SPS conditions used in most of the papers analyzed and groups the conditions by the cluster composition. The temperature conditions in most of the materials in clusters C1-C4 and C5-C9, where most of the alloying elements are not refractory metals, remain near 1000 °C, and that temperature could be considered a low sintering temperature for most of the core elements of these clusters (such as Fe, Ni, Co or Cr). Despite the scattered values regarding time, these values reach up to 60-80 min, but most of the studies maintain the time condition under 10 min, which can be considered a short sintering time. Thus, in most of the studied works, the

potential use of SPS to reach full density while maintaining good microstructural features in terms of grain size is fully harnessed. A couple of papers [48], [66], using these compositions, where the sintering temperature reaches up to over 1350 °C (even 1700 °C), have reported higher densities than most of the studied works. The final objective of these two articles was to develop a "cermet" using the HEA as binder and WC as the hard phase. To attain full microstructural integration of the WC in the binder, the sintering conditions were scaled up until the degree of integration was higher than average in these composite clusters.

After SPS, the second most common processing route to obtain PM HEAs is the conventional "press and sintering" route, which is the most extensively used route in mass production for conventional PM. Among the studied works, most use conventional uniaxial pressing, but in a few articles, cold isostatic pressing (CIP) has been used. In [188] is used pressurless sintering. Table S3 of the accompanying supplementary data, Appendix A, shows the pressing and sintering conditions of these PMHEAs. In most of the cases, the compacting pressure remains at values easily handled by the PM industry (under 500 MPa). Other issues are the sintering conditions. Here, the sintering is not enhanced, so the material is fully densified via adequate temperature and time. Compared with the temperatures used in SPS, we find slightly higher average temperatures, especially in some works aiming to develop a cermet [47], [68], [129], [157]. The protective atmosphere used is generally pure Ar and in some cases vacuum.

Two other significant minor processing methods are HP and HIP. These two cases involve enhanced sintering methods (simultaneously applying pressure and temperature), but usually, much longer times are required than those in SPS, despite the temperature remaining at low values. These longer times can produce significant grain growth despite the low temperatures. The HP and HIP conditions are detailed in Table S4 of the accompanying supplementary data, Appendix A. Only in one case [165], where the HP method is a "field assisted hot pressing" (FAHP) method, does the sintering time remain near those of SPS.

In [45] Fu et al. studied and compared the same PM HEA ($Al_{0.6}$NiFeCrCo, type C1) obtained by SPS (1000 °C/30 MPa/8 min) and HP (1000 °C/30 MPa/60 min). In both cases, a final FCC structure with some minor BCC is obtained, and the values for compression strength, strain to failure and hardness are quite similar (2150 MPa, 10.6% and 594 Hv vs. 2298 MPa, 10.8% and 570 Hv, respectively). The slightly smaller grain size in the SPS alloy, due to the shorter sintering time, results in a higher yield compression strength (1870 MPa in SPS vs. 1830 MPa in HP).

Beyond the "conventional" PM methods described above, some interesting PM alternatives exist. The first alternative is the development of a FeCoCrNi (C1 type) PM HEA by powder extrusion [108]. Powders are canned and degassed and then hot extruded at 1200 °C/60 min. The obtained tensile mechanical properties are very competitive relative to those of the equivalent "as-cast" alloy [191] even if we compare the alloy with a TWIP steel [192] (with much more complex processing and heat treatment). In Table 2 we can compare these results. The second alternative to conventional PM methods is a method wherein a PM HEA (CoCrFeMnNi, C3 type) is shaped by shock wave compaction at a pressure between 1 and 3 GPa [114]. This pressed alloy is further sintered in vacuum at 1100 °C for 2 h. The alloy exhibits a pure FCC structure (with some ZrO_2 contamination from the MA process) and full density, leading to promising tensile strength values, much higher than those of the same material processed by static compaction but far less than the same material processed by SPS [139].

A few materials under study are subjected to annealing after consolidation [39][58][141], but the main objective of the heat treatment is to ensure the formation of the FCC structure after the consolidation process.

Materials	Yield strength (MPa)	Ultimate tensile strength (MPa)	Elongation (%)	Ref.
FeCoCrNi HEA prepared by casting and cold rolling	205	580	70	[191]
TWIP steels: Fe68.25Mn27Al4.1Si0.52Nb0.05C0.08	383	548	61	[192]
FeCoCrNi PM HEAs by powder extrusion	359	712	56	[108]

Table 2. Comparison of some tensile properties of HEAs made by ingot casting and PM and a TWIP steel.

5. Processing by additive manufacturing.

Additive manufacturing is a good opportunity to consolidate HEAs. Once we have powders that can be mixed in an equimolar manner or that are fully prealloyed by MA, and especially by gas atomizing, this manufacturing method is a good way to produce parts with a very complex shape and specific properties. In Table S5 of the accompanying supplementary data, Appendix A, we summarize the main works found in the literature regarding manufacturing bulk parts by additive manufacturing (many articles related to “laser cladding” have not been considered in this review). Most of the HEAs developed by this technology belong to clusters 1, 3 and 4; that is, HEAs based on the core group of transition metals that constitute the main group of alloys are usually developed by PM, especially cluster 3, based on the Cantor alloy [3]. Only one work based on refractory HEAs was found [169].

Under the topic “additive manufacturing of metals”, we can find many technologies today. Most of these technologies use a laser beam as the power supply, but we can also find other energy sources such as electron beams. The selection of a method based on powder bed or powder feed systems is what truly determine many processing parameters and perhaps includes more restrictions in the alloying design. In [193]–[196] extended explanations of the different systems and their advantages and disadvantages can be found. Notably, powder bed systems require fully prealloyed powders. These powders are produced by gas atomizing to have a spherical shape and a specific size distribution that assures a good packing ratio and enough flowability in the powder to be handled. In powder bed systems, producing changes in the composition is not easy, because we must include all the alloying elements in the prealloyed powder. Preparing a bed of powders from a mix of atomized powders is not appropriate since any small change in the density of the powders belonging to the mix could produce severe segregations in the final composition of the bulk part. Segregations in the mix, when a solidification process is involved, means severe dimensional changes and deformed final parts. The most positive advantage of powder bed systems is that, by ensuring the quality of the prealloyed powder, we could guarantee a good final homogeneity and good dimensional control of the manufactured part.

On the other hand, powder feed methods allow different possibilities while managing the raw material. These methods can use two or more hoppers with different feeders that enable different combinations. For instance, we can place a prealloyed base powder in one hopper and in a second hopper, we can sequentially introduce a fifth or a sixth element with a completely different density. An example of this possibility is illustrated in [84] where in one hopper, an equiatomic mix of CoCrFeNi is introduced with similar density, and in the second hopper, a low-density Al powder is introduced to produce the HEA AlCoCrFeNi.

An interesting issue in additive manufacturing is whether tensile properties are affected by the growth direction of the consolidation. Fujieda et al. [78] developed a study wherein tensile features were compared between tensile samples extracted in the growth direction (tagged 0°) and in the perpendicular direction (tagged 90°). The work was performed for the HEA AlCoCrFeNi (C1 type), and the results were compared with those of the same material produced by casting. Table 3 compares those results and confirms that, indeed, the best features are obtained in the growth direction of the additive manufactured alloy.

Alloy	Yield Strength (MPa)	Ultimate Tensile Strength (MPa)	Elongation (%)
Casting	1308	1425	5.6
AM 0º	1015	1668	26.4
AM 90º	944	1447	14.5

Table 3. Tensile features of AM HEAs in the growth direction and at 90°, and compared with those of an equivalent cast HEA (from [78])

Another interesting analysis was developed by Joseph et al. [65] who studied the effect of HIP as a posttreatment on an AM HEA, in this case $Al_xCoCrFeNi$ (C1 type). In principle, HIP, which is widely used for casting alloys, could be beneficial to collapsing possible shrinkage defects produced during the AM process. This work concludes that this treatment does not significantly improve the AM product, mainly due to two negative effects (that compensate for the densification effect): coarsening in the microstructure, and the possible formation of a σ phase, which is always a risk in these alloys with such a high Cr content.

In addition, materials processed by additive manufacturing can be subjected to annealing, but in this case, the main objective was to release stresses after solidification [77].

6. Mechanical behaviour of PM HEAs

If we classify high-entropy materials into a specific family in the material world, it must be as a “structural material”, and as a structural material, the mechanical behavior is probably the most important feature required in this family of materials. In some of the figures developed for this paper, have been used results from many different sources. Despite in all the referred papers, authors have used standard tests to measure the mechanical properties, it was not possible to assure the same procedures to get all the analyzed results (especially in hardness, where the load in the Vickers hardness where different in most of the analyzed works, and for this reason is not included in Figures 17, 22 and 23). In this sense, readers are aware of the fact that these data must be treated with care.

6.1 Fine grain and twinning effect

The studied papers about HEAs produced by PM demonstrate that strengthening mechanisms that operate in the alloys are necessarily the same strengthening mechanisms that operate in

conventional HEAs. The effect of the solid solutions in alloys, which contain at least five different alloying elements with different structural properties, is very important. Such a high number of alloying elements produces important lattice distortions that can strongly influence the phase transformation, dislocation dynamics and yield of HEAs. Recently, a comprehensive work was published providing a basic understanding of this important issue [197]. However, leaving aside the solid solution effect, the observed twinning after deformation plays an important role in HEAs. Most HEAs possess, at least partially, an FCC structure that produces a twinning effect after deformation, and this twinning effect provides an additional deformation mode that increases the ductility. Twinning also introduces extra interfaces within the grains during deformation, producing a "dynamic Hall-Petch" effect that increases the work hardening rate and, as a consequence, the strength [198]. The strengthening mechanism of nanoscale twins can also be associated with the complicated interaction between dislocations and twin boundaries. Twin boundaries are believed to effectively block dislocation motion, especially when the thickness of the twin/matrix lamellae decreases down to the nanoscale, also reinforcing the Hall-Petch effect [199]. If we combine the high lattice deformation with the twinning effect and consider that twinning is observed in materials with a low stacking fault energy (SFE), the increase in the solute atoms strongly reduces the SFE and increases the nanotwinning tendency [200]. These effects have been widely studied in HEAs produced by ingot metallurgy but have also been confirmed in PMHEAs.

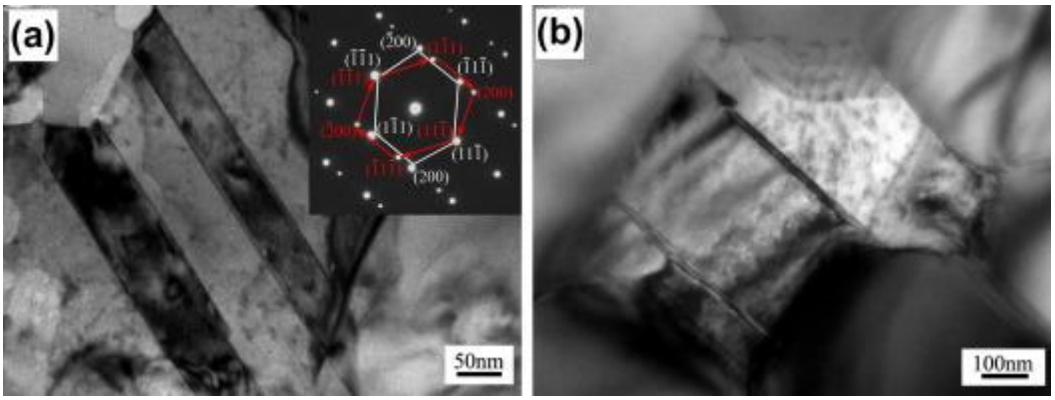

Figure 13 TEM microstructures and SAED pattern of a twinned FCC phase. (a) A twinned FCC grain with the corresponding SAED pattern and (b) a twinned FCC grain surrounded by Cr23C6 carbide, from [34] .

An example of this twinning effect is described in [99][34][149] for the alloys $CoNiFeAl_{0.6}Ti_{0.4}$, $CrCoNiFeAl_{0.6}Ti_{0.4}$ and $Al_{0.5}CrFeNiCo_{0.3}C_{0.2}$, respectively, made by MA and SPS. Figure 13 shows the transmission electron microscopy (TEM) images and corresponding selected-area electron diffraction (SAED) patterns of the FCC phase with nanoscale twins. The nanoscale twins were found only in the FCC phase, which was confirmed by energy dispersive X-ray spectroscopy (EDS)/TEM and the corresponding diffraction patterns.

In addition, [161] focused on the twinning effect in an AlCrCuFeNiZn HEA produced by MA. The stacking faults in this HEA are due to the solubility of Cu and Zn FCC with other solute atoms. With an increase in the Al content in a copper-aluminum alloy, the twin thicknesses decreased [201], [202]. Another important factor in this respect is that the twinning effect under stress is produced mainly in the compression mode, because the twinning produced by tensile load is negligible [13].

More possibilities to increase the twinning effect are reported in some studies on PMHEAs. One possibility is the use of reinforcing particles such as TiC [62]. Introducing particles that can act as hard hinges in the formation of deformation twins is associated with a lower SFE. Another possibility is the presence of dual microstructures. PM can more easily promote the formation of dual microstructures than other processing routes, and in the case of PMHEAs, dual microstructures could also be suitable for combining BCC and FCC structures [175]. A bimodal grain size distribution or ultrafine-grained microstructure could promote the accumulation of dislocations and thus achieve a high strain-hardening rate [203].

6.2 High-temperature behavior and high-strain-rate deformation

Although HEAs are a promising material for use as structural materials at high temperature [204], [205], fewer articles deal with the behavior of PMHEAs at high temperature.

In some of those works, a piece of Gleeble equipment, specially devoted to simulating thermomechanical treatments, evaluates the compression strength at different strain rates and temperatures. In [175] the behavior of two alloys, $TiNbTa_{0.5}Zr$ and $TiNbTa_{0.5}ZrAl_{0.2}$, in compression at 800 °C and promoting an engineering strain of 50% is analyzed. Specifically, the effect on the microstructure of the precipitates of Nb and Ta and the positive effect of adding Al is investigated. In these alloys, belonging to the C8 cluster where the predominant present phase is BCC, the mechanical behavior at high temperature is enhanced by the presence of precipitates in grain boundaries and the bimodal microstructure. Another example is the analysis of the $CrFeCoNiMo_{0.2}$ (cluster C3) alloy [109]. In this case, specimens were tested at different temperatures from 700 °C to 1100 °C. Here, the flow behavior at high temperature is improved by dynamic recovery and grain growth pinning by the precipitation of a Mo-rich σ phase. In addition, some information on the creep behavior under compression can be found. In [123] the compressive creep behavior of an oxide-dispersion-strengthened (ODS) CoCrFeMnNi PMHEA produced by SPS was studied. This work found that in the same material without and with dispersed oxides, the latter exhibited improved performance.

Alloy	σ_y (MPa)	σ_{max} (MPa)	ε (%)	Temperature (ºC)	Ref.
$Fe_{18}Ni_{23}Co_{25}Cr_{21}Mo_8WNb_3C_2$	1200	1452	3.9	25	[119]
$Fe_{18}Ni_{23}Co_{25}Cr_{21}Mo_8WNb_3C_2$	550	795	13.3	650	[119]
12Cr ODS ferritic	1200	1294	18	25	[206]
12Cr ODS ferritic	427	435	29	600	[206]

Table 4. Comparison of tensile properties from room temperature to 650 °C, from [119].

Few works provide information about tensile features at high temperature. In [119] a special PMHEA ($Fe_{18}Ni_{23}Co_{25}Cr_{21}Mo_8WNb_3C_2$) obtained by MA and HP with a 12 Cr ODS steel is compared. Table 4 shows that the PMHEA exhibits much higher tensile strength but lower ductility than the ODS steel.

Some PMHEAs subjected to a high strain deformation rate exhibit so-called “serrated yielding”. In Figure 14 [98] visually explains this concept. In [133]

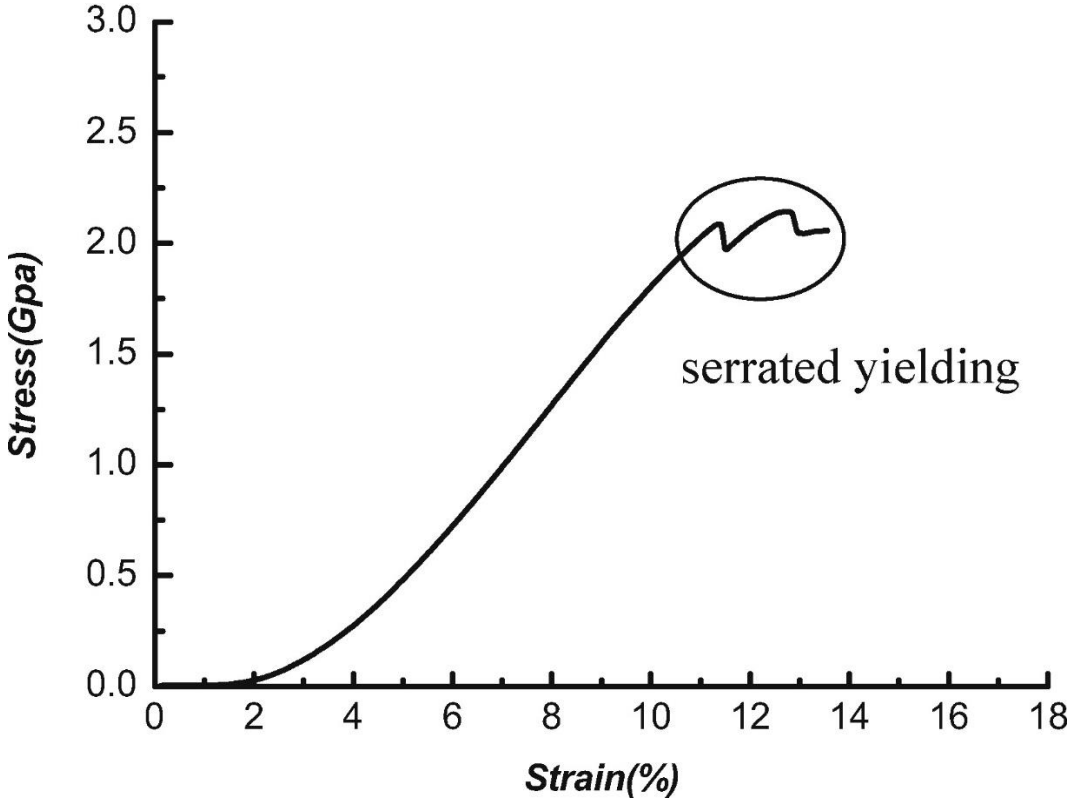

Figure 14. Stress-strain curve of $Al_{0.4}FeCrCo_{1.5}NiTi_{0.3}$ reinforced by nano-Al_2O_3 after SPS under compression. From [98].

different compressive tests (quasistatic at room temperature and different strain rates, quasistatic at different strain rates and different temperatures up to 900 °C and dynamic compressive tests) were performed over a PMHEA (CoCrFeMnNi). According to [21] this phenomenon is more accurate in PMHEA than in an as-cast HEA. The serrations observed on the stress-strain curves of the PM CoCrFeMnNi HEA are caused by the periodic pinning and unpinning process of dislocations in the grains due to the number of dispersed Cr-rich phase particles. A high deformation rate at room temperature also increases the serration yielding [107]. In [98], where tests are performed a low strain rate, the serration behavior is also observed but in this case, it is attributed to the Al_2O_3 reinforcements in the $Al_{0.4}FeCrCo_{1.5}NiTi_{0.3}$ PMHEA.

6.3 Compression behavior

Most of the papers dealing with mechanical behavior use compression tests to evaluate the mechanical behavior. Therefore, extensive information can be used to analyze this topic. Table S6 of the accompanying supplementary data, Appendix A, includes the results concerning yield strength, ultimate strength, deformation at fracture and hardness for many HEAs, including also HEA obtained by ingot casting [53], [207]–[218]. In the table, the alloy composition, the cluster to which the alloy belongs, the results regarding these properties, and the origin of the information are included. In addition, the processing route followed to obtain the alloy is included for comparison (i.e., if it is a PM route another specific route, or casting).

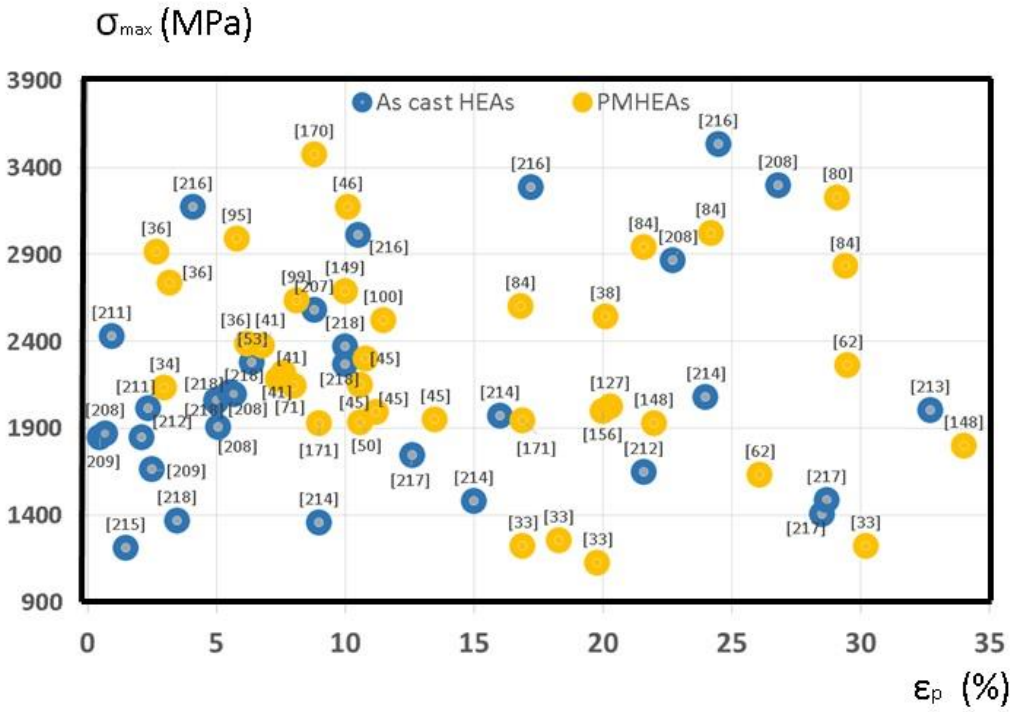

Figure 15. Ultimate compressive strength vs. deformation at fracture of different HEA.

Figure 15 displays the results concerning the ultimate compressive strength as a function of the deformation at fracture. When we analyze and compare these two properties in the figure, no tendency can be distinguished that could differentiate the materials obtained by conventional ingot casting from those obtained by PM. Perhaps the unique remarkable difference is that some HEAs obtained by casting exhibit a very low deformation at fracture but also a higher aptitude to attain higher levels of deformation, but the analyzed sample of papers in this graph does not allow us to extract clear conclusions. Figure 16 collects the results only taking into account the ones belonging to a specific cluster, that is, according to the composition, without considering if the processing is PM or ingot casting. Materials belonging to clusters C1, C3, and C4, based on NiCoFeCr, are spread throughout the figure, showing all the possibilities of strength and deformation. C3 materials exhibit less strength on average (but can reach higher levels of deformation), and C4 materials exhibit a lower level of deformation on average. Those materials are the most common in the literature regarding HEAs and are based on the core group of transition metals (3d transition metals from the 4th period) commonly used in ingot metallurgy. HEAs were developed, in part, from the Cantor alloy [3], based on these elements plus Mn. Leaving aside clusters C2-C5 (with only one alloy), the materials made with clusters C6-C8, that is, refractory HEAs, mainly composed of refractory metals (W, Ta, Nb, Mo, Zr) exhibit much less deformation at fracture.

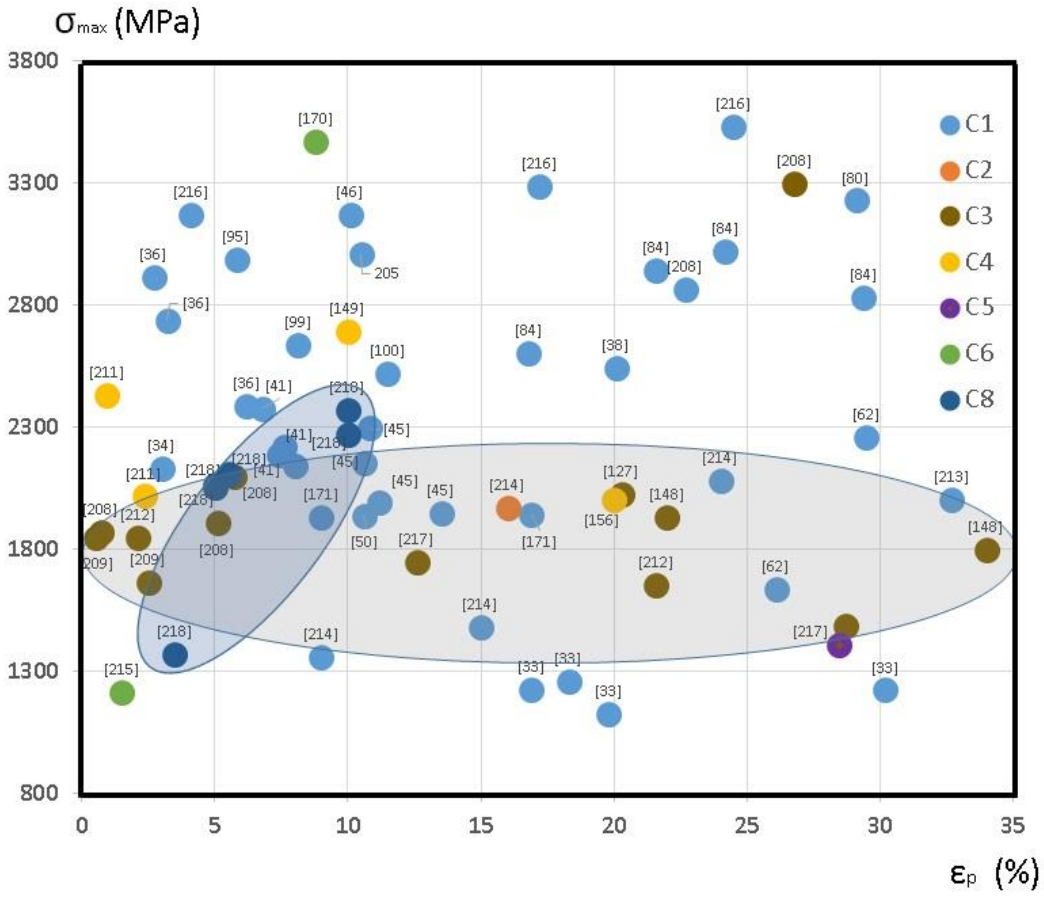

Figure 16. Ultimate compression strength vs. deformation at fracture considering the cluster composition.

However, if we analyze the hardness against the deformation at fracture (Figure 17), a slight improvement in the relationship of the hardness/deformation of the cast alloys against the PM alloys becomes more apparent. In any case, these results are based on many different materials (even

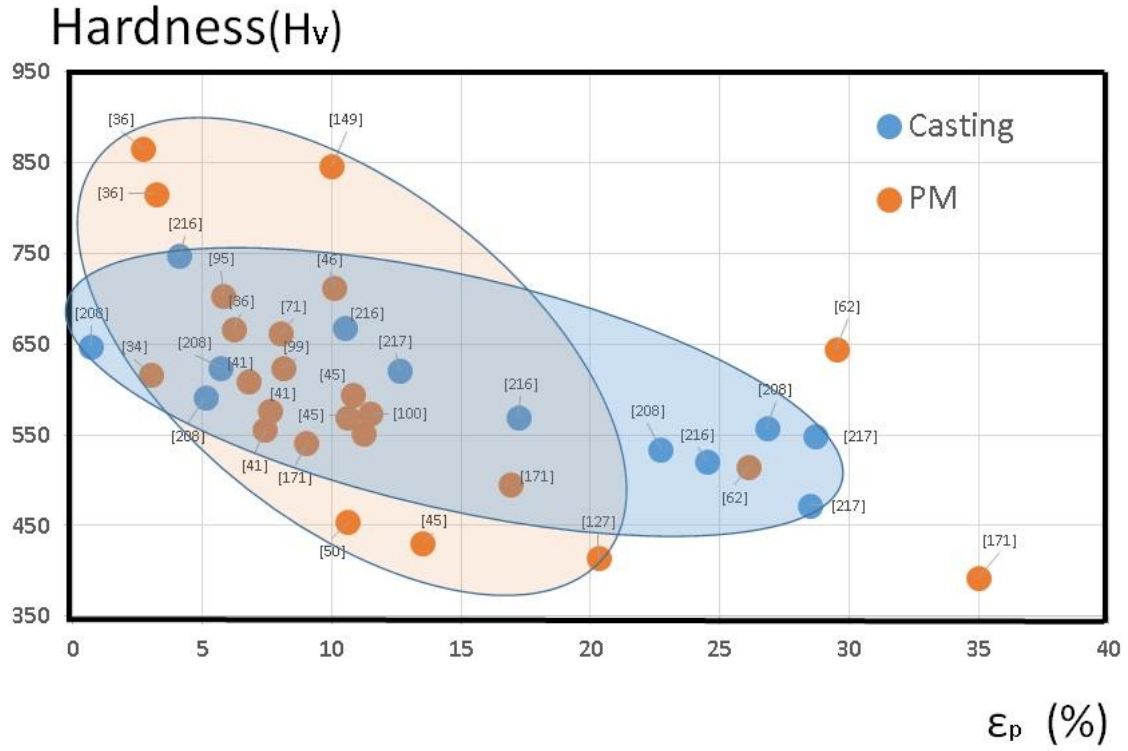

Figure 17. Hardness vs. deformation at fracture of different HEA.

compositions), manufactured under different processing conditions, and this is just an orientating tendency. Clearly, PM can compete in most fields to provide possibly required properties. Interestingly, the compositions and processing conditions of PMHEAs can be modified for a customized application, in contrast with ingot metallurgy.

6.4 Tensile behavior

Unfortunately, much less information about the tensile behavior of PMHEAs is available. Just a few papers regarding tensile features for these materials have been found. Table S7 of the accompanying supplementary data, Appendix A, shows some tensile results (those obtained from papers where reliable tensile data were provided), and results from as-cast HEA [34], [77], [205], [209], [219]–[230], rolled HEAs [26], [222], [224], [231]–[233], forged HEAs [220], HEAs obtained by high pressure torsion [198]. Other structural alloys belonging to the so-called structural materials are also included, like Ti base alloys [35], [234], [235], stainless steels [236], Ni base superalloys [237], ODS steels [206], [238] or intermetallics [239].

If we plot some of these results for analysis, some clusters of results can be distinguished in Figure 18. As-cast HEAs can be found in all the spaces of the figure, but could be appreciated in some groupings in the high values of deformation, being as these materials are the conventional structural alloys in this smaller range (and here Ti- based alloys show a little slightly bit better performance). Once again, like as in the compression results, the PMHEAs are distributed in all throughout the space of the graph, but also here this is not relevant at all due to because of the low number of samples. Only in one paper [77] compared the same material (CoCrFeNi HEA) made by additive manufacturing and arc melting, and the results for the PMHEA are clearly positive (σ_{max}/ε in PMHEA of 745 MPa/32% vs. 457 MPa/50%, yield strength of 600 MPa vs. 188 MPa). Furthermore, most of the tensile results for the PMHEAs came from materials produced by additive manufacturing. These are promising results, but

this information on this strategy is remarkably lacking, which makes it a good niche to research.

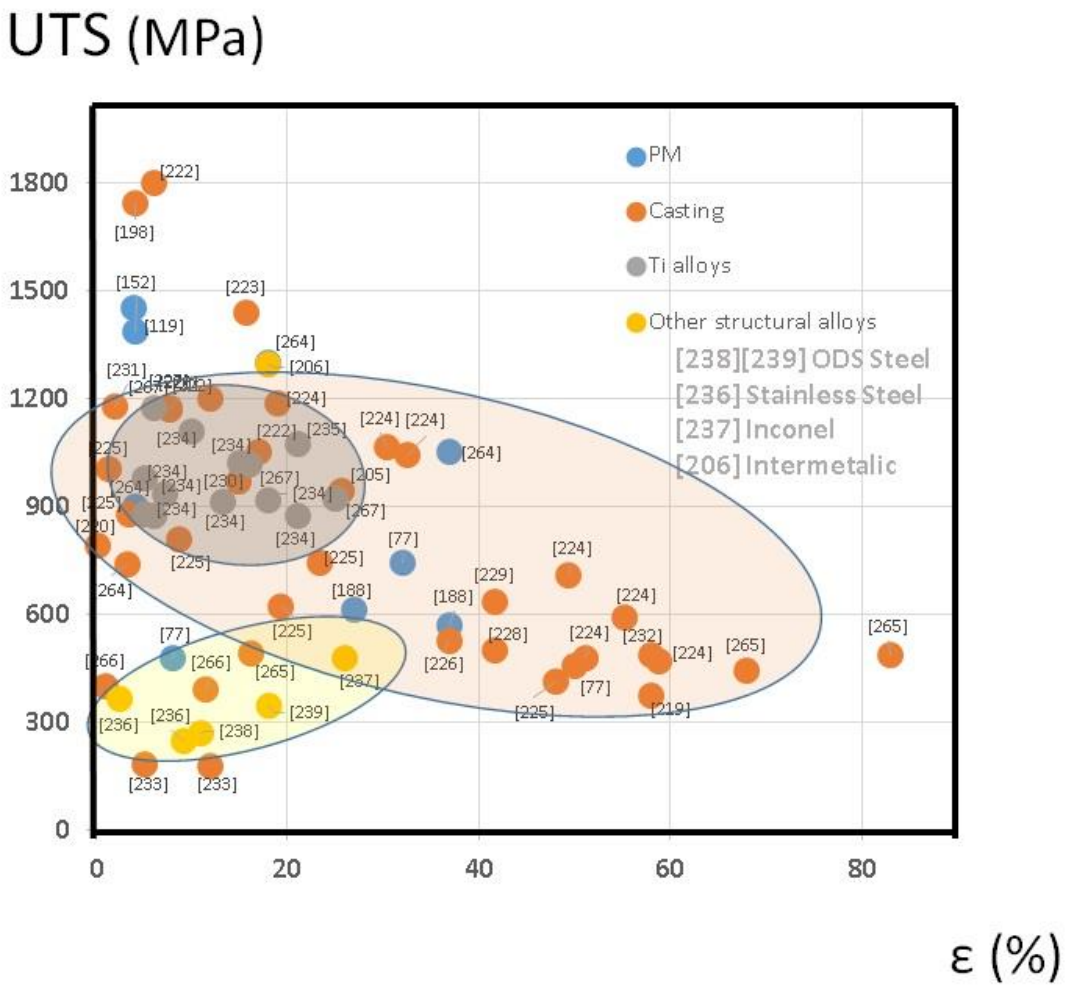

Figure 18. Tensile features for different HEAs and other structural alloys .

7. Special properties of PM HEAs

Clearly, HEAs have enormous potential as structural materials, especially because of their important mechanical properties, but other important abilities as structural materials beyond the mechanical properties can be found in HEAs. Here, we outline some of these abilities.

7.1 Corrosion and oxidation

The presence in the composition of an alloy of more than 20% (wt.) Cr in combination with Ti and Al powerfully suggests possible good corrosion or oxidation behavior. Among the works covered in this review, some of them focus on corrosion or oxidation, and among those, most of them belong to compositional clusters C1 to C4, in which Cr, Ti or Al are present.

Considering the HEAs in [32], [52], [54], [104], all of them belong to compositional clusters C1 and C2 made by conventional PM. Electrochemical corrosion is tested through potentiodynamic polarization curves, and better performance than that of stainless steel 304

was observed in all of these works. In [132], the electrochemical behavior of a C4 cluster was evaluated by measuring the pitting potential, the results were positive. This later work was devoted to the development of composites (HEA reinforced with SiC), and introducing reinforcements deteriorated the pitting corrosion behavior.

In [104] the pitting corrosion of three alloys (a CuZr alloy, labeled E2, a CuZrAlTiNi HEA, labeled E5, and stainless steel 304, obtained by MA and SPS) is evaluated by electrochemical polarization measurements using a potentiostat in an artificial seawater solution at a scan rate of 0.003 V/s. The artificial seawater mainly consisted of NaCl, $MgSO_4$, $MgCl_2$ and $CaCl_2$. The corrosion resistance of the as-sintered bulk samples in the seawater solution is demonstrated by the potentiodynamic polarization curves displayed in Figure *19*. The HEA sintered at 620 °C exhibits the highest corrosion potential (E_{corr}) and the lowest corrosion current density (i_{corr}) with a wider passive region. The HEA sintered at 959 °C possesses the best passivity behavior (the lowest i_{pass}) and a high pitting resistance (with the widest passive region). The corrosion rate (r_{corr}) can be calculated through Faraday's law, as shown in the equation below:

Equation 1 $R_{corr}=0.0327*(EW* i_{corr}/D)$

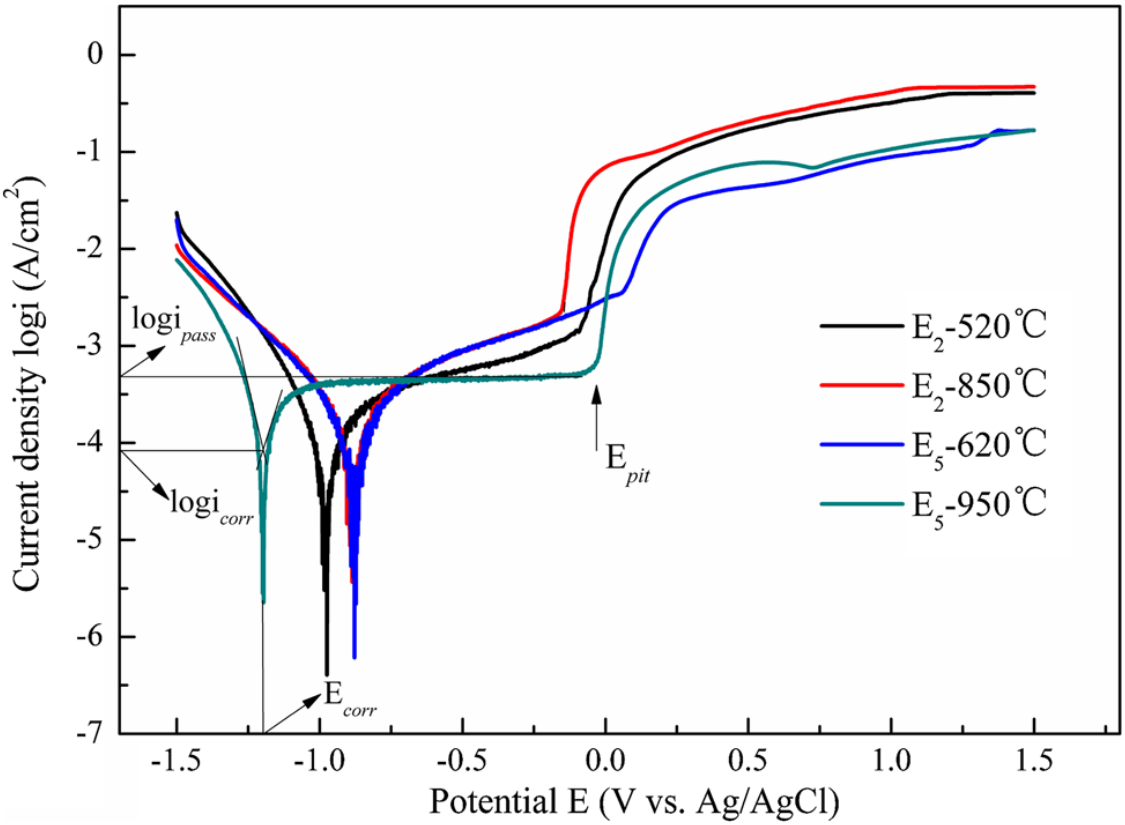

Figure 19. Potentiodynamic polarization curves of the as-sintered E2 (CuZr alloy) and E5 (CuZrAlTiNi HEA) bulk alloys at different sintering temperatures (from 520 ºC to 959 ºC), from [104].

where EW is the equivalent weight, and D is the density. Table 5 shows all these corrosion parameters (and also the pit potential and shows the best behavior of the HEA sintered at 620 against the stainless steel, tested under the same conditions.

Samples	E_{corr} (V)	i_{corr} (A/cm2)	i_{pass} (A/cm2)	E_{pit} (V)	E_{pit} - E_{corr} (V)	r_{corr}
E_2—520 ºC	-0.97 ± 0.01	(3.23 ± 0.31)x10^{-5}	(9.59 ± 0.28)x10^{-4}	-0.09 ± 0.06	0.88	0.38
E_2—850 ºC	-0.88 ± 0.09	(4.07 ± 0.44)x10-5	(1.90 ± 0.53)x10^{-3}	-0.15 ± 0.04	0.73	0.47
E_5—620 ºC	-0.87 ± 0.02	(3.47 ± 0.39)x10^{-5}	(3.59 ± 0.19)x10^{-3}	0.06 ± 0.03	0.93	0.37
E_5—950 ºC	-1.19 ± 0.02	(7.48 ± 0.54)x10^{-5}	(4.29 ± 0.22)x10^{-4}	-0.03 ± 0.06	1.16	0.79
304	-1.05 ± 0.04	(9.55 ± 0.25)x10^{-5}	(5.32 ± 0.31)x10^{-4}	0.09 ± 0.04	1.14	0.99

Table 5. Corrosion parameters of the samples tested (*as-sintered E2* -CuZr alloy- and E5 -CuZrAlTiNi HEA- bulk alloys at different sintering temperatures -from 520 ºC to 959 ºC-, in a seawater solution, from [104]

Only one work [84], has been found in which the behavior of the HEA is less competitive than that of stainless steel 304, and the reason should be related to the different aging treatments that were applied to the material, this time manufactured by direct laser fabrication.

If the performance against corrosion is quite good, the response against oxidation at high temperature is truly promising. In [47] a cermet based on an HEA (C1 cluster) was studied, and the oxidation tests were performed at the same time as cermets manufactured using conventional Ni/Co binders. The behavior in the HEA-based cermet is three times superior. Similar behavior can be found in [54] wherein in addition to the electrochemical corrosion, oxidation was studied. A unique study on a refractory HEA (C7 cluster) made by additive manufacturing can be found in [172] . Here, the behavior was studied at high temperature in air, and a good performance was observed, suggesting good possible fusion applications.

The results explained above suggest that the HEAs have good potential for a niche of applications requiring good corrosion/oxidation behavior.

7.2 Friction.

Friction and wear usually go together in the classification of properties, but we will devote some space to wear in the next paragraph. Through some slight modifications to the composition of the HEA which is suitable thanks to the flexibility of the PM process, important improvements have been made in the friction behavior of the alloys. Friction behavior is important in a wide number of applications, especially in bearings. The chapter devoted to composites based on HEAs (HEACMs) in [164], includes the profile of materials focused on here. In this later work, the advantages of PM for the development of this family of materials are highlighted because as-cast HEAs contain segregations, multiple phases, and brittle intermetallics at grain boundaries, all of which negatively influence the ductility and toughness and damage the friction features of these alloys.

Yadav et al. [165], [166] performed an interesting study adding Bi and Pb dispersoids to two different HEAs, AlCrFeMnV (C9 cluster) and CuCrFeTiZn (C5 cluster), respectively. In both cases, the friction coefficient was reduced, and the wear resistance was increased by approximately 20%. In both cases, the mechanical properties of the base HEA were not significantly affected. In [140] a similar study considering the addition of Mo to a base HEA (CoCrCuFe) was performed. The presence of the Mo introduced some precipitates into the microstructure that modify the friction behavior, reducing the friction with the increasing amount of Mo.

The works of Zhang et al. [120], [128] are in the same direction. In these studies, the base alloy was the core alloy of the C1-C4 clusters (CoCrFeNi), and the additions to the alloy were Ni coated with graphite, Ni coated with MoS_2 and S (added as FeS). The friction and wear

behavior from room temperature to 800 °C was studied. In all the cases, excellent self-lubrication behavior and good wear resistance were exhibited. The friction coefficient was always reduced, and the wear performance improved up to 5 times at room temperature. In addition, the mechanical properties were not highly compromised.

To end this section on the friction properties, an interesting work on the machinability of an HEA manufactured by AM [136] is discussed. Different machining conditions were applied to the CoCrFeNiMn alloy (C3 cluster), and the report concluded that with the suitable process combination, any practical surface quality and dimensional accuracy could be obtained.

7.3 Soft magnetic features

Ji et. al. [105] explored the soft magnetic features of a PM HEA (CoCrFeNiMn, C3 cluster). The hysteresis curve of the powders, after 60 h of MA, exhibits soft magnetic properties (see

Figure 20). The values of the saturated magnetization and the remanence ratio are higher and lower, respectively, than values available in the literature [240] for a similar cast alloy. This result indicates that the as-milled powder can be used as a soft magnetic material. Moreover, the powder exhibited superparamagnetic behavior, observed for magnetic particles with sizes under 10 nm [241]. Unfortunately, after SPS, the coarsening of the grains modified both the soft magnetic and the superparamagnetic features of the alloy.

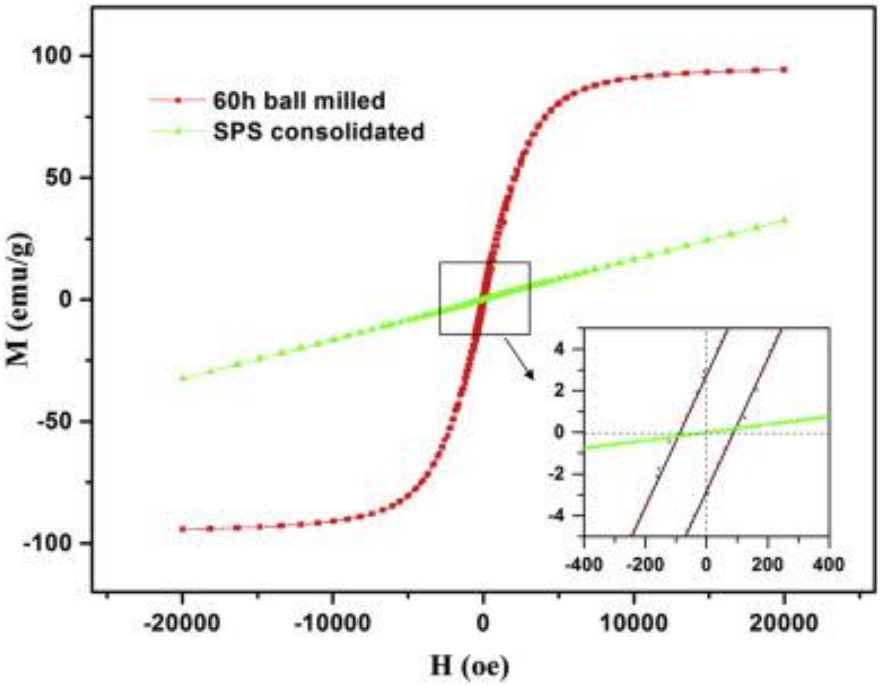

Figure 20. Magnetic hysteresis curves of the CoCrFeNiMn HEAs measured at room temperature, from [105].

In a similar way, is the study of Yu et. al. [106], but in this case succeeding in a PM consolidated HEA. In this paper, the change of just one element in the alloy leads to a drastic change in the magnetic response. With the same alloy than the previous work of Ji et. al. [105] a similar

result was obtained, but the Mn was changed to Cu in the composition (CoCrFeCuNi, also in the C3 cluster). The levels of the saturated magnetization, the remanence ratio and the coercivity, even after SPS, enable using this PM HEA in soft magnetic applications. The value obtained for the saturated magnetization is higher than that of the CoCrFeNiCuTi HEA obtained by casting [240].

These studies demonstrate that this is another promising field of application for PM HEAs.

7.4 Hydrogen storage

Hydrogen is considered a good alternative to fossil fuels, but its possible application is linked to the development of materials capable of storing it. Some works have demonstrated the possibility of some alloys with the BCC structure to react with hydrogen, thus constituting a promising hydrogen storage material [242]. Many HEA compositions can ensure the BCC structure with the proper combination of alloying elements (see Figure 6). Kunce et al. [151], [176] produced two PM HEAs by additive manufacturing, with two different compositions (TiZrNbMoV and ZrTiVCrFeNi, belonging to the C8 and C5 clusters), trying to exploit the BCC structure for hydrogen storage. The feasibility of this potential application was measured through pressure-composition-temperature experiments, and both alloys can absorb and desorb hydrogen (until the hydrogen is 1.8% and 0.59% in weight, respectively). In the context of this experimental setup, the alloys were unable to completely desorb hydrogen.

Similarly, in another study involving PM HEA [155] (MgZrTiFeCoNi, C4 cluster) tests were performed on the powder, and the phase transformation when the hydrogen was absorbed and desorbed was studied through *in situ* synchrotron XRD measurements. In this case, the samples could absorb and fully desorb 1.2% hydrogen by weight. Apparently, the structure changed from BCC to FCC during the absorption process and from FCC to BCC during the desorption process.

8. Alloying opportunities for PM HEAs

After the chapter related to special properties, and more in detail in the topic about “friction”, we have an example about “alloying opportunities” in PM. In this paragraph, what was explained in terms of alloying procedure, only can be possible through PM technology. Now, we will develop other alternatives that only can be introduced into the HEA field by using PM.

8.1 HEA-strengthen metal matrix composites **(MMCs)**

We found some works where HEA powders are used as a “reinforcement” in a metal matrix. The first example is a work developed by Chen et al. [76] where the selected matrix is Cu. In this work, an AlCoNiCrFe (C1 cluster) powder is used to reinforce pure Cu. The HEA powder was obtained by MA and then mixed (low-energy milling) and sintered (hot pressed at 800 °C/70 MPa/30 min). The composite was made by adding 10 and 20% (wt) HEA powder. The main result was an important increase in the compressive yield strength, without a significant decrease in the ultimate compression strength or the deformation at fracture.

One more typical configuration for MMCs is aluminum-based composites. In [243] using the AA6061 as the matrix and a conventional PM route (mix-cold compaction-sintering), an MMC is manufactured using a CrMnFeNiCu PM HEA (C5 cluster). Two different amounts of reinforcements (10 and 20% wt) were used, and in both cases, the compressive strength was

increased significantly (in the case of the 10% reinforcement, the fracture compressive strength was double that of the base alloy). In the work of Karthik et al. [244] an aluminum matrix (in this case an AA5083 alloy) and HEA as reinforcement (CoCrFeNi, C3 cluster) were also used, in this case using 12% (vol) as reinforcement. Interestingly, this work used an additive manufacturing method based on friction deposition using a friction stir welding equipment. The obtained composite significantly improved the mechanical properties relative to those of the matrix (i.e., the ultimate tensile strength increased from 300 MPa to 395 MPA and the HRB from 30 to 549), except the elongation, which reduced from 12% to 5%, as could be expected.

In this chapter, the work of Tan et al. [81]. is also of interest. In this case, an HEA was also used as a reinforcement (AlCoCrFeNi, C1 cluster), but the matrix, prepared from an amorphous Al alloy ($Al_{65}Cu_{16.5}Ti_{18.5}$) that was manufactured by MA, was more innovative. To avoid microstructural coarsening, the composite was consolidated by SPS. Here, both the matrix and composites exhibit a very brittle behavior, but the ultimate tensile strength of the composite increased from 1700 MPa to 3120 MPa.

Figure 21 shows the powders used and the microstructure of the composite.

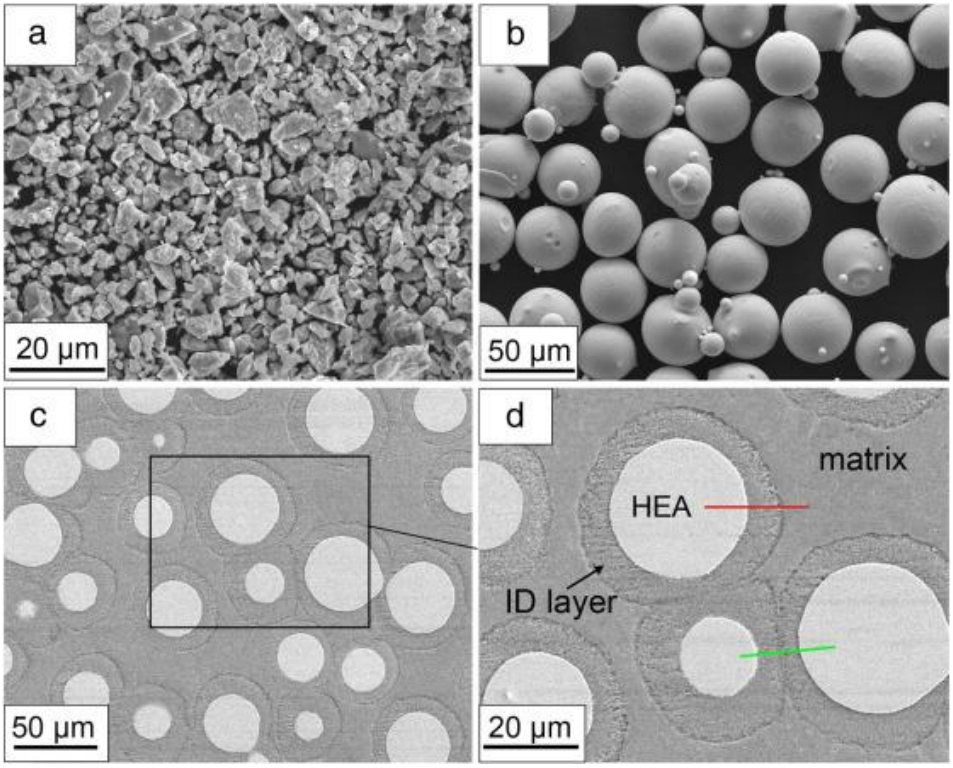

Figure 21. SEM images of the as-milled amorphous Al alloy powder (a), (b), the HEA gas-atomized particles and c) the composite; (d) magnified image corresponding to the area marked by the rectangular in (c), from [81].

8.2 Particle reinforced HEA composites **-HEA matrix composites- (HEAMCs)**

In this case, the MMCs are composed of an HEA matrix and reinforced with Al_2O_3 or SiC. Table S8 of the accompanying supplementary data, Appendix A, is displayed the composition, the

processing route and some compression properties and hardness of some works developed in this direction. In the bottom part of the table, some results regarding the same HEA without reinforcement and some other works from different authors for comparison. Although in most of the articles, the size of the reinforcement is in the range of nanometers, the effect of these reinforcements on the mechanical properties is not as important, as they improve only the compressive yield strength and the hardness.

There are another two other works, focused on the same material (CoCrMnNi, cluster C1 reinforced 5% - wt.- of SiC <50 nm, manufactured through MA + mMixing + HIP), but focused ion the electrochemical response (without reporting any information regarding mechanical properties). As could be expected, the presence of nanoparticles in the microstructure introduced local Cr- depleted zones, and this could promote an accelerateion of the corrosion process.

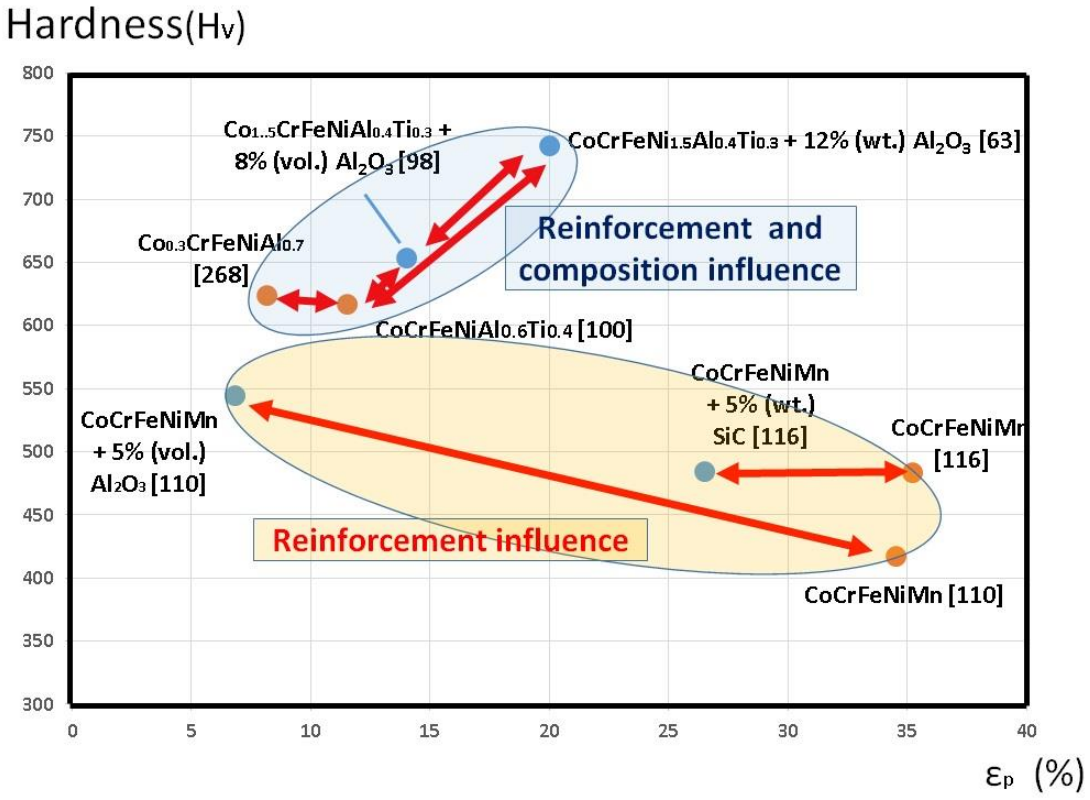

Figure 22. Ultimate compression strength vs. deformation at fracture for some HEA base composites and HEAs.

Figure 22 can help us analyze these results, considering that the plot shows differences in terms of composition and reinforcement, but differences also exist in other important variables such as the size of the reinforcement and the processing conditions. Clearly, the influence of reinforcement in conjunction with changes in composition can cause important changes in the mechanical properties, helping us to tailor the material to one specific application.

Sharma et al. [164] highlighted the possible role of these HEAMCs in applications requiring improved wear and friction properties beyond the required mechanical properties.

8.3 Cemented carbides/cermets

Cemented carbides (mainly based on WC as the hard phase and Co as the binder) and cermets (mainly based on TiCN as the hard phase and Co-Ni as the binder) have been competing for years in the cutting tool markets and in wear applications. However, for many different reasons, the last 15 years have seen a tendency both at the industrial level and in academia to find new materials for cutting and wear applications, trying to avoid Co and Ni as binders. Some of the reasons for this research are related to some specific properties such as resistance to corrosion or oxidation, but others are linked to the strategic role of Co and Ni in the global market and the health issues related to Co and Ni. Considering these circumstances, the appearance of HEAs as materials with a simple structural configuration (BCC or FCC), along with promising oxidation and corrosion performance, a promising behavior at high temperature and suitable for processing by PM, makes this new family of alloys a strong candidate to be used as binders in hardmetals.

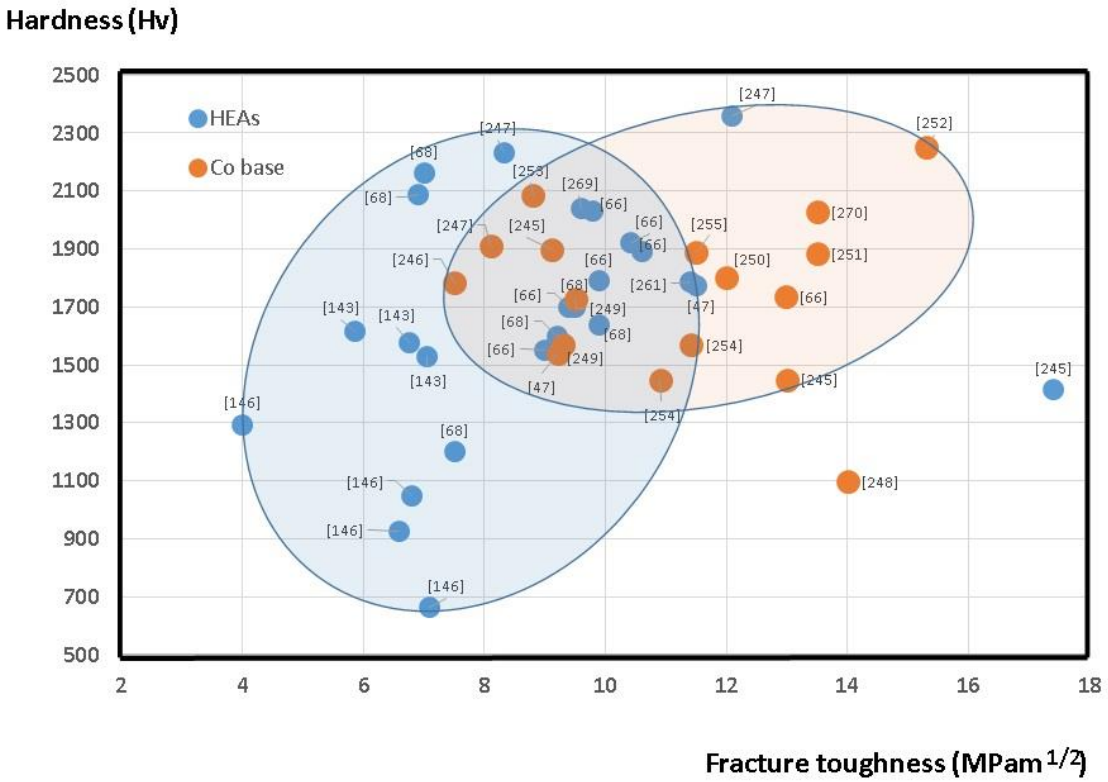

Figure 23. Hardness vs. fracture toughness of different cermets and cemented carbides made with HEA binders, and some conventional Co-based materials for comparison.

Since the appearance of PM HEAs, many works were performed to try to analyze the feasibility of these materials as a binder, especially since 2014 ([47], [150], [245]) and 2015 [48]. Over the last few months, there has been a dramatic increase in papers dealing with this topic ([62], [129], [160], [168]). Many of these papers deal with improving the oxidation behavior [47] or the wear behavior [131], [138], [157], [245] and the relationship between the fracture toughness and hardness (always in comparison with the conventional cermets/cemented carbides based on Co or Co-Ni). In this latter respect, Figure 23 analyzes some results from different articles and compares these results with some traditional Co-WC [245]–[252] or Co-WC-VC [45], [95], [253]–[255] hardmetals produced by equivalent processing routes. Table S9 of the accompanying supplementary data, Appendix A, includes information regarding the binder phase (an HEA or a Co-based binder), as well as the hard phases and the processing route, including results concerning hardness and fracture toughness.

This figure shows how PMHEAs are competitive with other conventional hardmetals. In a large space, the range of properties is similar, and we have to consider that most of materials processed with conventional composition have been manufactured with hard phases from nanosized powders and materials with enhanced fracture toughness [256]. Most of the HEAs used in these studies belong to the C1 cluster. Refractory HEAs (clusters C6-C7-C8) with, in principle, higher hardness and presumably better behavior at high temperature could be good candidates to develop cermets and cemented carbides [164].

One important issue to be solved in the development of cermets is the wetting behavior of the binder in the hard phase, in this case the HEA on the TiC or the TiNC. This topic has been treated in some works [48], [150], [160]. Some of these studies have performed wetting studies using the sessile drop test on TiCN substrates, which demonstrated the very good wetting of the HEA.

To finalize this chapter, it is also interesting to mention that [138] suggests that HEAs can also be a good binder to manufacture diamond tools.

8.4 Oxide dispersion strengthened (ODS) alloys: HEAODS

Three works were found related to this topic, two performed by Hadraba et al. [115], [123] and the third by Moravcik et al. [257]. This very interesting strategy may open a completely new research area of high interest. In the first two works, an HEA (CoCrFeNiMn, C3 cluster) was manufactured by MA and SPS (1150 °C/50 MPA/5 min). The same alloy was produced by adding oxygen, Y and Ti during the MA step to produce dispersed oxides on the order of 0.3% (wt). The mechanical properties (in compression and tension) and the creep behavior in uniaxial compression mode (between 700 and 800 °C) were tested in these studies. The results were quite promising because the yield strength (both at compression and tension) and the ultimate tensile strength increased on the order of 30% in the case of the ODS alloy, and in the tests performed at 800 °C, the response increased by up to 70%. In addition, the results of the compression creep study showed better performance in the ODS HEA. No work has compared these HEAODSs with ODS steels tested under the same conditions, but the values obtained can be considered promising. The negative aspect is, similar to that of the ODS steels, the ductility was much lower in the HEAODSs than that of the original alloy.

In [257] the HEA (CoCrFeNiTi, C4 cluster) is also manufactured by MA and SPS (1150 ºC/30 MPa/20 min.). After the MA a powder with a preferential FCC phase is obtained, but after SPS some intermetallic (Ni_3Ti type) can be found. In this work after the SPS consolidation, the bulk material is submitted to different annealing temperatures (700, 900 and 1100 ºC) under Ar atmosphere. After the annealing grain growth is produced and some dispersed oxides and also the above mentioned intermetallics finely dispersed in the structure make some changes in the mechanical behavior. The highest values for tensile strength are obtained for the SPS materials but an slightly decrease in the UTS values (from 1569 MPa to 1467 MPa) are compensated with an important increase of the elongation in the annealed materials (from 6 to 14%).

9. Future work

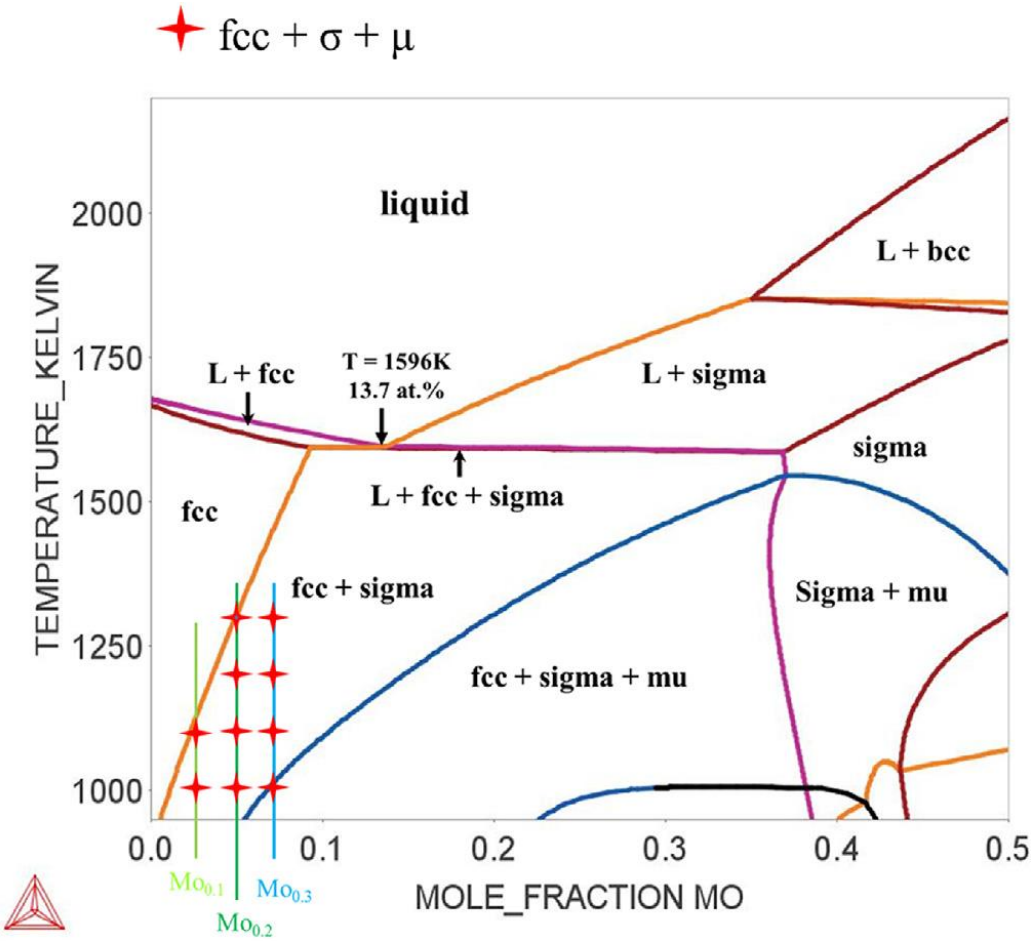

Figure 24. The pseudo binary phase diagram of the (CoCrFeNi)-Mo alloy system. The star stands for a mixture of the FCC, σ and μ phases in the Mox (x = 0.1, 0.2 and 0.3) at 973 K (700 ºC), 1073 K (800 ºC), 1173 K (900 ºC) and 1273 K (1000 ºC). From [147].

Many studies have been performed on PM HEAs, but many further work could be done to improve the knowledge of this family of materials. Today, so many instruments are available that can be used in materials science that the space to explore any field of materials is unlimited. In the next sections, some ideas are introduced to offer some possible research

lines to those who want to be introduced to the PM HEA field, to enable them to develop knowledge in those spaces with room for innovation. These points are not exhaustive, and some matters are not covered, but all the proposed topics can be considered important.

9.1 Thermodynamic modeling.

Today, there are many tools to develop accurate thermodynamic calculations to predict the expected phases for a determined composition at a specific temperature. In a complex system such as an HEA, using these tools to have an idea about what we can estimate for a certain combination of elements could be an important advantage. For instance, we have seen in many works how the structural composition could change by modifying the composition of one single element such as Al [44], [55], [126], Ti [85], [172], Fe [33], Mn [177] or the modification of two elements, such as Al-Ti [67] or Cu-V [171]. Through thermodynamical calculations, those changes could be calculated and predicted before investigating them experimentally. One example is shown in [147], Figure 24, wherein a pseudobinary phase diagram (CoFeCrNi)-Mo (obtained with the help of Thermo-Calc software, based on the Calphad method [258]) is analyzed for the possible presence of σ and μ phases depending on the Mo content. On the diagram are marked lines and stars with the composition of the (σ+μ) precipitates on the γ matrix, for each of the studied alloys (Mo0.1, Mo0.2 and Mo0.3).

In all the papers studied to prepare this review, only a few used any kind of thermodynamical calculations. More than the abovementioned paper highlight the use of Thermo-Calc to predict the present phases (FCC, BCC, liquid) as a function of the temperature in the AlCoCrFeNi system [58] and to predict the presence of graphite in an HEA-based cemented carbide as a function of the carbon content [174]. Thermo-Calc was also used in [175] to predict the present phases (HCP, BCC and liquid) as a function of the temperature in the $TiNbTa_{0.5}Zr$ and $TiNbTa_{0.5}ZrAl_{0.2}$ systems. In [153] another thermodynamic software, JMAtPro [259], was used to simulate the phase equilibrium in the solidification of the NiCrCoTiV system.

In their review of nanocomposites and HEAs, Sharma et al. [164] emphasized the important role of thermodynamical calculations in the design of new possibilities in this field.

9.2 Thermal analysis.

Many thermal analysis techniques could be applied in the development of PM HEAs that could help to reduce the weight of experimentalism in the development of the final proposed alloy. However, only a few techniques focus on some specific steps of the processes. Differential scanning calorimetry (DSC) and differential thermal analysis (DTA) have been widely used to analyze the phase transformation in the atomized or mechanically alloyed powders before the consolidation step (i.e., [143], [160] among many others), but only a few works use these kinds of techniques to study the consolidated material manufacture by the conventional PM route [141], [162]) or AM ([77], [260]). In [65] and [167] thermal analysis techniques are used to evaluate changes with different cooling or heating rates. In the case of [12] CCT (continuous cooling temperature) diagrams are developed (later the application to heat treatments will also be discussed). Dilatometry, which is a highly useful technique used in the development of many PM families of materials, is scarcely used for PM HEAs [124].

Information about the appearances or disappearances of desired phases (such as a specific BCC or FCC phase) or undesired phases (σ phase, carbides or intermetallics, for example), the real melting point of any HEA system, the kinetics of the transformations in the phases, the dimensional behavior with the temperature or the possible undesired oxidation processes could be analyzed and studied with thermal analysis techniques. This is another good opportunity for studying this family of materials.

9.3 Structural and microstructural knowledge of the PM HEAs

In most of the analyzed works, the present phases have been thoroughly studied by XRD and/or TEM. However, only a few studies are complemented with an electron back-scattered diffraction (EBSD) analysis. In the world of HEAs, in principle, the size of the grain in the microstructure, the orientation of the phases, the twinning effect, etc. are much important than in other families of alloys because they are one multicomponent alloy, usually with only one main phase in the microstructure. For this reason, small changes in some microstructural features could be crucial to improving the mechanical properties, and here, the role of EBSD could be important. For example, [34], [100], [145], [148] analyzed twinning and its effects on the mechanical properties (using TEM), but only in the last work was EBSD used to demonstrate the main conclusions.

Nevertheless, some interesting uses of EBSD have been found for different purposes. In many works [51], [89], [113], [130], [135], [137] where the shaping method is an AM technique, it is important to analyze the effect of the growth direction on the consolidation, grain size and grain orientation, and the mechanical properties. Thus, EBSD has been used profusely in these works. In other articles, the shaping method exhibited a special influence on the grain size and its orientation, such as shock wave compaction [114] or hot extrusion [261]. EBSD is important when a tool is needed to easily distinguish the FCC and the BCC phases with the same chemical composition [88] or when the grain size is crucial in the range of properties to be studied, as in the case in the creep mode [123] or in the ODS alloys [115]. To finish with this topic, we also mention those works where the heritage of the grain from the powder is important in the further development of the processing, which is the case when we modify the grain size and the size distribution of the original powder [121].

In alloys with high complexity in terms of alloying elements such as the HEAs, the partitioning of the different elements in the different grains/phases of the microstructure and the possible correlation with those microstructural features that affect the properties could be an interesting area of study. This information can be obtained by many techniques linked with electron microscopy and perhaps the most powerful technique, by atom probe. The use of this technique is scarce in the analyzed papers [84], [118].

9.4 Heat treatments

Heat treating monophasic or biphasic alloys, wherein phases are stable in most of the range of temperatures and the solubility does not change as a function of the phases, appears to make no sense at first glance. However, many papers have signaled that heat treatments may be promising for PM HEAs.

In [103] an AlCoCuZnNi (cluster C2) PM HEA was developed by MA and SPS. The main obtained phase was FCC after both MA and SPS. SPS was applied at different temperatures, and the formation of a minor phase with an ordered FCC structure $L1_2$ that precipitated in the main FCC phase was detected. Those precipitates change in size and shape depending on the

temperature as does the measured hardness. This $L1_2$ phase exhibited a stoichiometry close to that of $Co_9Al_6Ni_3(Cu,Zn)$. The authors explained the strengthening mechanism by comparing it with the mechanism of the γ' (Ni_3Al) phase in Ni-based superalloys that precipitate in the γ phase, which is a solid solution of Ni with the other elements. The presence of these ordered precipitates (in volume, shape, size) modifies the mechanical behavior of the superalloys at high temperature and the coherency strain between the precipitates and the matrix. There is clearly an opportunity for heat treatments of PM HEAs.

Another example can be found in [80] where the AlCoCrFeNi (cluster C1) PM HEA is made by dry mixing and SPS. After SPS, an FCC phase and two different BCC phases (one ordered and one disordered) are found in the microstructure. The microstructural configuration of these phases is a network of the FCC phase and surrounding grains containing a matrix of the ordered BCC with precipitates of the disordered BCC (see Figure 25).

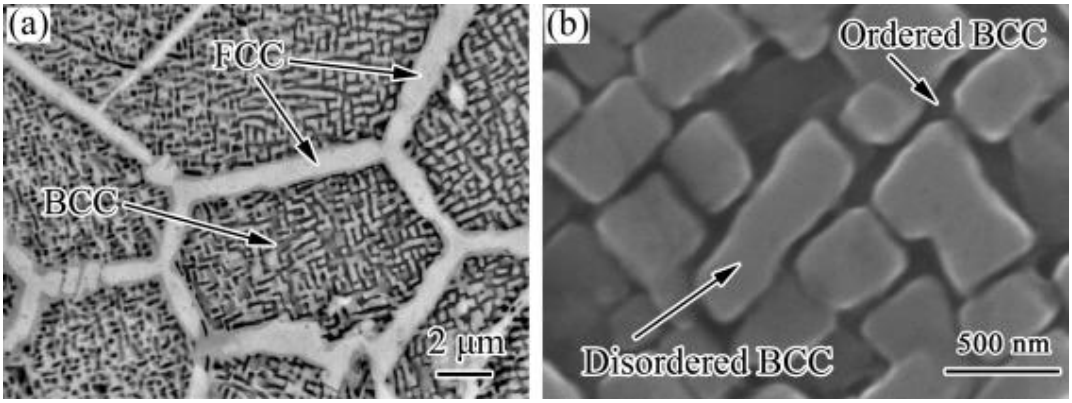

Figure 25. Microstructures of the SPSed AlCoCrFeNiHEA:(a) low-magnification back-scattered electron image (BEI), (b) high-magnification secondary electron image (SEI) of the BCC phase, from [80]

In right image of Figure 25, the microstructure is quite similar to the γ/γ' structure in Ni-based superalloys. As in the previous example, the size, distribution and morphology of these phases are temperature/time dependent, and the coherent strain between the phases is responsible for the final mechanical properties. The advantages of having a dual microstructure with BCC and FCC that could combine hardness and ductility could also be beneficial for wear applications [164]. In paragraph 6.1 was also discussed how a bimodal grain structure enhance the twin effect and the mechanical properties.

In the two previous examples, simply adjusting the temperature can substantially modify the relationship among the present phases and their influence on the microstructure and the mechanical properties. Using temperature to finely tune the microstructure is clearly a research field to be explored.

However, changes in the main phase are not the only desirable changes. In PM, many other phases can appear and disappear in HEAs; most of these phases are undesirable, but a convenient treatment could be used to improve the microstructural features and properties. Among these phases, a σ phase was observed in many compositions [58], [67], [177] among many others), as well as carbides, especially $Cr_{23}C_6$ [85], [116], [131] and intermetallics such as Al_3Ti ([81]). All of these phases can be properly treated (through heat treatments) to optimize their presence in the microstructure.

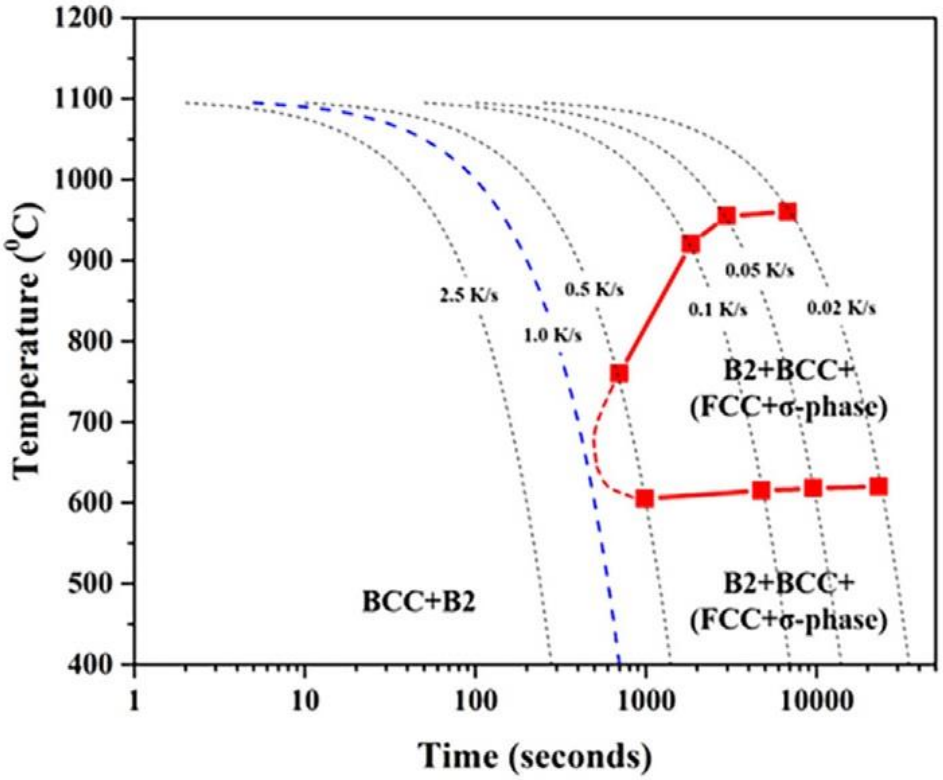

Figure 26. Cooling curve transformation diagram for $Al_{0.85}$CoCrFeNi HEA, from[65].

In this sense, a very interesting approach was demonstrated in [65]. In this work, three different PM HEAs with different Al contents (Al_xCoCrFeNi, cluster C1) were tested. The samples were manufactured from gas-atomized powders and HIP. The HIP treatment was adapted to produce different cooling rates and thus to prepare continuous cooling diagrams (Figure 26). This type of diagram enables the planning of possible heat treatments that could control the presence of the σ phase. In this work, the presence of the σ phase produced a notable loss of ductility, which could be avoided with the proper cooling rate.

"The highest strength conventional metals and alloys used at high temperatures almost always rely on the controlled distribution of a second phase" [16]. This common strategy to increase strength in most structural materials is also suitable for HEAs, and an appropriate way to follow this recommendation is heat treatment.

9.5 Mechanical properties at high temperature

The main review papers published on HEAs [5], [8], [18], [42] emphasized the potential of these alloys for high-temperature applications. Some reviews have specifically focused on the high potential of these materials for high-temperature applications [204], [205]. However, in chapter 7 of this review, a few papers are discussed that deal with tensile properties, and in particular, an unusually high number of papers discussed the behavior of PM HEAs at high temperature. To validate PM as an alternative processing route to produce HEAs, this manufacturing strategy must be shown to be competitive in the high-temperature niche. Therefore, high-temperature properties are the last topic proposed for future work. This topic has been covered less than the other topics, but it may be the most important gap in the literature to fill.

9.6 High pressure torsion.

It has been found just a recent work on this topic, and related HEAs [262]**. A HEA (CoCrFeMnNi, C3 cluster) is developed by using high pressure torsion directly form elemental powders. A high pressure of 5 GPa is used and bulk material with a very fine grain and extremely high hardness (over 6700 MPa) is obtained. Without any further heat treatment, just using pressure, a FCC+BCC structure is obtained. This work is the first one published in this field and opens another interesting field of research.**

10. Summary

This review article has covered the field of HEAs consolidated by PM. In this sense, this review focused on powder development and PM consolidation and the related properties obtained by this processing route demonstrated in papers dealing with this central matter. In addition, potential opportunities for PM to produce "different" HEAs are also discussed since PM offers some alternative routes to obtain special compositions. Moreover, PM represents an easy way to obtain some special materials (especially composites) that are difficult to obtain by conventional casting routes. This review shows that the potential of PM is vast, and the level of the obtained properties is highly competitive with HEAs obtained by ingot casting for many different fields. PMHEAs may even be more competitive with traditional materials for the HEAs in some specific applications. However, this review demonstrates that considerable work must be done to provide the market with reasons to use PM instead of other processing routes. Now that PM is established as a processing route, further research must be conducted to cover properly the topic.

11. Appendix A. Supplementary data

Supplementary data related to this article can be found at http://XXXXXXXXXXX

12. Aknowledgements.

Authors wish to thank Dr. Mario Torralba for his help in the statistical analysis developed in the section 2 of this paper.

13. References.

[1] M. Radetzki, "Seven thousand years in the service of humanity—the history of copper, the red metal," *Resour. Policy*, vol. 34, no. 4, pp. 176–184, Dec. 2009.

[2] Y.-W. Kim, "Intermetallic alloys based on gamma titanium aluminide," *JOM*, vol. 41, no. 7, pp. 24–30, Jul. 1989.

[3] B. Cantor, I. T. H. Chang, P. Knight, and A. J. B. Vincent, "Microstructural development in equiatomic multicomponent alloys," *Mater. Sci. Eng. A*, vol. 375–377, pp. 213–218, Jul. 2004.

[4] J.-W. Yeh *et al.*, "Nanostructured High-Entropy Alloys with Multiple Principal Elements: Novel Alloy Design Concepts and Outcomes," *Adv. Eng. Mater.*, vol. 6, no. 5, pp. 299–303, May 2004.

[5] D. B. Miracle and O. N. Senkov, "A critical review of high entropy alloys and related concepts," *Acta Mater.*, vol. 122, pp. 448–511, Jan. 2017.

[6] J.-W. Yeh, "Recent progress in high-entropy alloys," *Ann. Chim. Sci. des Matériaux*, vol. 31, no. 6, pp. 633–648, Dec. 2006.

[7] M.-H. Tsai and J.-W. Yeh, “High-Entropy Alloys: A Critical Review,” *Mater. Res. Lett.*, vol. 2, no. 3, pp. 107–123, 2014.
[8] Y. F. Ye, Q. Wang, J. Lu, C. T. Liu, and Y. Yang, “High-entropy alloy: challenges and prospects,” *Mater. Today*, vol. 19, no. 6, pp. 349–362, 2016.
[9] E. J. Pickering and N. G. Jones, “High-entropy alloys: a critical assessment of their founding principles and future prospects,” *Int. Mater. Rev.*, vol. 61, no. 3, pp. 183–202, 2016.
[10] B. Cantor, “Multicomponent and High Entropy Alloys,” *Entropy*, vol. 16, no. 9, pp. 4749–4768, 2014.
[11] M.-H. Tsai, “Physical Properties of High Entropy Alloys,” *Entropy*, vol. 15, no. 12, pp. 5338–5345, 2013.
[12] Y. Zhang, T. Zuo, Y. Cheng, and P. K. Liaw, “High-entropy Alloys with High Saturation Magnetization, Electrical Resistivity, and Malleability,” *Sci. Rep.*, vol. 3, p. 1455, Mar. 2013.
[13] Y. Shi, B. Yang, and P. K. Liaw, “Corrosion-Resistant High-Entropy Alloys: A Review,” *Metals (Basel).*, vol. 7, no. 2, 2017.
[14] Y. Qiu, M. A. Gibson, H. L. Fraser, and N. Birbilis, “Corrosion characteristics of high entropy alloys,” *Mater. Sci. Technol.*, vol. 31, no. 10, pp. 1235–1243, 2015.
[15] S. John Mary, R. Nagalakshmi, S. Rajendran, and R. Epshipha, “High entropy alloys and corrosion resistance. A bird’s eye view,” *Eur. Chem. Bull.*, vol. 3, no. 12, pp. 1031–1035, 2014.
[16] D. B. Miracle, J. D. Miller, O. N. Senkov, C. Woodward, M. D. Uchic, and J. Tiley, “Exploration and Development of High Entropy Alloys for Structural Applications,” *Entropy*, vol. 16, no. 1, pp. 494–525, 2014.
[17] D. B. Miracle, “Critical Assessment 14: High entropy alloys and their development as structural materials,” *Mater. Sci. Technol.*, vol. 31, no. 10, pp. 1142–1147, 2015.
[18] Y. Zhang *et al.*, “Microstructures and properties of high-entropy alloys,” *Prog. Mater. Sci.*, vol. 61, pp. 1–93, 2014.
[19] B. Gludovatz, A. Hohenwarter, D. Catoor, E. H. Chang, E. P. George, and R. O. Ritchie, “A fracture-resistant high-entropy alloy for cryogenic applications,” *Science (80-.).*, vol. 345, no. 6201, pp. 1153–1158, 2014.
[20] H. Y. Diao, R. Feng, K. A. Dahmen, and P. K. Liaw, “Fundamental deformation behavior in high-entropy alloys: An overview,” *Curr. Opin. Solid State Mater. Sci.*, vol. 21, no. 5, pp. 252–266, Oct. 2017.
[21] W. Li, P. K. Liaw, and Y. Gao, “Fracture resistance of high entropy alloys: A review,” *Intermetallics*, vol. 99, pp. 69–83, 2018.
[22] B. S. Murty, J. W. Yeh, and S. Ranganathan, *High-Entropy Alloys*. Elsevier Science, 2014.
[23] M. C. Gao, J.-W. Yeh, P. K. Liaw, and Y. Zhang, Eds., *High-Entropy Alloys*. Cham: Springer International Publishing, 2016.
[24] S. Varalakshmi, M. Kamaraj, and B. S. Murty, “Synthesis and characterization of nanocrystalline AlFeTiCrZnCu high entropy solid solution by mechanical alloying,” *J. Alloys Compd.*, vol. 460, no. 1, pp. 253–257, 2008.
[25] K. B. Zhang *et al.*, “Nanocrystalline CoCrFeNiCuAl high-entropy solid solution synthesized by mechanical alloying,” *Journal of Alloys and Compounds*, vol. 485, no. 1. pp. L31–L34, 2009.
[26] Y.-L. Chen *et al.*, “Alloying behavior of binary to octonary alloys based on Cu–Ni–Al–Co–Cr–Fe–Ti–Mo during mechanical alloying,” *J. Alloys Compd.*, vol. 477, no. 1–2, pp. 696–705, May 2009.
[27] C. C. Koch, “Nanocrystalline high-entropy alloys,” *J. Mater. Res.*, vol. 32, no. 18, pp. 3435–3444, 2017.
[28] A. Kumar and M. Gupta, “An Insight into Evolution of Light Weight High Entropy Alloys: A Review,” *Metals (Basel).*, vol. 6, no. 9, 2016.

[29] O. N. Senkov, G. B. Wilks, D. B. Miracle, C. P. Chuang, and P. K. Liaw, “Refractory high-entropy alloys,” *Intermetallics*, vol. 18, no. 9, pp. 1758–1765, Sep. 2010.
[30] J.-W. Yeh, “Alloy Design Strategies and Future Trends in High-Entropy Alloys,” *JOM*, vol. 65, no. 12, pp. 1759–1771, 2013.
[31] G. W. Milligan and M. C. Cooper, “A Study of the Comparability of External Criteria for Hierarchical Cluster Analysis,” *Multivariate Behav. Res.*, vol. 21, no. 4, pp. 441–458, 1986.
[32] X.-W. Qiu, “Microstructure and properties of AlCrFeNiCoCu high entropy alloy prepared by powder metallurgy,” *J. Alloys Compd.*, vol. 555, pp. 246–249, Apr. 2013.
[33] F. Yuhu, Z. Yunpeng, G. Hongyan, S. Huimin, and H. Li, “AlNiCrFexMo0.2CoCu High Entropy Alloys Prepared by Powder Metallurgy,” *Rare Met. Mater. Eng.*, vol. 42, no. 6, pp. 1127–1129, Jun. 2013.
[34] S. Fang, W. Chen, and Z. Fu, “Microstructure and mechanical properties of twinned Al0.5CrFeNiCo0.3C0.2 high entropy alloy processed by mechanical alloying and spark plasma sintering,” *Mater. Des.*, vol. 54, pp. 973–979, 2014.
[35] C. S. babu, K. Sivaprasad, V. Muthupandi, and J. A. Szpunar, “Characterization of Nanocrystalline AlCoCrCuNiFeZn High Entropy Alloy Produced by Mechanical Alloying,” *Procedia Mater. Sci.*, vol. 5, pp. 1020–1026, Jan. 2014.
[36] Z. Fu, W. Chen, Z. Chen, H. Wen, and E. J. Lavernia, “Influence of Ti addition and sintering method on microstructure and mechanical behavior of a medium-entropy Al0.6CoNiFe alloy,” *Mater. Sci. Eng. A*, vol. 619, pp. 137–145, Dec. 2014.
[37] H. Zhang, Y. Pan, Y. He, and H. Jiao, “Microstructure and properties of 6FeNiCoSiCrAlTi high-entropy alloy coating prepared by laser cladding,” *Appl. Surf. Sci.*, vol. 257, no. 6, pp. 2259–2263, 2011.
[38] Y. Shaofeng, Z. Yan, C. Jialin, Z. Chen, and C. Weiping, “Microstructure and Properties of Al0.4FeCrNiCo1.5Ti0.3 High Entropy Alloy Prepared by MA-HP Technique,” *Rare Met. Mater. Eng.*, vol. 43, no. 12, pp. 2948–2952, Dec. 2014.
[39] W. Ji *et al.*, “Mechanical alloying synthesis and spark plasma sintering consolidation of CoCrFeNiAl high-entropy alloy,” *J. Alloys Compd.*, vol. 589, pp. 61–66, 2014.
[40] G. Zhu, Y. Liu, and J. Ye, “Fabrication and properties of Ti(C,N)-based cermets with multi-component AlCoCrFeNi high-entropy alloys binder,” *Mater. Lett.*, vol. 113, pp. 80–82, Dec. 2013.
[41] Z. Chen, W. Chen, B. Wu, X. Cao, L. Liu, and Z. Fu, “Effects of Co and Ti on microstructure and mechanical behavior of Al0.75FeNiCrCo high entropy alloy prepared by mechanical alloying and spark plasma sintering,” *Mater. Sci. Eng. A*, vol. 648, pp. 217–224, 2015.
[42] Y.-L. Chen, Y.-H. Hu, C.-W. Tsai, J.-W. Yeh, S.-K. Chen, and S.-Y. Chang, “Structural evolution during mechanical milling and subsequent annealing of Cu–Ni–Al–Co–Cr–Fe–Ti alloys,” *Mater. Chem. Phys.*, vol. 118, no. 2–3, pp. 354–361, Dec. 2009.
[43] F. J. Baldenebro-Lopez, J. M. Herrera-Ramírez, S. P. Arredondo-Rea, C. D. Gómez-Esparza, and R. Martínez-Sánchez, “Simultaneous effect of mechanical alloying and arc-melting processes in the microstructure and hardness of an AlCoFeMoNiTi high-entropy alloy,” *J. Alloys Compd.*, vol. 643, pp. S250–S255, 2015.
[44] R. Sriharitha, B. S. Murty, and R. S. Kottada, “Phase formation in mechanically alloyed AlxCoCrCuFeNi (x = 0.45, 1, 2.5, 5 mol) high entropy alloys,” *Intermetallics*, vol. 32, pp. 119–126, 2013.
[45] Z. Fu, W. Chen, H. Wen, Z. Chen, and E. J. Lavernia, “Effects of Co and sintering method on microstructure and mechanical behavior of a high-entropy Al0.6NiFeCrCo alloy prepared by powder metallurgy,” *J. Alloys Compd.*, vol. 646, pp. 175–182, Oct. 2015.
[46] W. Chen, Z. Fu, S. Fang, Y. Wang, H. Xiao, and D. Zhu, “Processing, microstructure and properties of Al0.6CoNiFeTi0.4 high entropy alloy with nanoscale twins,” *Mater. Sci. Eng. A*, vol. 565, pp. 439–444, Mar. 2013.

[47] G. Zhu, Y. Liu, and J. Ye, “Early high-temperature oxidation behavior of Ti(C,N)-based cermets with multi-component AlCoCrFeNi high-entropy alloy binder,” *Int. J. Refract. Met. Hard Mater.*, vol. 44, pp. 35–41, 2014.
[48] W. Ji *et al.*, “Fabrication and properties of TiB2-based cermets by spark plasma sintering with CoCrFeNiTiAl high-entropy alloy as sintering aid,” *J. Eur. Ceram. Soc.*, vol. 35, no. 3, pp. 879–886, Mar. 2015.
[49] P. Veronesi, R. Rosa, E. Colombini, and C. Leonelli, “Microwave-Assisted Preparation of High Entropy Alloys,” *Technologies*, vol. 3, no. 4, pp. 182–197, Oct. 2015.
[50] Z. Fu *et al.*, “Microstructure and strengthening mechanisms in an FCC structured single-phase nanocrystalline Co25Ni25Fe25Al7.5Cu17.5 high-entropy alloy,” *Acta Mater.*, vol. 107, pp. 59–71, Apr. 2016.
[51] H. Shiratori *et al.*, “Relationship between the microstructure and mechanical properties of an equiatomic AlCoCrFeNi high-entropy alloy fabricated by selective electron beam melting,” *Mater. Sci. Eng. A*, vol. 656, pp. 39–46, 2016.
[52] X. Qiu, C. Huang, M. Wu, C. Liu, and Y. Zhang, “Structure and properties of AlCrFeNiCuTi six principal elements equimolar alloy,” *J. Alloys Compd.*, vol. 658, pp. 1–5, Feb. 2016.
[53] K. B. Zhang *et al.*, “Microstructure and mechanical properties of CoCrFeNiTiAlx high-entropy alloys,” *Mater. Sci. Eng. A*, vol. 508, no. 1–2, pp. 214–219, May 2009.
[54] A. Raphel, S. Kumaran, K. V. Kumar, and L. Varghese, “Oxidation and Corrosion resistance of AlCoCrFeTiHigh Entropy Alloy,” *Mater. Today Proc.*, vol. 4, no. 2, pp. 195–202, Jan. 2017.
[55] P. Wang, X. Cheng, H. Cai, Y. Xue, and Y. Zhang, “Influence of increasing Al concentration on phase, microstructure and mechanical behaviors of Ni1.5CoFeCu1−xAlxV0.5 high entropy alloys,” *Mater. Sci. Eng. A*, vol. 708, pp. 523–536, Dec. 2017.
[56] H. Prasad, S. Singh, and B. B. Panigrahi, “Mechanical activated synthesis of alumina dispersed FeNiCoCrAlMn high entropy alloy,” *J. Alloys Compd.*, vol. 692, pp. 720–726, 2017.
[57] J. Li, W. Craeghs, C. Jing, S. Gong, and F. Shan, “Microstructure and physical performance of laser-induction nanocrystals modified high-entropy alloy composites on titanium alloy,” *Mater. Des.*, vol. 117, pp. 363–370, Mar. 2017.
[58] S. Mohanty *et al.*, “Powder metallurgical processing of equiatomic AlCoCrFeNi high entropy alloy: Microstructure and mechanical properties,” *Mater. Sci. Eng. A*, vol. 679, pp. 299–313, Jan. 2017.
[59] C.-C. Yang, J. L. Hang Chau, C.-J. Weng, C.-S. Chen, and Y.-H. Chou, “Preparation of high-entropy AlCoCrCuFeNiSi alloy powders by gas atomization process,” *Mater. Chem. Phys.*, vol. 202, pp. 151–158, Dec. 2017.
[60] R. S. Ganji, P. Sai Karthik, K. Bhanu Sankara Rao, and K. V. Rajulapati, “Strengthening mechanisms in equiatomic ultrafine grained AlCoCrCuFeNi high-entropy alloy studied by micro- and nanoindentation methods,” *Acta Mater.*, vol. 125, pp. 58–68, Feb. 2017.
[61] S. Riva, A. Tudball, S. Mehraban, N. P. Lavery, S. G. R. Brown, and K. V. Yusenko, “A novel High-Entropy Alloy-based composite material,” *J. Alloys Compd.*, vol. 730, pp. 544–551, Jan. 2018.
[62] S. Yang, J. Pi, W. Yang, H. Zhou, and D. Zhu, “Deformation twinning structure and interface in a FCC-based Al0.3FeNiCo1.2CrCu high-entropy alloy matrix composites,” *Mater. Lett.*, vol. 214, pp. 50–52, Mar. 2018.
[63] S. Yang, X. Yan, K. Yang, and Z. Fu, “Effect of the addition of nano-Al2O3 on the microstructure and mechanical properties of twinned Al0.4FeCrCoNi1.2Ti0.3 alloys,” *Vacuum*, vol. 131, pp. 69–72, Sep. 2016.
[64] K. B. Zhang, Z. Y. Fu, J. Y. Zhang, W. M. Wang, S. W. Lee, and K. Niihara, “Characterization of nanocrystalline CoCrFeNiTiAl high-entropy solid solution processed by mechanical alloying,” *J. Alloys Compd.*, vol. 495, no. 1, pp. 33–38, 2010.

[65] J. Joseph, P. Hodgson, T. Jarvis, X. Wu, N. Stanford, and D. M. Fabijanic, “Effect of hot isostatic pressing on the microstructure and mechanical properties of additive manufactured AlxCoCrFeNi high entropy alloys,” *Mater. Sci. Eng. A*, vol. 733, pp. 59–70, Aug. 2018.

[66] W. Luo, Y. Liu, Y. Luo, and M. Wu, “Fabrication and characterization of WC-AlCoCrCuFeNi high-entropy alloy composites by spark plasma sintering,” *J. Alloys Compd.*, vol. 754, pp. 163–170, Jul. 2018.

[67] A. Erdogan, T. Yener, and S. Zeytin, “Fast production of high entropy alloys (CoCrFeNiAlxTiy) by electric current activated sintering system,” *Vacuum*, vol. 155, pp. 64–72, Sep. 2018.

[68] P. L. Zhou, D. H. Xiao, P. F. Zhou, and T. C. Yuan, “Microstructure and properties of ultrafine grained AlCrFeCoNi/WC cemented carbides,” *Ceram. Int.*, Jun. 2018.

[69] E. Colombini, R. Rosa, L. Trombi, M. Zadra, A. Casagrande, and P. Veronesi, “High entropy alloys obtained by field assisted powder metallurgy route: SPS and microwave heating,” *Mater. Chem. Phys.*, vol. 210, pp. 78–86, May 2018.

[70] K. V. Yusenko *et al.*, “High-pressure high-temperature tailoring of High Entropy Alloys for extreme environments,” *J. Alloys Compd.*, vol. 738, pp. 491–500, Mar. 2018.

[71] C. Wang, W. Ji, and Z. Fu, “Mechanical alloying and spark plasma sintering of CoCrFeNiMnAl high-entropy alloy,” *Adv. Powder Technol.*, vol. 25, no. 4, pp. 1334–1338, 2014.

[72] R. Sriharitha, B. S. Murty, and R. S. Kottada, “Alloying, thermal stability and strengthening in spark plasma sintered AlxCoCrCuFeNi high entropy alloys,” *J. Alloys Compd.*, vol. 583, pp. 419–426, 2014.

[73] I. Kunce, M. Polanski, K. Karczewski, T. Plocinski, and K. J. Kurzydlowski, “Microstructural characterisation of high-entropy alloy AlCoCrFeNi fabricated by laser engineered net shaping,” *J. Alloys Compd.*, vol. 648, pp. 751–758, Nov. 2015.

[74] C. D. Gómez-Esparza *et al.*, “Series of Nanocrystalline NiCoAlFe(Cr, Cu, Mo, Ti) High-Entropy Alloys produced by Mechanical Alloying,” *Mater. Res.*, vol. 19, no. suppl 1, pp. 39–46, Aug. 2016.

[75] C. D. Gómez-Esparza *et al.*, “Microstructure of NiCoAlFeCuCr multi-component systems synthesized by mechanical alloying,” *J. Alloys Compd.*, vol. 509, pp. S279–S283, Jun. 2011.

[76] J. Chen *et al.*, “Fabrication and mechanical properties of AlCoNiCrFe high-entropy alloy particle reinforced Cu matrix composites,” *J. Alloys Compd.*, vol. 649, pp. 630–634, 2015.

[77] Y. Brif, M. Thomas, and I. Todd, “The use of high-entropy alloys in additive manufacturing,” *Scr. Mater.*, vol. 99, pp. 93–96, Apr. 2015.

[78] T. Fujieda *et al.*, “First demonstration of promising selective electron beam melting method for utilizing high-entropy alloys as engineering materials,” *Mater. Lett.*, vol. 159, pp. 12–15, 2015.

[79] J. Joseph, T. Jarvis, X. Wu, N. Stanford, P. Hodgson, and D. M. Fabijanic, “Comparative study of the microstructures and mechanical properties of direct laser fabricated and arc-melted AlxCoCrFeNi high entropy alloys,” *Mater. Sci. Eng. A*, vol. 633, pp. 184–193, 2015.

[80] A. Zhang, J. Han, J. Meng, B. Su, and P. Li, “Rapid preparation of AlCoCrFeNi high entropy alloy by spark plasma sintering from elemental powder mixture,” 2016.

[81] Z. Tan, L. Wang, Y. Xue, P. Zhang, T. Cao, and X. Cheng, “High-entropy alloy particle reinforced Al-based amorphous alloy composite with ultrahigh strength prepared by spark plasma sintering,” *Mater. Des.*, vol. 109, pp. 219–226, Nov. 2016.

[82] J. Joseph, N. Stanford, P. Hodgson, and D. M. Fabijanic, “Tension/compression asymmetry in additive manufactured face centered cubic high entropy alloy,” *Scr. Mater.*, vol. 129, pp. 30–34, Mar. 2017.

[83] P. Veronesi, E. Colombini, R. Rosa, C. Leonelli, and M. Garuti, “Microwave processing of high entropy alloys: A powder metallurgy approach,” *Chem. Eng. Process. Process Intensif.*, vol. 122, pp. 397–403, Dec. 2017.
[84] R. Wang, K. Zhang, C. Davies, and X. Wu, “Evolution of microstructure, mechanical and corrosion properties of AlCoCrFeNi high-entropy alloy prepared by direct laser fabrication,” *J. Alloys Compd.*, vol. 694, pp. 971–981, 2017.
[85] S. Nam, M. J. Kim, J. Y. Hwang, and H. Choi, “Strengthening of Al0.15CoCrCuFeNiTix–C (x = 0, 1, 2) high-entropy alloys by grain refinement and using nanoscale carbides via powder metallurgical route,” *J. Alloys Compd.*, vol. 762, pp. 29–37, Sep. 2018.
[86] S. Praveen, B. S. Murty, and R. S. Kottada, “Alloying behavior in multi-component AlCoCrCuFe and NiCoCrCuFe high entropy alloys,” *Mater. Sci. Eng. A*, vol. 534, pp. 83–89, 2012.
[87] T. Lu *et al.*, “The influence of nanocrystalline CoNiFeAl0.4Ti0.6Cr0.5 high-entropy alloy particles addition on microstructure and mechanical properties of SiCp/7075Al composites,” *Mater. Sci. Eng. A*, vol. 726, pp. 126–136, 2018.
[88] R. M. Pohan *et al.*, “Microstructures and mechanical properties of mechanically alloyed and spark plasma sintered Al0.3CoCrFeMnNi high entropy alloy,” *Mater. Chem. Phys.*, vol. 210, pp. 62–70, May 2018.
[89] K. Kuwabara, H. Shiratori, T. Fujieda, K. Yamanaka, Y. Koizumi, and A. Chiba, “Mechanical and Corrosion Properties of AlCoCrFeNi High-Entropy Alloy Fabricated with Selective Electron Beam Melting,” *Addit. Manuf.*, Jun. 2018.
[90] Z. Fu *et al.*, “Influence of Cr removal on the microstructure and mechanical behaviour of a high-entropy Al0.8Ti0.2CoNiFeCr alloy fabricated by powder metallurgy,” *Powder Metall.*, vol. 61, no. 2, pp. 106–114, 2018.
[91] E. Colombini *et al.*, “SPS-assisted Synthesis of SICp reinforced high entropy alloys: reactivity of SIC and effects of pre-mechanical alloying and post-annealing treatment,” *Powder Metall.*, vol. 61, no. 1, pp. 64–72, 2018.
[92] S. Varalakshmi, M. Kamaraj, and B. S. Murty, “Processing and properties of nanocrystalline CuNiCoZnAlTi high entropy alloys by mechanical alloying,” *Mater. Sci. Eng. A*, vol. 527, no. 4, pp. 1027–1030, Feb. 2010.
[93] Y.-L. Chen, Y.-H. Hu, C.-A. Hsieh, J.-W. Yeh, and S.-K. Chen, “Competition between elements during mechanical alloying in an octonary multi-principal-element alloy system,” *J. Alloys Compd.*, vol. 481, no. 1–2, pp. 768–775, Jul. 2009.
[94] S. Varalakshmi, M. Kamaraj, and B. S. Murty, “Formation and Stability of Equiatomic and Nonequiatomic Nanocrystalline CuNiCoZnAlTi High-Entropy Alloys by Mechanical Alloying,” *Metall. Mater. Trans. A*, vol. 41, no. 10, pp. 2703–2709, Oct. 2010.
[95] Z. Fu *et al.*, “Microstructure and mechanical behavior of a novel Co20Ni20Fe20Al20Ti20 alloy fabricated by mechanical alloying and spark plasma sintering,” *Mater. Sci. Eng. A*, vol. 644, pp. 10–16, 2015.
[96] P. Wang, H. Cai, and X. Cheng, “Effect of Ni/Cr ratio on phase, microstructure and mechanical properties of NixCoCuFeCr2−x (x = 1.0, 1.2, 1.5, 1.8 mol) high entropy alloys,” *J. Alloys Compd.*, vol. 662, pp. 20–31, Mar. 2016.
[97] N. H. Tariq, M. Naeem, B. A. Hasan, J. I. Akhter, and M. Siddique, “Effect of W and Zr on structural, thermal and magnetic properties of AlCoCrCuFeNi high entropy alloy,” *J. Alloys Compd.*, vol. 556, pp. 79–85, Apr. 2013.
[98] S. Yang, Y. Zhang, X. Yan, H. Zhou, J. Pi, and D. Zhu, “Deformation twins and interface characteristics of nano-Al2O3 reinforced Al0.4FeCrCo1.5NiTi0.3 high entropy alloy composites,” *Mater. Chem. Phys.*, vol. 210, pp. 240–244, May 2018.
[99] W. Chen, Z. Fu, S. Fang, H. Xiao, and D. Zhu, “Alloying behavior, microstructure and mechanical properties in a FeNiCrCo0.3Al0.7 high entropy alloy,” *Mater. Des.*, vol. 51, pp. 854–860, Oct. 2013.
[100] Z. Fu, W. Chen, S. Fang, D. Zhang, H. Xiao, and D. Zhu, “Alloying behavior and

deformation twinning in a CoNiFeCrAl0.6Ti0.4 high entropy alloy processed by spark plasma sintering," *J. Alloys Compd.*, vol. 553, pp. 316–323, Mar. 2013.
[101] S. Varalakshmi, G. Appa Rao, M. Kamaraj, and B. S. Murty, "Hot consolidation and mechanical properties of nanocrystalline equiatomic AlFeTiCrZnCu high entropy alloy after mechanical alloying," *J. Mater. Sci.*, vol. 45, no. 19, pp. 5158–5163, Oct. 2010.
[102] W. Ge *et al.*, "Characterization and properties of CuZrAlTiNi high entropy alloy coating obtained by mechanical alloying and vacuum hot pressing sintering," *Adv. Powder Technol.*, vol. 28, no. 10, pp. 2556–2563, Oct. 2017.
[103] S. Mohanty, N. P. Gurao, and K. Biswas, "Sinter ageing of equiatomic Al20Co20Cu20Zn20Ni20 high entropy alloy via mechanical alloying," *Mater. Sci. Eng. A*, vol. 617, pp. 211–218, 2014.
[104] W. Ge, Y. Wang, C. Shang, Z. Zhang, and Y. Wang, "Microstructures and properties of equiatomic CuZr and CuZrAlTiNi bulk alloys fabricated by mechanical alloying and spark plasma sintering," *J. Mater. Sci.*, vol. 52, no. 10, pp. 5726–5737, May 2017.
[105] W. Ji *et al.*, "Alloying behavior and novel properties of CoCrFeNiMn high-entropy alloy fabricated by mechanical alloying and spark plasma sintering," *Intermetallics*, vol. 56, pp. 24–27, Jan. 2015.
[106] P. F. Yu *et al.*, "The high-entropy alloys with high hardness and soft magnetic property prepared by mechanical alloying and high-pressure sintering," *Intermetallics*, vol. 70, pp. 82–87, 2016.
[107] B. Wang *et al.*, "Mechanical Properties and Microstructure of the CoCrFeMnNi High Entropy Alloy Under High Strain Rate Compression," *J. Mater. Eng. Perform.*, vol. 25, no. 7, pp. 2985–2992, Jul. 2016.
[108] B. Liu *et al.*, "Microstructure and mechanical properties of equimolar FeCoCrNi high entropy alloy prepared via powder extrusion," *Intermetallics*, vol. 75, pp. 25–30, 2016.
[109] J. Wang *et al.*, "Flow behavior and microstructures of powder metallurgical CrFeCoNiMo0.2 high entropy alloy during high temperature deformation," *Mater. Sci. Eng. A*, vol. 689, pp. 233–242, Mar. 2017.
[110] Ł. Rogal, D. Kalita, and L. Litynska-Dobrzynska, "CoCrFeMnNi high entropy alloy matrix nanocomposite with addition of Al2O3," *Intermetallics*, vol. 86, pp. 104–109, 2017.
[111] N. Eißmann, B. Klöden, T. Weißgärber, and B. Kieback, "High-entropy alloy CoCrFeMnNi produced by powder metallurgy," *Powder Metall.*, vol. 60, no. 3, pp. 184–197, 2017.
[112] C. Shang *et al.*, "CoCrFeNi(W1−xMox) high-entropy alloy coatings with excellent mechanical properties and corrosion resistance prepared by mechanical alloying and hot pressing sintering," *Mater. Des.*, vol. 117, pp. 193–202, Mar. 2017.
[113] C. Haase, F. Tang, M. B. Wilms, A. Weisheit, and B. Hallstedt, "Combining thermodynamic modeling and 3D printing of elemental powder blends for high-throughput investigation of high-entropy alloys – Towards rapid alloy screening and design," *Mater. Sci. Eng. A*, vol. 688, pp. 180–189, 2017.
[114] D. Yim *et al.*, "Shock wave compaction and sintering of mechanically alloyed CoCrFeMnNi high-entropy alloy powders," *Mater. Sci. Eng. A*, vol. 708, pp. 291–300, Dec. 2017.
[115] H. Hadraba *et al.*, "Oxide dispersion strengthened CoCrFeNiMn high-entropy alloy," *Mater. Sci. Eng. A*, vol. 689, pp. 252–256, Mar. 2017.
[116] Ł. Rogal, D. Kalita, A. Tarasek, P. Bobrowski, and F. Czerwinski, "Effect of SiC nano-particles on microstructure and mechanical properties of the CoCrFeMnNi high entropy alloy," *J. Alloys Compd.*, vol. 708, pp. 344–352, 2017.
[117] Y. Liu, J. Wang, Q. Fang, B. Liu, Y. Wu, and S. Chen, "Preparation of superfine-grained high entropy alloy by spark plasma sintering gas atomized powder," *Intermetallics*, vol. 68, pp. 16–22, 2016.
[118] P. Sathiyamoorthi, J. Basu, S. Kashyap, K. G. Pradeep, and R. S. Kottada, "Thermal stability and grain boundary strengthening in ultrafine-grained CoCrFeNi high entropy

alloy composite," *Mater. Des.*, vol. 134, pp. 426–433, Nov. 2017.
[119] C. Sun, P. Li, S. Xi, Y. Zhou, S. Li, and X. Yang, "A new type of high entropy alloy composite Fe18Ni23Co25Cr21Mo8WNb3C2 prepared by mechanical alloying and hot pressing sintering," *Mater. Sci. Eng. A*, vol. 728, pp. 144–150, 2018.
[120] A. Zhang, J. Han, B. Su, and J. Meng, "A promising new high temperature self-lubricating material: CoCrFeNiS0.5 high entropy alloy," *Mater. Sci. Eng. A*, vol. 731, pp. 36–43, 2018.
[121] D. Yim *et al.*, "Compaction behavior of water-atomized CoCrFeMnNi high-entropy alloy powders," *Mater. Chem. Phys.*, vol. 210, pp. 95–102, May 2018.
[122] S. Praveen, J. Basu, S. Kashyap, and R. S. Kottada, "Exceptional resistance to grain growth in nanocrystalline CoCrFeNi high entropy alloy at high homologous temperatures," *J. Alloys Compd.*, vol. 662, pp. 361–367, Mar. 2016.
[123] F. Dobeš, H. Hadraba, Z. Chlup, A. Dlouhý, M. Vilémová, and J. Matějíček, "Compressive creep behavior of an oxide-dispersion-strengthened CoCrFeMnNi high-entropy alloy," *Mater. Sci. Eng. A*, vol. 732, pp. 99–104, 2018.
[124] R. B. Mane and B. B. Panigrahi, "Effect of alloying order on non-isothermal sintering kinetics of mechanically alloyed high entropy alloy powders," *Mater. Lett.*, vol. 217, pp. 131–134, Apr. 2018.
[125] H. Cheng, W. Chen, X. Liu, Q. Tang, Y. Xie, and P. Dai, "Effect of Ti and C additions on the microstructure and mechanical properties of the FeCoCrNiMn high-entropy alloy," *Mater. Sci. Eng. A*, vol. 719, pp. 192–198, Mar. 2018.
[126] M. D. Alcalá, C. Real, I. Fombella, I. Trigo, and J. M. Córdoba, "Effects of milling time, sintering temperature, Al content on the chemical nature, microhardness and microstructure of mechanochemically synthesized FeCoNiCrMn high entropy alloy," *J. Alloys Compd.*, vol. 749, pp. 834–843, 2018.
[127] Y. Xie, H. Cheng, Q. Tang, W. Chen, W. Chen, and P. Dai, "Effects of N addition on microstructure and mechanical properties of CoCrFeNiMn high entropy alloy produced by mechanical alloying and vacuum hot pressing sintering," *Intermetallics*, vol. 93, pp. 228–234, Feb. 2018.
[128] A. Zhang, J. Han, B. Su, P. Li, and J. Meng, "Microstructure, mechanical properties and tribological performance of CoCrFeNi high entropy alloy matrix self-lubricating composite," *Mater. Des.*, vol. 114, pp. 253–263, 2017.
[129] I. L. Velo, F. J. Gotor, M. D. Alcalá, C. Real, and J. M. Córdoba, "Fabrication and characterization of WC-HEA cemented carbide based on the CoCrFeNiMn high entropy alloy," *J. Alloys Compd.*, vol. 746, pp. 1–8, 2018.
[130] Z. G. Zhu *et al.*, "Hierarchical microstructure and strengthening mechanisms of a CoCrFeNiMn high entropy alloy additively manufactured by selective laser melting," *Scr. Mater.*, vol. 154, pp. 20–24, Sep. 2018.
[131] R. Zhou, G. Chen, B. Liu, J. Wang, L. Han, and Y. Liu, "Microstructures and wear behaviour of (FeCoCrNi)1-x(WC)x high entropy alloy composites," *Int. J. Refract. Met. Hard Mater.*, vol. 75, pp. 56–62, Sep. 2018.
[132] Z. Szklarz, J. Lekki, P. Bobrowski, M. B. Szklarz, and Ł. Rogal, "The effect of SiC nanoparticles addition on the electrochemical response of mechanically alloyed CoCrFeMnNi high entropy alloy," *Mater. Chem. Phys.*, vol. 215, pp. 385–392, Aug. 2018.
[133] B. Wang, X. Huang, A. Fu, Y. Liu, and B. Liu, "Serration behavior and microstructure of high entropy alloy CoCrFeMnNi prepared by powder metallurgy," *Mater. Sci. Eng. A*, vol. 726, pp. 37–44, May 2018.
[134] R. Zhou *et al.*, "Microstructures and mechanical properties of C-containing FeCoCrNi high-entropy alloy fabricated by selective laser melting," *Intermetallics*, vol. 94, pp. 165–171, 2018.
[135] R. Li, P. Niu, T. Yuan, P. Cao, C. Chen, and K. Zhou, "Selective laser melting of an equiatomic CoCrFeMnNi high-entropy alloy: Processability, non-equilibrium

microstructure and mechanical property," *J. Alloys Compd.*, vol. 746, pp. 125–134, 2018.
[136] J. Guo, M. Goh, Z. Zhu, X. Lee, M. L. S. Nai, and J. Wei, "On the machining of selective laser melting CoCrFeMnNi high-entropy alloy," *Mater. Des.*, vol. 153, pp. 211–220, 2018.
[137] A. Piglione, B. Dovgyy, C. Liu, C. M. Gourlay, P. A. Hooper, and M. S. Pham, "Printability and microstructure of the CoCrFeMnNi high-entropy alloy fabricated by laser powder bed fusion," *Mater. Lett.*, vol. 224, pp. 22–25, Aug. 2018.
[138] M. Zhang, W. Zhang, Y. Liu, B. Liu, and J. Wang, "FeCoCrNiMo high-entropy alloys prepared by powder metallurgy processing for diamond tool applications," *Powder Metall.*, vol. 61, no. 2, pp. 123–130, 2018.
[139] S.-H. Joo *et al.*, "Structure and properties of ultrafine-grained CoCrFeMnNi high-entropy alloys produced by mechanical alloying and spark plasma sintering," *J. Alloys Compd.*, vol. 698, pp. 591–604, Mar. 2017.
[140] Q. Yang, Y. Tang, Y. Wen, Q. Zhang, D. Deng, and X. Nai, "Microstructures and properties of CoCrCuFeNiMox high-entropy alloys fabricated by mechanical alloying and spark plasma sintering," *Powder Metall.*, vol. 61, no. 2, pp. 115–122, 2018.
[141] R. B. Mane, R. Y., and B. B. Panigrahi, "Sintering mechanism of CoCrFeMnNi high-entropy alloy powders," *Powder Metall.*, vol. 61, no. 2, pp. 131–138, 2018.
[142] S. Praveen, B. S. Murty, and R. S. Kottada, "Phase Evolution and Densification Behavior of Nanocrystalline Multicomponent High Entropy Alloys During Spark Plasma Sintering," *JOM*, vol. 65, no. 12, pp. 1797–1804, 2013.
[143] Z.-W. He, M.-Z. Wang, X.-L. Hao, Q. Zou, and Y.-C. Zhao, "Novel cemented carbide produced with TiN0.3 and high-entropy alloys," *Rare Met.*, vol. 36, no. 6, pp. 494–500, Jun. 2017.
[144] S. Praveen, A. Anupam, R. Tilak, and R. S. Kottada, "Phase evolution and thermal stability of AlCoCrFe high entropy alloy with carbon as unsolicited addition from milling media," *Mater. Chem. Phys.*, vol. 210, pp. 57–61, 2018.
[145] Z. Qiu, C. Yao, K. Feng, Z. Li, and P. K. Chu, "Cryogenic deformation mechanism of CrMnFeCoNi high-entropy alloy fabricated by laser additive manufacturing process," *Int. J. Light. Mater. Manuf.*, vol. 1, no. 1, pp. 33–39, Mar. 2018.
[146] A. G. de la Obra, M. A. Avilés, Y. Torres, E. Chicardi, and F. J. Gotor, "A new family of cermets: Chemically complex but microstructurally simple," *Int. J. Refract. Met. Hard Mater.*, vol. 63, pp. 17–25, Feb. 2017.
[147] W. H. Liu *et al.*, "Ductile CoCrFeNiMox high entropy alloys strengthened by hard intermetallic phases," *Acta Mater.*, vol. 116, pp. 332–342, Sep. 2016.
[148] B. Wu, W. Chen, Z. Jiang, Z. Chen, and Z. Fu, "Influence of Ti addition on microstructure and mechanical behavior of a FCC-based Fe30Ni30Co30Mn10 alloy," *Mater. Sci. Eng. A*, vol. 676, pp. 492–500, Oct. 2016.
[149] Z. Fu, W. Chen, H. Xiao, L. Zhou, D. Zhu, and S. Yang, "Fabrication and properties of nanocrystalline Co0.5FeNiCrTi0.5 high entropy alloy by MA–SPS technique," *Mater. Des.*, vol. 44, pp. 535–539, Feb. 2013.
[150] C.-M. Lin, C.-W. Tsai, S.-M. Huang, C.-C. Yang, and J.-W. Yeh, "New TiC/Co1.5CrFeNi1.5Ti0.5 Cermet with Slow TiC Coarsening During Sintering," *JOM*, vol. 66, no. 10, pp. 2050–2056, Oct. 2014.
[151] I. Kunce, M. Polanski, and J. Bystrzycki, "Structure and hydrogen storage properties of a high entropy ZrTiVCrFeNi alloy synthesized using Laser Engineered Net Shaping (LENS)," *Int. J. Hydrogen Energy*, vol. 38, no. 27, pp. 12180–12189, 2013.
[152] I. Moravcik *et al.*, "Microstructure and mechanical properties of Ni1,5Co1,5CrFeTi0,5 high entropy alloy fabricated by mechanical alloying and spark plasma sintering," *Mater. Des.*, vol. 119, pp. 141–150, Apr. 2017.
[153] Z. Cai, G. Jin, X. Cui, Y. Li, Y. Fan, and J. Song, "Experimental and simulated data about

microstructure and phase composition of a NiCrCoTiV high-entropy alloy prepared by vacuum hot-pressing sintering," *Vacuum*, vol. 124, pp. 5–10, Feb. 2016.
[154] B. Liu, J. Wang, J. Chen, Q. Fang, and Y. Liu, "Ultra-High Strength TiC/Refractory High-Entropy-Alloy Composite Prepared by Powder Metallurgy," *JOM*, vol. 69, no. 4, pp. 651–656, Apr. 2017.
[155] G. Zepon *et al.*, "Hydrogen-induced phase transition of MgZrTiFe0.5Co0.5Ni0.5 high entropy alloy," *Int. J. Hydrogen Energy*, vol. 43, no. 3, pp. 1702–1708, Jan. 2018.
[156] Z. Fu *et al.*, "Fcc nanostructured TiFeCoNi alloy with multi-scale grains and enhanced plasticity," *Scr. Mater.*, vol. 143, pp. 108–112, Jan. 2018.
[157] E. Holmström *et al.*, "High entropy alloys: Substituting for cobalt in cutting edge technology," *Appl. Mater. Today*, vol. 12, pp. 322–329, Sep. 2018.
[158] Z. Cai, X. Cui, Z. Liu, Y. Li, M. Dong, and G. Jin, "Microstructure and wear resistance of laser cladded Ni-Cr-Co-Ti-V high-entropy alloy coating after laser remelting processing," *Opt. Laser Technol.*, vol. 99, pp. 276–281, 2018.
[159] S. Varalakshmi, M. Kamaraj, and B. S. Murty, "Synthesis and characterization of nanocrystalline AlFeTiCrZnCu high entropy solid solution by mechanical alloying," *J. Alloys Compd.*, vol. 460, no. 1–2, pp. 253–257, Jul. 2008.
[160] E. Prieto *et al.*, "Processing of a new high entropy alloy: AlCrFeMoNiTi," *Powder Metall.*, vol. 61, no. 3, pp. 258–265, 2018.
[161] N. T. B. N. Koundinya, C. Sajith Babu, K. Sivaprasad, P. Susila, N. Kishore Babu, and J. Baburao, "Phase Evolution and Thermal Analysis of Nanocrystalline AlCrCuFeNiZn High Entropy Alloy Produced by Mechanical Alloying," *J. Mater. Eng. Perform.*, vol. 22, no. 10, pp. 3077–3084, Oct. 2013.
[162] O. Maulik, D. Kumar, S. Kumar, D. M. Fabijanic, and V. Kumar, "Structural evolution of spark plasma sintered AlFeCuCrMgx (x = 0, 0.5, 1, 1.7) high entropy alloys," *Intermetallics*, vol. 77, pp. 46–56, 2016.
[163] S. Mridha, S. Samal, P. Y. Khan, K. Biswas, and Govind, "Processing and Consolidation of Nanocrystalline Cu-Zn-Ti-Fe-Cr High-Entropy Alloys via Mechanical Alloying," *Metall. Mater. Trans. A*, vol. 44, no. 10, pp. 4532–4541, Oct. 2013.
[164] A. S. Sharma, S. Yadav, K. Biswas, and B. Basu, "High-entropy alloys and metallic nanocomposites: Processing challenges, microstructure development and property enhancement," *Mater. Sci. Eng. R Reports*, vol. 131, pp. 1–42, Sep. 2018.
[165] S. Yadav, A. Kumar, and K. Biswas, "Wear behavior of high entropy alloys containing soft dispersoids (Pb, Bi)," *Mater. Chem. Phys.*, vol. 210, pp. 222–232, May 2018.
[166] S. Yadav, S. Sarkar, A. Aggarwal, A. Kumar, and K. Biswas, "Wear and mechanical properties of novel (CuCrFeTiZn)100-xPbx high entropy alloy composite via mechanical alloying and spark plasma sintering," *Wear*, vol. 410, pp. 93–109, 2018.
[167] D. Kumar, O. Maulik, S. Kumar, Y. V. S. S. Prasad, and V. Kumar, "Phase and thermal study of equiatomic AlCuCrFeMnW high entropy alloy processed via spark plasma sintering," *Mater. Chem. Phys.*, vol. 210, pp. 71–77, 2018.
[168] M. Murali, S. P. K. Babu, J. Majhi, A. Vallimanalan, and R. Mahendran, "Processing and characterisation of nano crystalline AlCoCrCuFeTix high-entropy alloy," *Powder Metall.*, vol. 61, no. 2, pp. 139–148, 2018.
[169] H. Dobbelstein, M. Thiele, E. L. Gurevich, E. P. George, and A. Ostendorf, "Direct Metal Deposition of Refractory High Entropy Alloy MoNbTaW," *Phys. Procedia*, vol. 83, pp. 624–633, Jan. 2016.
[170] B. Kang, J. Lee, H. J. Ryu, and S. H. Hong, "Ultra-high strength WNbMoTaV high-entropy alloys with fine grain structure fabricated by powder metallurgical process," *Mater. Sci. Eng. A*, vol. 712, pp. 616–624, 2018.
[171] P. Wang, H. Cai, S. Zhou, and L. Xu, "Processing, microstructure and properties of Ni1.5CoCuFeCr0.5−xVx high entropy alloys with carbon introduced from process control agent," *J. Alloys Compd.*, vol. 695, pp. 462–475, Feb. 2017.

[172] O. A. Waseem, J. Lee, H. M. Lee, and H. J. Ryu, “The effect of Ti on the sintering and mechanical properties of refractory high-entropy alloy TixWTaVCr fabricated via spark plasma sintering for fusion plasma-facing materials,” *Mater. Chem. Phys.*, vol. 210, pp. 87–94, 2018.
[173] O. A. Waseem and H. J. Ryu, “Powder Metallurgy Processing of a WxTaTiVCr High-Entropy Alloy and Its Derivative Alloys for Fusion Material Applications,” *Sci. Rep.*, vol. 7, no. 1, p. 1926, 2017.
[174] D. Linder, E. Holmström, and S. Norgren, “High entropy alloy binders in gradient sintered hardmetal,” *Int. J. Refract. Met. Hard Mater.*, vol. 71, pp. 217–220, Feb. 2018.
[175] Y. Cao, Y. Liu, B. Liu, and W. Zhang, “Precipitation behavior during hot deformation of powder metallurgy Ti-Nb-Ta-Zr-Al high entropy alloys,” *Intermetallics*, vol. 100, pp. 95–103, Sep. 2018.
[176] I. Kunce, M. Polanski, and J. Bystrzycki, “Microstructure and hydrogen storage properties of a TiZrNbMoV high entropy alloy synthesized using Laser Engineered Net Shaping (LENS),” *Int. J. Hydrogen Energy*, vol. 39, no. 18, pp. 9904–9910, Jun. 2014.
[177] A. Raza, B. Kang, J. Lee, H. J. Ryu, and S. H. Hong, “Transition in microstructural and mechanical behavior by reduction of sigma-forming element content in a novel high entropy alloy,” *Mater. Des.*, vol. 145, pp. 11–19, May 2018.
[178] R. Song, L. Wei, C. Yang, and S. Wu, “Phase formation and strengthening mechanisms in a dual-phase nanocrystalline CrMnFeVTi high-entropy alloy with ultrahigh hardness,” *J. Alloys Compd.*, vol. 744, pp. 552–560, May 2018.
[179] O. Senkov, D. Isheim, D. Seidman, and A. Pilchak, “Development of a Refractory High Entropy Superalloy,” *Entropy*, vol. 18, no. 3, p. 102, Mar. 2016.
[180] Y. Zhang, Y. J. Zhou, J. P. Lin, G. L. Chen, and P. K. Liaw, “Solid-Solution Phase Formation Rules for Multi-component Alloys,” *Adv. Eng. Mater.*, vol. 10, no. 6, pp. 534–538, 2008.
[181] S. GUO and C. T. LIU, “Phase stability in high entropy alloys: Formation of solid-solution phase or amorphous phase,” *Prog. Nat. Sci. Mater. Int.*, vol. 21, no. 6, pp. 433–446, Dec. 2011.
[182] F. Tian, L. K. Varga, N. Chen, J. Shen, and L. Vitos, “Empirical design of single phase high-entropy alloys with high hardness,” *Intermetallics*, vol. 58, pp. 1–6, 2015.
[183] S. Guo, Q. Hu, C. Ng, and C. T. Liu, “More than entropy in high-entropy alloys: Forming solid solutions or amorphous phase,” *Intermetallics*, vol. 41, pp. 96–103, Oct. 2013.
[184] S. Guo, C. Ng, J. Lu, and C. T. Liu, “Effect of valence electron concentration on stability of fcc or bcc phase in high entropy alloys,” *J. Appl. Phys.*, vol. 109, no. 10, p. 103505, May 2011.
[185] M.-H. Tsai, K.-Y. Tsai, C.-W. Tsai, C. Lee, C.-C. Juan, and J.-W. Yeh, “Criterion for Sigma Phase Formation in Cr- and V-Containing High-Entropy Alloys,” *Mater. Res. Lett.*, vol. 1, no. 4, pp. 207–212, 2013.
[186] K. Górecki, J. Zýka, J. Malek, J. Horvát, J. Čapek, and P. Bała, “Sintering and heat treatment of Al $_{15}$ Ti $_{5}$ Co $_{35}$ Ni $_{25}$ Fe $_{20}$ high-entropy alloy,” *IOP Conf. Ser. Mater. Sci. Eng.*, vol. 179, p. 012027, Feb. 2017.
[187] X.-W. Qiu, Y.-P. Zhang, L. He, and C. Liu, “Microstructure and corrosion resistance of AlCrFeCuCo high entropy alloy,” *J. Alloys Compd.*, vol. 549, pp. 195–199, 2013.
[188] K. Eymann *et al.*, “Consolidation of mechanically alloyed nanocrystalline Cu–Nb–ZrO2 powder by spark plasma sintering,” *J. Alloys Compd.*, vol. 535, pp. 62–69, 2012.
[189] X.-W. Qiu and C.-G. Liu, “Microstructure and properties of Al2CrFeCoCuTiNix high-entropy alloys prepared by laser cladding,” *J. Alloys Compd.*, vol. 553, pp. 216–220, Mar. 2013.
[190] Z. A. Munir, U. Anselmi-Tamburini, and M. Ohyanagi, “The effect of electric field and pressure on the synthesis and consolidation of materials: A review of the spark plasma sintering method,” *J. Mater. Sci.*, vol. 41, no. 3, pp. 763–777, Feb. 2006.
[191] A. Gali and E. P. George, “Tensile properties of high- and medium-entropy alloys,”

Intermetallics, vol. 39, pp. 74–78, Aug. 2013.
[192] S. Curtze and V.-T. Kuokkala, "Dependence of tensile deformation behavior of TWIP steels on stacking fault energy, temperature and strain rate," *Acta Mater.*, vol. 58, no. 15, pp. 5129–5141, Sep. 2010.
[193] E. C. Santos, M. Shiomi, K. Osakada, and T. Laoui, "Rapid manufacturing of metal components by laser forming," *Int. J. Mach. Tools Manuf.*, vol. 46, no. 12–13, pp. 1459–1468, Oct. 2006.
[194] D. D. Gu, W. Meiners, K. Wissenbach, and R. Poprawe, "Laser additive manufacturing of metallic components: materials, processes and mechanisms," *Int. Mater. Rev.*, vol. 57, no. 3, pp. 133–164, 2012.
[195] W. E. Frazier, "Metal Additive Manufacturing: A Review," *J. Mater. Eng. Perform.*, vol. 23, no. 6, pp. 1917–1928, Jun. 2014.
[196] S. Gorsse, C. Hutchinson, M. Gouné, and R. Banerjee, "Additive manufacturing of metals: a brief review of the characteristic microstructures and properties of steels, Ti-6Al-4V and high-entropy alloys," *Sci. Technol. Adv. Mater.*, vol. 18, no. 1, pp. 584–610, 2017.
[197] Q. He and Y. Yang, "On Lattice Distortion in High Entropy Alloys," *Front. Mater.*, vol. 5, p. 42, 2018.
[198] F. Otto, A. Dlouhý, C. Somsen, H. Bei, G. Eggeler, and E. P. George, "The influences of temperature and microstructure on the tensile properties of a CoCrFeMnNi high-entropy alloy," *Acta Mater.*, vol. 61, no. 15, pp. 5743–5755, Sep. 2013.
[199] B. Cai *et al.*, "Deformation mechanisms of Mo alloyed FeCoCrNi high entropy alloy: In situ neutron diffraction," *Acta Mater.*, vol. 127, pp. 471–480, Apr. 2017.
[200] S. K. C. Ch.-W. Tsai, Y.-L. Chen, M.-H. Tsai, J.W. Yeh, T.T. Shun, "Deformation and annealing behaviors of high-entropy alloy Al0.5CoCrCuFeNi," *J. Alloys Compd.*, vol. 486, no. 1–2, pp. 427–435, Nov. 2009.
[201] E. El-Danaf, S. R. Kalidindi, and R. D. Doherty, "Influence of grain size and stacking-fault energy on deformation twinning in fcc metals," *Metall. Mater. Trans. A*, vol. 30, no. 5, pp. 1223–1233, May 1999.
[202] K. L. Y. Zhang, N.R. Tao, "Effect of stacking-fault energy on deformation twin thickness in Cu–Al alloys," *Scr. Mater.*, vol. 60, no. 4, pp. 211–213, Feb. 2009.
[203] E. Ma, "Eight routes to improve the tensile ductility of bulk nanostructured metals and alloys," *JOM*, vol. 58, no. 4, pp. 49–53, 2006.
[204] S. Praveen and H. S. Kim, "High-Entropy Alloys: Potential Candidates for High-Temperature Applications – An Overview," *Adv. Eng. Mater.*, vol. 20, no. 1, p. 1700645.
[205] Y. Lu *et al.*, "A Promising New Class of High-Temperature Alloys: Eutectic High-Entropy Alloys," *Sci. Rep.*, vol. 4, p. 6200, Aug. 2014.
[206] A. Chauhan, D. Litvinov, and J. Aktaa, "High temperature tensile properties and fracture characteristics of bimodal 12Cr-ODS steel," *J. Nucl. Mater.*, vol. 468, pp. 1–8, Jan. 2016.
[207] Y. J. Zhou, Y. Zhang, Y. L. Wang, and G. L. Chen, "Solid solution alloys of AlCoCrFeNiTix with excellent room-temperature mechanical properties," *Appl. Phys. Lett.*, vol. 90, no. 18, p. 181904, Apr. 2007.
[208] Y. Dong, K. Zhou, Y. Lu, X. Gao, T. Wang, and T. Li, "Effect of vanadium addition on the microstructure and properties of AlCoCrFeNi high entropy alloy," *Mater. Des.*, vol. 57, pp. 67–72, May 2014.
[209] G. A. Salishchev *et al.*, "Effect of Mn and V on structure and mechanical properties of high-entropy alloys based on CoCrFeNi system," *J. Alloys Compd.*, vol. 591, pp. 11–21, Apr. 2014.
[210] N. D. Stepanov, D. G. Shaysultanov, G. A. Salishchev, and M. A. Tikhonovsky, "Structure and mechanical properties of a light-weight AlNbTiV high entropy alloy," *Mater. Lett.*, vol. 142, pp. 153–155, Mar. 2015.
[211] Y. J. Zhou, Y. Zhang, Y. L. Wang, and G. L. Chen, "Microstructure and compressive

properties of multicomponent Alx(TiVCrMnFeCoNiCu)100−x high-entropy alloys," *Mater. Sci. Eng. A*, vol. 454–455, pp. 260–265, Apr. 2007.
[212] X. F. Wang, Y. Zhang, Y. Qiao, and G. L. Chen, "Novel microstructure and properties of multicomponent CoCrCuFeNiTix alloys," *Intermetallics*, vol. 15, no. 3, pp. 357–362, Mar. 2007.
[213] Y. P. Wang, B. S. Li, M. X. Ren, C. Yang, and H. Z. Fu, "Microstructure and compressive properties of AlCrFeCoNi high entropy alloy," *Mater. Sci. Eng. A*, vol. 491, no. 1–2, pp. 154–158, Sep. 2008.
[214] B. S. Li, Y. P. Wang, M. X. Ren, C. Yang, and H. Z. Fu, "Effects of Mn, Ti and V on the microstructure and properties of AlCrFeCoNiCu high entropy alloy," *Mater. Sci. Eng. A*, vol. 498, no. 1–2, pp. 482–486, Dec. 2008.
[215] O. N. Senkov, G. B. Wilks, J. M. Scott, and D. B. Miracle, "Mechanical properties of Nb25Mo25Ta25W25 and V20Nb20Mo20Ta20W20 refractory high entropy alloys," *Intermetallics*, vol. 19, no. 5, pp. 698–706, May 2011.
[216] S. G. Ma and Y. Zhang, "Effect of Nb addition on the microstructure and properties of AlCoCrFeNi high-entropy alloy," *Mater. Sci. Eng. A*, vol. 532, pp. 480–486, Jan. 2012.
[217] Y. Dong, Y. Lu, J. Kong, J. Zhang, and T. Li, "Microstructure and mechanical properties of multi-component AlCrFeNiMox high-entropy alloys," *J. Alloys Compd.*, vol. 573, pp. 96–101, Oct. 2013.
[218] O. N. Senkov, C. Woodward, and D. B. Miracle, "Microstructure and Properties of Aluminum-Containing Refractory High-Entropy Alloys," *JOM*, vol. 66, no. 10, pp. 2030–2042, Oct. 2014.
[219] M. J. Yao, K. G. Pradeep, C. C. Tasan, and D. Raabe, "A novel, single phase, non-equiatomic FeMnNiCoCr high-entropy alloy with exceptional phase stability and tensile ductility," *Scr. Mater.*, vol. 72–73, pp. 5–8, Feb. 2014.
[220] A. V. Kuznetsov, D. G. Shaysultanov, N. D. Stepanov, G. A. Salishchev, and O. N. Senkov, "Tensile properties of an AlCrCuNiFeCo high-entropy alloy in as-cast and wrought conditions," *Mater. Sci. Eng. A*, vol. 533, pp. 107–118, Jan. 2012.
[221] Z. Tang *et al.*, "Tensile ductility of an AlCoCrFeNi multi-phase high-entropy alloy through hot isostatic pressing (HIP) and homogenization," *Mater. Sci. Eng. A*, vol. 647, pp. 229–240, Oct. 2015.
[222] I. S. Wani *et al.*, "Ultrafine-Grained AlCoCrFeNi2.1 Eutectic High-Entropy Alloy," *Mater. Res. Lett.*, vol. 4, no. 3, pp. 174–179, 2016.
[223] Y. Dong, X. Gao, Y. Lu, T. Wang, and T. Li, "A multi-component AlCrFe2Ni2 alloy with excellent mechanical properties," *Mater. Lett.*, vol. 169, pp. 62–64, Apr. 2016.
[224] W. H. Liu *et al.*, "Ductile CoCrFeNiMox high entropy alloys strengthened by hard intermetallic phases," *Acta Mater.*, vol. 116, pp. 332–342, Sep. 2016.
[225] W. H. Liu, J. Y. He, H. L. Huang, H. Wang, Z. P. Lu, and C. T. Liu, "Effects of Nb additions on the microstructure and mechanical property of CoCrFeNi high-entropy alloys," *Intermetallics*, vol. 60, pp. 1–8, May 2015.
[226] S. G. Ma *et al.*, "Superior high tensile elongation of a single-crystal CoCrFeNiAl0.3 high-entropy alloy by Bridgman solidification," *Intermetallics*, vol. 54, pp. 104–109, Nov. 2014.
[227] J. Y. He *et al.*, "Effects of Al addition on structural evolution and tensile properties of the FeCoNiCrMn high-entropy alloy system," *Acta Mater.*, vol. 62, pp. 105–113, Jan. 2014.
[228] T.-T. Shun and Y.-C. Du, "Microstructure and tensile behaviors of FCC Al0.3CoCrFeNi high entropy alloy," *J. Alloys Compd.*, vol. 479, no. 1–2, pp. 157–160, Jun. 2009.
[229] T. Zuo, S. Ren, P. K. Liaw, and Y. Zhang, "Processing effects on the magnetic and mechanical properties of FeCoNiAl0.2Si0.2 high entropy alloy," *Int. J. Miner. Metall. Mater.*, vol. 20, no. 6, pp. 549–555, Jun. 2013.
[230] Y. D. Wu *et al.*, "A refractory Hf25Nb25Ti25Zr25 high-entropy alloy with excellent

structural stability and tensile properties," *Mater. Lett.*, vol. 130, pp. 277–280, Sep. 2014.
[231] C.-W. Tsai, M.-H. Tsai, K.-Y. Tsai, S.-Y. Chang, J.-W. Yeh, and A.-C. Yeh, "Microstructure and tensile properties of Al0.5CoCrCuFeNi alloys produced by simple rolling and annealing," *Mater. Sci. Technol.*, vol. 31, no. 10, pp. 1178–1183, 2015.
[232] Y. Deng, C. C. Tasan, K. G. Pradeep, H. Springer, A. Kostka, and D. Raabe, "Design of a twinning-induced plasticity high entropy alloy," *Acta Mater.*, vol. 94, pp. 124–133, Aug. 2015.
[233] C.-W. Tsai, M.-H. Tsai, J.-W. Yeh, and C.-C. Yang, "Effect of temperature on mechanical properties of Al0.5CoCrCuFeNi wrought alloy," *J. Alloys Compd.*, vol. 490, no. 1–2, pp. 160–165, Feb. 2010.
[234] M. Niinomi, "Mechanical properties of biomedical titanium alloys," *Mater. Sci. Eng. A*, vol. 243, no. 1–2, pp. 231–236, Mar. 1998.
[235] J. W. Lu *et al.*, "Microstructure and mechanical properties of new high strength beta-titanium alloy Ti-1300," *Mater. Sci. Eng. A*, vol. 621, pp. 182–189, Jan. 2015.
[236] J. Chen and B. Young, "Stress–strain curves for stainless steel at elevated temperatures," *Eng. Struct.*, vol. 28, no. 2, pp. 229–239, Jan. 2006.
[237] V. Venkatesh and H. J. Rack, "Elevated temperature hardening of INCONEL 690," *Mech. Mater.*, vol. 30, no. 1, pp. 69–81, Sep. 1998.
[238] R. Schaeublin, T. Leguey, P. Spätig, N. Baluc, and M. Victoria, "Microstructure and mechanical properties of two ODS ferritic/martensitic steels," *J. Nucl. Mater.*, vol. 307–311, pp. 778–782, Dec. 2002.
[239] R. S. Sundar and S. C. Deevi, "High-temperature strength and creep resistance of FeAl," *Mater. Sci. Eng. A*, vol. 357, no. 1–2, pp. 124–133, Sep. 2003.
[240] K. B. Zhang *et al.*, "Annealing on the structure and properties evolution of the CoCrFeNiCuAl high-entropy alloy," *J. Alloys Compd.*, vol. 502, no. 2, pp. 295–299, Jul. 2010.
[241] S. R. Shinde *et al.*, "Co-occurrence of Superparamagnetism and Anomalous Hall Effect in Highly Reduced Cobalt-Doped Rutile ${\mathrm{TiO}}_{2\ensuremath{-}\ensuremath{\delta}}$ Films," *Phys. Rev. Lett.*, vol. 92, no. 16, p. 166601, 2004.
[242] M. Aoki, T. Noritake, A. Ito, M. Ishikiriyama, and S. Towata, "Improvement of cyclic durability of Ti–Cr–V alloy by Fe substitution," *Int. J. Hydrogen Energy*, vol. 36, no. 19, pp. 12329–12332, Sep. 2011.
[243] V. S. R.K. Prabakaran, A.N. Sait, "Synthesis and characteristization of high entropy alloy (CrMnFeNiCu) reinforced AA6061 aluminium matrix composite," *Mech. Mech. Eng.*, vol. 21, no. 2, pp. 415–424, 2017.
[244] G. M. Karthik, S. Panikar, G. D. J. Ram, and R. S. Kottada, "Additive manufacturing of an aluminum matrix composite reinforced with nanocrystalline high-entropy alloy particles," *Mater. Sci. Eng. A*, vol. 679, pp. 193–203, 2017.
[245] C.-S. Chen, C.-C. Yang, H.-Y. Chai, J.-W. Yeh, and J. L. H. Chau, "Novel cermet material of WC/multi-element alloy," *Int. J. Refract. Met. Hard Mater.*, vol. 43, pp. 200–204, Mar. 2014.
[246] T. T. Shen *et al.*, "Effects of LaB6 addition on the microstructure and mechanical properties of ultrafine grained WC–10Co alloys," *J. Alloys Compd.*, vol. 509, no. 4, pp. 1236–1243, Jan. 2011.
[247] P.-F. Zhou, D.-H. Xiao, and T.-C. Yuan, "Comparison between ultrafine-grained WC–Co and WC–HEA-cemented carbides," *Powder Metall.*, vol. 60, no. 1, pp. 1–6, 2017.
[248] M. S. El-Eskandarany, A. A. Mahday, H. . Ahmed, and A. . Amer, "Synthesis and characterizations of ball-milled nanocrystalline WC and nanocomposite WC–Co powders and subsequent consolidations," *J. Alloys Compd.*, vol. 312, no. 1–2, pp. 315–325, Nov. 2000.
[249] L. SUN, C. JIA, C. LIN, and R. CAO, "VC Addition Prepared Ultrafine WC-11Co Composites

by Spark Plasma Sintering," *J. Iron Steel Res. Int.*, vol. 14, no. 5, pp. 85–89, Sep. 2007.
[250] S. I. Cha, S. H. Hong, and B. K. Kim, "Spark plasma sintering behavior of nanocrystalline WC–10Co cemented carbide powders," *Mater. Sci. Eng. A*, vol. 351, no. 1–2, pp. 31–38, Jun. 2003.
[251] H.-C. Kim, I.-J. Shon, I.-K. Jeong, I.-Y. Ko, J.-K. Yoon, and J.-M. Doh, "Rapid sintering of ultra fine WC and WC-Co hard materials by high-frequency induction heated sintering and their mechanical properties," *Met. Mater. Int.*, vol. 13, no. 1, pp. 39–45, Feb. 2007.
[252] A. Michalski and D. Siemiaszko, "Nanocrystalline cemented carbides sintered by the pulse plasma method," *Int. J. Refract. Met. Hard Mater.*, vol. 25, no. 2, pp. 153–158, Mar. 2007.
[253] C. Lin, E. Kny, G. Yuan, and B. Djuricic, "Microstructure and properties of ultrafine WC–0.6VC–10Co hardmetals densified by pressure-assisted critical liquid phase sintering," *J. Alloys Compd.*, vol. 383, no. 1–2, pp. 98–102, Nov. 2004.
[254] D. Sivaprahasam, S. B. Chandrasekar, and R. Sundaresan, "Microstructure and mechanical properties of nanocrystalline WC–12Co consolidated by spark plasma sintering," *Int. J. Refract. Met. Hard Mater.*, vol. 25, no. 2, pp. 144–152, Mar. 2007.
[255] L. H. Zhu, Q. W. Huang, and H. F. Zhao, "Preparation of nanocrystalline WC-10Co-0.8VC by spark plasma sintering," *J. Mater. Sci. Lett.*, vol. 22, pp. 1631–1633, 2003.
[256] Z. Z. Fang, X. Wang, T. Ryu, K. S. Hwang, and H. Y. Sohn, "Synthesis, sintering, and mechanical properties of nanocrystalline cemented tungsten carbide – A review," *Int. J. Refract. Met. Hard Mater.*, vol. 27, no. 2, pp. 288–299, 2009.
[257] I. Moravcik *et al.*, "Synergic strengthening by oxide and coherent precipitate dispersions in high-entropy alloy prepared by powder metallurgy," *Scr. Mater.*, vol. 157, pp. 24–29, 2018.
[258] J.-O. Andersson, T. Helander, L. Höglund, P. Shi, and B. Sundman, "Thermo-Calc & DICTRA, computational tools for materials science," *Calphad*, vol. 26, no. 2, pp. 273–312, Jun. 2002.
[259] N. Saunders, U. K. Z. Guo, X. Li, A. P. Miodownik, and J.-P. Schillé, "Using JMatPro to model materials properties and behavior," *JOM*, vol. 55, no. 12, pp. 60–65, 2003.
[260] H. R. Sistla, J. W. Newkirk, and F. Frank Liou, "Effect of Al/Ni ratio, heat treatment on phase transformations and microstructure of AlxFeCoCrNi2−x (x = 0.3, 1) high entropy alloys," *Mater. Des.*, vol. 81, pp. 113–121, Sep. 2015.
[261] B. Cai *et al.*, "Deformation mechanisms of Mo alloyed FeCoCrNi high entropy alloy: In situ neutron diffraction," *Acta Mater.*, vol. 127, pp. 471–480, Apr. 2017.
[262] A. Kilmametov *et al.*, "High-pressure torsion driven mechanical alloying of CoCrFeMnNi high entropy alloy," *Scr. Mater.*, vol. 158, pp. 29–33, 2019.
[263] G. Zhu, Y. Liu, and J. Ye, "Fabrication and properties of Ti(C,N)-based cermets with multi-component AlCoCrFeNi high-entropy alloys binder," 2013.
[264] I. Moravcik, J. Cizek, P. Gavendova, S. Sheikh, S. Guo, and I. Dlouhy, "Effect of heat treatment on microstructure and mechanical properties of spark plasma sintered AlCoCrFeNiTi0.5 high entropy alloy," 2016.
[265] X. Qiu, "Microstructure, hardness and corrosion resistance of Al<inf>2</inf>CoCrCuFeNiTi<inf>x</inf>high-entropy alloy coatings prepared by rapid solidification," *J. Alloys Compd.*, vol. 735, pp. 359–364, 2018.
[266] T. Fujieda *et al.*, "CoCrFeNiTi-based high-entropy alloy with superior tensile strength and corrosion resistance achieved by a combination of additive manufacturing using selective electron beam melting and solution treatment," *Mater. Lett.*, vol. 189, pp. 148–151, Feb. 2017.
[267] G. A. Salishchev *et al.*, "Effect of Mn and V on structure and mechanical properties of high-entropy alloys based on CoCrFeNi system," *J. Alloys Compd.*, vol. 591, pp. 11–21, Apr. 2014.
[268] Z. Tang *et al.*, "Tensile ductility of an AlCoCrFeNi multi-phase high-entropy alloy through

hot isostatic pressing (HIP) and homogenization," *Mater. Sci. Eng. A*, vol. 647, pp. 229–240, Oct. 2015.
[269] W.-F. Ho, "A comparison of tensile properties and corrosion behavior of cast Ti–7.5Mo with c.p. Ti, Ti–15Mo and Ti–6Al–4V alloys," *J. Alloys Compd.*, vol. 464, no. 1–2, pp. 580–583, Sep. 2008.
[270] Z. Fu, W. Chen, S. Fang, and X. Li, "Effect of Cr addition on the alloying behavior, microstructure and mechanical properties of twinned CoFeNiAl0.5Ti0.5 alloy," *Mater. Sci. Eng. A*, vol. 597, pp. 204–211, Mar. 2014.
[271] N. N. Guo *et al.*, "Microstructure and mechanical properties of in-situ MC-carbide particulates-reinforced refractory high-entropy Mo0.5NbHf0.5ZrTi matrix alloy composite," *Intermetallics*, vol. 69, pp. 74–77, Feb. 2016.
[272] F. Zhang, J. Shen, and J. Sun, "The effect of phosphorus additions on densification, grain growth and properties of nanocrystalline WC–Co composites," *J. Alloys Compd.*, vol. 385, no. 1–2, pp. 96–103, Dec. 2004.

Supplementary data.

MA method	Grinding media	Process control agent	Cluster Composition	Time to reach the alloy	Obtained phase (minor)	Ref.
Planetary	WC vial and balls	Toluene	C5	15h	BCC	[24]
Vibratory	Hardened steel vial and balls/Ar	No	C1	24h 36h 24h	BCC FCC BCC	[26], [42]
Planetary	Hardened steel vial and balls	Toluene	C1 C3	15h	FCC FCC (BCC)	[142]
Planetary	Stainless steel vial and balls	n-heptane	C1	60h	BCC (FCC)	[25]
Vibratory	Steel+argon	No	C1	24h	BCC	[93]
Planetary	WC vial and balls	Toluene	C2	20h	BCC	[94]
Planetary	WC	Toluene	C2	20h	BCC	[92]
Planetary	Stainless steel	n-heptane	C1	18h	BSS	[64]
Vibratory	Hardened steel vial and balls/Ar	Methanol	C1	30h	FCC	[75]
Planetary	Hard chorme steel	No	C1	15h 15h	BCC FCC (BCC)	[86]
Planetary	Stainless steel vial/WC balls/Ar	No	C1	30h	BCC	[99]
Planetary	Stainless steel vial/WC balls	No	C1	30h	BCC	[100]
Planetary	Stailess sttels vial and balls/Ar	No	C1	30h	BCC	[263]
Planetary	WC vial and balls	Toluene	C1	20h 15h	BCC+FCC BCC	[44]
Planetary	Stainless steel vial, WC balls/Ar	No	C1	30h	FCC	[46]
Planetary	Stainless steel vial and balls	n-heptane	C1	50h 40h 30h	BCC	[97]
Planetary	Stainless steel vial and balls/Ar	n-heptane	C1	30h	BCC	[71]
Planetary	Stainless steel vial/WC balls/Ar	No	C1	38h	BCC+FCC	[34]
Planetary	Hardened steel	Toluene	C1	30h	BCC	[35]
Planetary	Stainless steel vial/WC balls/Ar	Ethanol	C1	38h	BCC (FCC)	[36]

					FCC	
Planetary	Stailess sttels vial and balls/Ar	Ethanol	C1	20h	BCC	[38]
Planetary	Stainless steel	n-heptane	C1	18h	BCC	[39]
Planetary	Stainless steel vial/WC balls/Ar	Ethanol	C1	30h	BCC+FCC	[41]
Planetary	Stainless steel vial/WC balls/Ar	No	C1	30h	BCC+FCC	[95]
Planetary	WC vial and balls/Ar	Ethanol	C1	38h	BCC+FCC	[45]
Planetary	Chrome steel balls	Toluene	C1	24h	BCC	[76]
Vibratory	Hardened steel vial and balls/Ar	Methanol	C1	10h	BCC	[43]
Milling bowl	Hardened steel vial, chromium balls	Methanol	C1	24h	BCC	[264]
Planetary	Stainless steel vial and balls/Ar	No	C1	66h	BCC+FCC FCC	[96]
Vibratory	Hardened steel vial and balls	Methanol	C1	20h	BCC+FCC BCC	[74]
Planetary	Zirconia vial and balls/Ar	No	C1	40h	BCC+FCC	[57]
High energy ball mill	Stainless steel vial and balls	Toluene	C1	70h	BCC+FCC FCC FCC	[55]
Vibratory	Hardened steel vial and balls/Ar	No	C1	20h	FCC	[60]
Planetary	WC vial and balls/Ar	No	C1	25h	BCC+FCC	[58]
Planetary		Toluene	C1	20h	BCC+FCC	[56]
High energy ball mill	WC vial and balls	Toluene	C1	10h	BCC	[54]
Planetary	Steels balls/Ar	No	C1	35h	FCC	[69]
Planetary	Stainless steel vial and balls/Ar	No	C1	55h	FCC	[62]
Planetary	Stainless steel vial and balls/Ar	No	C1	50h	FCC	[98]
Planetary	WC vial and balls	Ethanol	C1	40h	BCC+FCC	[66]
Planetary	Stainless steel vial and balls	n-heptane	C1	36h	FCC	[88]
Planetary	Steel balls an vials/Ar	No	C1		BCC+FCC	[91]

Planetary	WC vial ad balls	No	C1	45h	FCC+BCC	[90]
Planetary	WC vial and balls/Ar	No	C2	15h	BCC	[103]
High energy ball mill	Ar	No	C2	10h 20h	FCC+HCP (Zr) Amorphous	[104]
Planetary	Stainless steel vial and balls/Ar	No	C2	200h	Amorphous	[102]
Planetary	Stainless steel vial and balls	n-heptane	C3	30h	BCC+FCC	[105]
Planetary	WC vial and balls	Toluene	C3	25h	BCC+FCC	[106]
Planetary	Stainless steel vial, WC balls/Ar	Ciclohexane	C3	30h	FCC	[148]
Planetary	Steel vial and balls	Toluene	C3	15h	FCC	[118]
Planetary	Stainless steel vial and balls	n-heptane	C3	35h	FCC	[116]
Planetary	Hardened steel vial and balls/vacuum	No	C3	24h	FCC	[115]
Planetary	Zirconia balls/Ar	No	C3	20min	FCC	[139]
Planetary	Zirconia balls/Ar	No	C3	1h	FCC	[114]
Planetary	Stainless steel vial and balls	n-heptane	C3	35h	FCC	[110]
Planetary	Tempered steel vial, sainless steel balls	No	C3	10h	FCC	[146]
Planetary	Steel vial and balls	Toluene	C3	15h	BCC	[144]
Shaker rod mill	Stainless steel containers and rods	No	C3	24h	FCC	[119]
Planetary	WC vial and balls	Toluene	C3	15h	FCC FCC BCC+FCC	[124]
Planetary	Stainless steel vial and balls	n-heptane	C3	45h	FCC	[125]
Planetary	Tempered steel vial and balls/Ar	No	C3	10h	FCC	[126]
Planetary	Stainless steel vial and balls/Ar	n-heptane	C3	45h	FCC	[127]
Planetary	Tempered steel vial and balls/Ar	No	C3	10h	FCC	[129]
Planetary	Stainless steel vial and balls	n-heptane	C3	35h	FCC	[132]
Planetary	WC vial and balls	Toluene	C3	15 min	BCC (FCC)	[141]
Planetary	Stainless steels vial and balls	Ethanol	C3	20h	FCC	[138]

Ball mill		No	C3	60h	FCC	[140]
Planetary	Stainless steel vial/WC balls	No	C4	45h	BCC (FCC)	[149]
Planetary	Hardened tool steel vial, chrome steel balls	Toluene	C4	30h	BCC (FCC)	[152]
Planetary	Stainless steel vial and balls/Ar Stainless steels vial and balls/3MPa H_2	No	C4	24h	BCC FCC	[155]
Planetary	Stainles steel vial and balls	Ciclohexane	C4	40h	FCC	[156]
Planetary	Hardened Steel	Toluene	C5	30h	BCC	[161]
Planetary	WC vial and balls/Ar	No	C5	25h	BCC	[165]
Planetary	WC vial and balls	Toluene	C5	20h	BCC	[168]
Planetary	Stainless steels vial and balls	Toluene	C6	42h	BCC+FCC	[171]
Ball mill	Steel vial, WC balls/Ar	No	C6	6h	BCC	[170]
Planetary	Tool steel vial, WC balls/Ar	No	C9	15h	BCC	[177]
Planetary	WC vial and balls	Ethanol	C9	40h	BCC	[178]

Table S1. Processing conditions and phase obtained after the process after MA.

SPS Conditions	Cluster composition	Ref.
800-850 ºC/30-80MPa/10-15 min	C1-C4	[60], [64], [71], [85], [105]
900-1000ºC/30-90 MPa/5-80 min	C1-C4	[34], [41], [46], [55], [58], [63], [69], [86], [88], [91], [95], [99], [100], [102], [103], [107], [109], [114], [122], [133], [139], [140], [142], [144], [148], [149], [171], [188]
1100-1150 ºC/30-50 MPa/5-30 min	C1-C4	[38], [115], [120], [123], [128], [131], [138], [152]
1200-1250 ºC/30-60 MPa/5-20 min	C1-C4	[69], [80]
1350 ºC/30 MPa/5 min	C1-C4	[66]
1700 ºC/30 MPa/5 min	C1-C4	[48]
800 ºC/50 MPa/5 min	C5-C9	[162]
900 ºC/45-50 MPa/5-15 min	C5-C9	[163], [167], [168]
1100-1150 ºC/40-50 MPa/5 min	C5-C9	[177], [178]
1500 ºC/50 MPa/10 min	C6-C7	[172]
1600 ºC/50 MPa/10 min	C6-C7	[173]
1700 ºC/50 MPa/5 min	C6-C7	[170]

Table S2. SPS conditions for the different groups of materials.

Press	Sintering	Cluster composition	Ref.
300/400 MPa	1000 ºC/1h/Ar	C1	[56], [186]
300 MPa	1200 ºC/2min	C1	[83]
310 MPa	1300 ºC/2h/Ar	C1	[33]
100 MPa	1450 ºC/1h/Ar	C1	[47]
200 MPa	1450 ºC/2h/Ar	C1	[68]
	1800 ºC/2h/Ar	C1	[32], [265]
70 MPa	1150 ºC/Ar	C3	[124]
1000 MPa	1200 ºC/2h/vacuum	C3	[122]
200 MPa (CIP)	1400 ºC/1h/Ar	C3	[126]
200 MPa (CIP)	1450 ºC/1h/Ar	C3	[129]
	1500 ºC/3h/vacuum	C4	[157]
1500 MPa	1100 ºC/3h	C5	[43]
200 MPa (CIP)	1300 ºC/16h/vacuum	C8	[175]

Table S3. Press and sintering conditions in each cluster of alloys.

Hot press conditions	**Cluster composition**	**Ref.**
800/900 ºC/30/50MPa/30/60 min	C1-C4	[92], [127]
1000-1050 ºC/30-50 MPa/15-120 min	C1-C4	[36], [38], [45], [119], [125]
1150 ºC/25 MPa/60 min	C1-C4	[153]
850 ºC/200 MPa/120 min	C5-C9	[161]
900 ºC/50 MPa/5 min (FAHP)	C5-C9	[165]
1200 ºC/35 MPa	C5-C9	[160]
HIP conditions	**Cluster composition**	**Ref.**
1100 ºC/300 MPa/180 min	C1	[65]
800 ºC/1000 MPa/60 min	C2	[94]
1000 ºC/150 MPa/15 min	C3	[110], [132]

Table S4. Processing conditions when HP and HIP is used.

Cluster	AM Technology	AM System	Ref.
C1	LMD	Powder feed	[57], [73]
	DMD		[260]
	DLF		[79], [82], [84]
	SLM	Powder bed	[77]
	SEBM		[51], [78], [89]
C3	LMD	Powder feed	[113]
	DLF		[145]
	SLM	Powder bed	[130], [134]–[136]
	LPBF		[137]
	SEBM		[188]
C4	LMD	Powder feed	[151]
	SEBM	Powder bed	[266]
C6	DMD	Powder feed	[169]

LMD: Laser Melting Deposition
DMD: Direct Melting Deposition
DLF: Direct Laser Fabrication
SLM: Selective Laser Melting
SEBM: Selective Electron Bean Melting
LPBF: Laser Powder Bed Fusion

Table S5. Table AM technologies used in PMHEAs.

Alloy	Cluster	Process	σ_y (MPa)	σ_{max} (MPa)	ε_p (%)	Hardness (H_v)	Ref.
$FeNiCrCo_{0.3}Al_{0.7}$	C1	SPS	2033	2635	8.12	624	[99]
$Al_{0.6}CoNiFeTi_{0.4}$	C1	SPS	2732	3172	10.1	712	[46]
$CoFeNiCrAl_{0.6}Ti_{0.4}$	C1	SPS	2080	2520	11.5	573	[100]
$AlNiCrFe_{0.5}Mo_{0.2}CoCu$	C1	Press and sintering	1132	1258	18.3		[33]
$AlNiCrFeMo_{0.2}CoCu$	C1	Press and sintering	818	1222	16.9		[33]
$AlNiCrFe_{1.5}Mo_{0.2}CoCu$	C1	Press and sintering	536	1124	19.8		[33]
$AlNiCrFe_{2}Mo_{0.2}CoCu$	C1	Press and sintering	436	1221	30.2		[33]
$Co_{0.5}FeNiCrTi_{0.5}$	C4	SPS	2650	2690	10.0	846	[149]
$Al_{0.5}CrFeNiCo_{0.3}C_{0.2}$	C1	SPS		2131	3	617	[34]
AlCoNiFe	C1	HP		2913	2.7	865	[36]
AlCoNiFe	C1	SPS		2386	6.2	667	[36]
TiAlCoNiFe	C1	HP		2737	3.2	816	[36]
$Al_{0.4}FeCrNiCo_{1.5}Ti_{0.3}$	C1	HP	2130	2540	20.1		[38]
CoCrFeNiAl	C1	SPS		1907		625	[39]
CoCrFeNiMnAl	C1	SPS		2142	8	662	[71]
$Al_{0.5}FeNiCr$	C1	SPS	1741	2184	7.4	556	[41]
$Al_{0.5}FeNiCrCo$	C1	SPS	1938	2221	7.6	577	[41]
$Al_{0.5}FeNiCrTi_{0.25}$	C1	SPS	1926	2376	6.8	609	[41]
CoNiFeAlTi	C1	SPS		2988	5.8	704	[95]
CoCrFeNiMn	C3	SPS		1987		646	[105]
AlNiFeCr	C1	SPS	1607	1992	11.2	552	[45]
AlNiFeCr	C1	HP	1420	1948	13.5	431	[45]
AlNiFeCrCo	C1	SPS	1870	2150	10.6	570	[45]
AlNiFeCrCo	C1	HP	1830	2298	10.8	594	[45]
AlCoCrFeNi	C1	SPS	1262	3228	29.1		[80]

$Fe_{30}Ni_{30}Co_{30}Mn_{10}$	C3	SPS		1798	34		[148]
$Fe_{27}Ni_{27}Co_{26}Mn_{10}Ti_{10}$	C3	SPS		1928	22		[148]
$Co_{25}Ni_{25}Fe_{25}Al_{7.5}Cu_{17.5}$	C1	SPS		1936	10.6	454	[50]
$Ni_{1.5}CoFeCu_{0.9}Al_{0.1}V_{0.5}$	C1	SPS	1219		35	393	[171]
$Ni_{1.5}CoFeCu_{0.9}Al_{0.1}V_{0.5}$	C1	SPS	1504	1942	16.9	495	[171]
$Ni_{1.5}CoFeCu_{0.9}Al_{0.1}V_{0.5}$	C1	SPS	1721	1931	9	541	[171]
AlCoCrFeNi	C1	DLF+ aging at 600 ºC	1310	2600	16.8		[84]
AlCoCrFeNi	C1	DLF+ aging at 800 ºC	1170	2940	21.6		[84]
AlCoCrFeNi	C1	DLF+ aging at 1000 ºC	1070	2830	29.4		[84]
AlCoCrFeNi	C1	DLF+ aging at 1200 ºC	1130	3020	24.2		[84]
WNbMoTaV	C6	SPS	2612	3472	8.8		[170]
CoCrFeNiMn	C3	HP	1314	2026	20.3	415	[127]
$Ti_{20}Fe_{30}Co_{30}Ni_{30}$	C4	SPS	1800	2000	20		[156]
$Al_{0.3}FeNiCo_{1.2}CrCu$	C1	SPS	1275	1635	26.1	515	[62]
$Al_{0.3}FeNiCo_{1.2}CrCu$ +TiC	C1	SPS	1730	2260	29.5	645	[62]
CoFeNiCrAlTi	C1	Casting	1860	2.58	8.8		[207]
TiVCrMnFeCoNi	C4	Casting	1312	1312	0		[211]
TiVCrMnFeCoNiAl	C4	Casting	1862	2431	0.95		[211]
$Ti_{10}V_{10}Cr_{10}Mn_{10}Fe_{10}Ni_{10}Co_{10}Al_{20}$	C4	Casting	1465	2016	2.35		[211]
$Ti_{7.5}V_{7.5}Cr_{7.5}Mn_{7.5}Fe_{7.5}Co_{7.5}Ni_{7.5}Co_{7.5}Al_{40}$	C4	Casting	1461	1461	0		[211]
CoCrCuFeNi	C3	Casting	230	888	50.2		[212]
$CoCrCuFeNiTi_{0.5}$	C3	Casting	700	1650	21.6		[212]
$CoCrCuFeNiTi_{0.8}$	C3	Casting	1042	1848	2.11		[212]
CoCrCuFeNiTi	C3	Casting	1272	1272	0		[212]
FeNiCrCoAl	C1	Casting	1251	2004	32.7		[213]
AlCrFeCoNiCu	C1	Casting	1303	2081	24		[214]
AlCrFeCoNiCuMn	C1	Casting	1005	1480	15		[214]
AlCrFeCoNiCuTi	C1	Casting	1234	1356	9		[214]

AlCrFeCoNiCuV	C2	Casting	1469	1970	16		[214]
CoFeNiCrAlTi	C1	Casting		2.28	6.4		[53]
NbMoTaW	C6	Casting	1058	1211	1.5		[215]
VNbMoTaW	C6	Casting	1246	1270	0.5		[215]
AlCoCrFeNi	C1	Casting	1373	3531	24.5	520	[216]
$AlCoCrFeNb_{0.1}Ni$	C1	Casting	1641	3285	17.2	569	[216]
$AlCoCrFeNb_{0.25}Ni$	C1	Casting	1959	3008	10.5	668	[216]
$AlCoCrFeNb_{0.5}Ni$	C1	Casting	2473	3170	4.1	747	[216]
AlCrFeNi	C5	Casting	2926	1406	28.5	472	[217]
$AlCrFeNiMo_{0.2}$	C3	Casting	3222	1487	28.7	548	[217]
$AlCrFeNiM_{0.5}$	C3	Casting	2643	1748	12.6	621	[217]
$AlCrFeNiMo_{0.8}$	C3	Casting	1512	1512	0	853	[217]
$AlMo_{0.5}NbTa_{0.5}TiZr$	C8	Casting	2000	2368	10		[218]
$AlNb_{1.5}Ta_{0.5}Ti_{1.5}Zr_{0.5}$	C8	Casting	1280	1367	3.5		[218]
$Al_{0.4}Hf_{0.6}NbTaTiZr$	C8	Casting	1841	2269	10		[218]
$Al_{0.3}NbTaTi_{1.4}Zr_{1.3}$	C8	Casting	1965	2054	5		[218]
$Al_{0.3}NbTa_{0.8}Ti_{1.4}V_{0.2}Zr_{1.3}$	C8	Casting	1965	2061	5		[218]
$Al_{0.5}NbTa_{0.8}Ti_{1.5}V_{0.2}Zr$	C8	Casting	2035	2105	5.5		[218]
AlCoCrFeNi	C1	Casting	1378	2864	22.7	534	[208]
$AlCoCrFeNiV_{0.2}$	C3	Casting	1492	3297	26.8	557	[208]
$AlCoCrFeNiV_{0.5}$	C3	Casting	1597	1907	5.1	591	[208]
$AlCoCrFeNiV_{0.8}$	C3	Casting	1695	2097	5.7	624	[208]
AlCoCrFeNiV	C3	Casting	1726	1867	0.7	648	[208]
CoCrFeNi	C1	Casting	190	1000	75		[209]
CoCrFeNiV	C3	Casting	1435	1665	2.5		[209]
CoCrFeNiMnV	C3	Casting	1660	1845	0.5		[209]
AlNbTiV		Casting	1020	1318	5		[210]

Table S6. Compression strength and hardness for different HEAs.

Alloy	Cluster	Process	$\sigma_{0.2}$ (MPa)	σ_{max} (MPa)	ε (%)	Ref.
$Ni_{1.5}Co_{1.5}CrFeTi_{0.5}$		SPS	1308	1384	4	[152]
CoCrFeNi	C1	AM (SLM)- 50 μm layer	402	480	8	[77]
CoCrFeNi	C1	AM (SLM)-20 μm layer	600	745	32	[77]
CoCrFeNiMn	C3	SPS	161	613	27	[188]
CoCrFeNiMn	C3	SPS	194	571	37	[188]
$Co_{1.5}CrFeNi_{1.5}Ti_{0.5}Mo_{0.1}$	C4	Arc melting	550	740	3.2	[266]
$Co_{1.5}CrFeNi_{1.5}Ti_{0.5}Mo_{0.1}$	C4	AM (SEBM)	750	900	4	[266]
$Co_{1.5}CrFeNi_{1.5}Ti_{0.5}Mo_{0.1}$	C4	AM (SEBM)+annealing	900	1300	18	[266]
$Co_{1.5}CrFeNi_{1.5}Ti_{0.5}Mo_{0.1}$	C4	AM (SEBM)+wáter quenching	800	1050	37	[266]
$Fe_{18}Ni_{23}Co_{25}Cr_{21}Mo_8WNb_3C_2$		Hot Pressing	1200	1452	3.9	[119]
CoCrFeNi	C1	Arc melted	147	413	48	[225]
$CoCrFeNiNb_{0.103}$	C1	Arc melted	317	622	19.2	[225]
$CoCrFeNiNb_{0.155}$	C1	Arc melted	321	744	23.3	[225]
$CoCrFeNiNb_{0.206}$	C1	Arc melted	402	807	8.6	[225]
$CoCrFeNiNb_{0.309}$	C1	Arc melted	478	879	3.5	[225]
$CoCrFeNiNb_{0.412}$	C1	Arc melted	637	1004	1.3	[225]
CoCrFeNi	C1	Arc melted	188	457	50	[77]
$AlCoCrFeNi_{2.1}$	C1	Arc melted	75	944	25.6	[205]
$Al_{0.3}CoCrFeNi$	C1	Arc melted	275	528	37	[226]
$Al_{11}(CoCrFeMnNi)_{89}$	C1	Arc melted	832	1174	7.7	[227]
CoCrFeNi	C1	Arc melted	140	488	83	[267]
CoCrFeMnNi	C1	Arc melted	215	491	71	[267]
$Al_{0.5}CrCuFeNi_2$		Arc melted	363	500	16.1	[228]
$FeCoNiAl_{0.2}Si_{0.2}$		Arc melted	280	636	41.6	[229]
HfNbTiZr	C8	Arc melted and homogenized	879	969	14.9	[230]
$Fe_{40}Mn_{27}Ni_{26}Co_5Cr_2$	C1	Arc melted and homogenized	95	375	58	[219]
AlCoCrCuFeNi	C1	Arc melted and homogenized	790	790	0.2	[220]

CoCrFeNi	C1	Arc melted and annealed	130	458	87	[267]
CoCrFeNiMn	C1	Arc melted and annealed	162	443	68	[267]
$Al_{0.5}CrCuFeNi_2$	C1	Rolled	1055	1179	2	[231]
$Al_{0.5}CoCrCuFeNi$	C1	Rolled	1284	1344	7.6	[231]
AlCoCrCuFeNi	C1	Forged	1040	1170	1	[220]
$Fe_{40}Mn_{40}Co_{10}Cr_{10}$	C3	Rolled + homogenized	240	489	58	[232]
AlCoCrFeNi	C1	As cast	395	400	1	[268]
AlCoCrFeNi	C1	As cast+HIP	295	393	11.5	[268]
$Al_{0.5}CoCrCuFeNi$	C1	Rolled	180	185	5	[233]
$Al_{0.5}CoCrCuFeNi$	C1	Rolled+annealed	160	180	12	[233]
$AlCoCrFeNi_{2.1}$	C1	As cast	620	1050	17	[222]
$AlCoCrFeNi_{2.1}$	C1	Cold Rolled	1625	1800	6	[222]
$AlCoCrFeNi_{2.1}$	C1	Annealed	1100	1200	12	[222]
$AlCrFe_2Ni_2$	C1	As cast	796	1437	15.7	[223]
CoCrFeNi	C1	As cast	155	472	58.9	[224]
$CoCrFeNiMo_{0.1}$	C3	As cast	199	479	51.1	[224]
$CoCrFeNiMo_{0.2}$	C3	As cast	255	590	55.2	[224]
$CoCrFeNiMo_{0.3}$	C3	As cast	305	710	49.3	[224]
$CoCrFeNiMo_{0.3}$	C3	Rolled	815	1186	18.9	[224]
$CoCrFeNiMo_{0.3}$	C3	Rolled	647	1042	32.5	[224]
$CoCrFeNiMo_{0.3}$	C3	Rolled+annealed	684	1067	30.4	[224]
CoCrFeNiMn	C3	High Pressure Torsion	1400	1740	4	[198]
Ti-7.5Mo		as-cast	737	1019	16	[269]
Ti-15Mo		as-cast	745	921	25	[269]
Ti-6Al-4V		as-cast	999	1173	6	[269]
Ti-20Cr-0.2Si		as-cast	669	874	6	[234]
Ti-25Pd-5Cr		as-cast	659	880	5	[234]
Ti-6Al-4V		as-cast	847	976	5.1	[234]
Ti-6Al-7Nb		as-cast	817	933	7.1	[234]
Ti-5Al-2.5Fe		as-cast	895	1020	15	[234]

Ti-29Nb-13Ta-4.6Zr		as-aged	864	911	13.2	[234]
Ti-15Zr-4Nb-4Ta-0.2Pd		as-aged	806	919	18	[234]
Ti-15Sn-4Nb-2Ta-0.2Pd		as-aged	1020	1109	10	[234]
Ti-15Mo		as-annealed	544	874	21	[234]
Ti-5Al-3Zr-4Cr-4Mo-4V		hot rolled + heat treated	1034	1075	21	[235]
Duplex Stainless Steel			329	366	2.4	[236]
304 Stainless Steel			179	248	9.1	[236]
Inconel 680			150	478	26	[237]
ODS Steel+0.3%Ytria			210	272	11	[238]
12Cr-ODS ferritic			1200	1294	18	[206]
Intermetallic FeAl			345	350	18	[239]

Table S7. Tensile feature of some PMHEAs, HEAs and other structural alloys.

Matrix	Reinforcement	Processing	σ_y (MPa)	σ_{max} (MPa)	ε_p (%)	Hardness (H_v)	Ref.
$Al_{0.4}FeCrCoNi_{1.5}Ti_{0.3}$ Cluster C4	12% (wt.) Al_2O_3 (<20 nm)	All components in MA+SPS (1000 ºC/30 MPa/10 min	-	2250	20	743	[63]
CoCrFeMnNi Cluster C3	5% (vol.) Al_2O_3 (<35 nm)	HEA by MA and mix with Al_2O_3+HIP (1000 ºC/150 MPa/15 min.	1600	1930	6.8	545	[110]
$Al_{0.4}FeCrCo_{1.5}NiTi_{0.3}$ Cluster C1	8% (vol.) Al_2O_3 (<20 nm)	All components in MA+SPS (1000 ºC/30 MPa/10 min	2050	2140	14	654	[98]
FeCoCrNiMn Cluster C3	5% (wt.) SiC (<50 nm)	MA+ mix with SiC+HIP (1000 ºC/150 MPa/15 min)	1480	2390	26.5	485	[116]
FeCoCrNiAl Cluster C1	10% (wt.) SiC (< 40 μm)	Mix+SPS (1000 ªC/60 MPa/5min+annealing (1200 ºC/5h)				795	[91]
FeCoCrNiAl Cluster C1	10% (wt.) SiC (< 40 μm)	MA+SPS (1000 ªC/60 MPa/5min+annealing (1200 ºC/5h)				951	[91]
$CoNiFeCrAl_{0.6}Ti_{0.4}$ Cluster C1	-	MA+SPS (1000 ºC/30 MPa/8 min.)	2080	2520	11.5	617	[100]
$FeNiCrCo_{0.3}Al_{0.7}$ Cluster C1	-	MA+SPS (1000 ºC/30 MPa/8 min.)	2030	2630	8.12	624	[270]
CoCrFeMnNi Cluster C3	-	MA+HIP (1000 ºC/150 MPa/15 min.	1180	2660	34.5	418	[110]
FeCoCrNiMn Cluster C3	-	MA+ mix with SiC+HIP (1000 ºC/150 MPa/15 min)	1180	2660	35.5	484	[116]

Table S8. MMCs from HEAs used as binder.

Processing	Binder	Hard phase	Fracture toughness (MPam1/2)	Hardness (Hv)	Ref.
Press+sint. (1450 ºC)	Ni-Co (15% wt.)	TiCN-WC-Mo2C-TaC	9.21	1538	[47]
Press+sint. (1450 ºC)	AlCoCrFeNi (15% wt.)	TiCN-WC-Mo2C-TaC	11.5	1773	[47]
Press+sint. (1500 ºC)	CoCrFeMnNi (20% wt.)	TiTaNbCN	6.6	928	[146]
Press+sint. (1500 ºC)	CoCrFeNiV (20% wt.)	TiTaNbCN	4	1295	[146]
Press+sint. (1500 ºC)	CoCrFeMnNiC (20% wt.)	TiTaNbCN	7.1	663	[146]
Press+sint. (1500 ºC)	CoCrFeNiVC (20% wt.)	TiTaNbCN	6.8	1048	[146]
SPS (1250 ºC)	AlCoCrCuFeNi (5% wt.)	WC	9.6	2040	[271]
SPS (1250 ºC)	AlCoCrCuFeNi (10% wt.)	WC	10.41	1922	[66]
SPS (1250 ºC)	AlCoCrCuFeNi (15% wt.)	WC	9.4	1700	[66]
SPS (1250 ºC)	AlCoCrCuFeNi (20% wt.)	WC	9	1550	[66]
SPS (1200 ºC)	AlCoCrCuFeNi (10% wt.)	WC	9.8	2030	[66]
SPS (1300 ºC)	AlCoCrCuFeNi (10% wt.)	WC	10.6	1890	[66]
SPS (1350 ºC)	AlCoCrCuFeNi (10% wt.)	WC	9.9	1790	[66]
SPS (1250 ºC)	Co (10%)	WC	12.99	1736	[66]
Press+sint. (1300 ºC)	AlCrFeCoNi (10% wt.)	WC	7.5	1200	[68]
Press+sint. (1400 ºC)	AlCrFeCoNi (10% wt.)	WC	7	2160	[68]
Press+sint. (1450 ºC)	AlCrFeCoNi (10% wt.)	WC	6.9	2090	[68]
Press+sint. (1300 ºC)	AlCrFeCoNi (20% wt.)	WC	9.2	1600	[68]
Press+sint. (1400 ºC)	AlCrFeCoNi (20% wt.)	WC	9.5	1701	[68]
Press+sint. (1450 ºC)	AlCrFeCoNi (20% wt.)	WC	9.9	1640	[68]
Press+sint. (1450 ºC)	Co (10% wt.)	WC	7.5	1784	[246]
Press+sint (1500 ºC)	AlCoCrFeNi (15% wt.)	TiCN-WC-Mo2C-TaC	11.4	1787	[263]
Press+sint (1200 ºC)	Al0.5CrCoCuFeNi (20% wt.)	WC	17.4	1413	[245]

	Co (10% wt.)	WC	9.1	1900	[245]
	Co (18% wt.)	WC	13	1450	[245]
Hot Press. (1500 ºC)	Co (10% wt.)		8.1	1910	[247]
Hot Press. (1500 ºC)	AlFeCoNiCrTi (10% wt.)	WC	8.33	2231	[247]
Hot Press. (1500 ºC)	AlFeCoNiCrTi (20% wt.)	WC	12.1	2358	[247]
SPS (1450 ºC)	CoCrNiCuMn (5% wt.)	TiN0.3	5.85	1614	[143]
SPS (1450 ºC)	CoCrNiCuMn (7% wt.)	TiN0.3	6.75	1575	[143]
SPS (1450 ºC)	CoCrNiCuMn (10% wt.)	TiN0.3	7.05	1529	[143]
Hot press. (1300 ºC)	Co (10% wt.)	WC-VC	8.8	2084	[253]
Hot press. (1700 ºC)	Co (14% wt.)	WC	14	1100	[248]
SPS (1150 ºC)	Co (10% wt.)	WC	13.5	2030	[272]
SPS (1100ºC)	Co (12% wt.)	WC-VC	10.9	1450	[254]
SPS (1100 ºC)	Co (12% wt.)	WC-VC	11.42	1570	[254]
SPS (1240 ºC)	Co (10% wt.)	WC	9.3	1569	[249]
SPS (1240 ºC)	Co (10% wt.)	WC-VC	9.5	1726	[249]
SPS (1200 ºC)	Co (10% wt.)	WC-VC	11.5	1887	[255]
SPS (1000 ºC)	Co (10% wt.)	WC	12	1800	[250]
HFIHS (1200 ºC)	Co (10% wt.)	WC	13.5	1886	[251]
PPS (1100 ºC)	Co (12% wt.)	WC	15.3	2250	[252]

Table S9. Composition and properties of the materials plotted in Figure 23.

References

[1] M. Radetzki, “Seven thousand years in the service of humanity—the history of copper, the red metal,” *Resour. Policy*, vol. 34, no. 4, pp. 176–184, Dec. 2009.

[2] Y.-W. Kim, “Intermetallic alloys based on gamma titanium aluminide,” *JOM*, vol. 41, no. 7, pp. 24–30, Jul. 1989.

[3] B. Cantor, I. T. H. Chang, P. Knight, and A. J. B. Vincent, “Microstructural development in equiatomic multicomponent alloys,” *Mater. Sci. Eng. A*, vol. 375–377, pp. 213–218, Jul. 2004.

[4] J.-W. Yeh *et al.*, “Nanostructured High-Entropy Alloys with Multiple Principal Elements: Novel Alloy Design Concepts and Outcomes,” *Adv. Eng. Mater.*, vol. 6, no. 5, pp. 299–303, May 2004.

[5] D. B. Miracle and O. N. Senkov, “A critical review of high entropy alloys and related concepts,” *Acta Mater.*, vol. 122, pp. 448–511, Jan. 2017.

[6] J.-W. Yeh, “Recent progress in high-entropy alloys,” *Ann. Chim. Sci. des Matériaux*, vol. 31, no. 6, pp. 633–648, Dec. 2006.

[7] M.-H. Tsai and J.-W. Yeh, “High-Entropy Alloys: A Critical Review,” *Mater. Res. Lett.*, vol. 2, no. 3, pp. 107–123, 2014.

[8] Y. F. Ye, Q. Wang, J. Lu, C. T. Liu, and Y. Yang, “High-entropy alloy: challenges and prospects,” *Mater. Today*, vol. 19, no. 6, pp. 349–362, 2016.

[9] E. J. Pickering and N. G. Jones, “High-entropy alloys: a critical assessment of their founding principles and future prospects,” *Int. Mater. Rev.*, vol. 61, no. 3, pp. 183–202, 2016.

[10] B. Cantor, “Multicomponent and High Entropy Alloys,” *Entropy*, vol. 16, no. 9, pp. 4749–4768, 2014.

[11] M.-H. Tsai, “Physical Properties of High Entropy Alloys,” *Entropy*, vol. 15, no. 12, pp. 5338–5345, 2013.

[12] Y. Zhang, T. Zuo, Y. Cheng, and P. K. Liaw, “High-entropy Alloys with High Saturation Magnetization, Electrical Resistivity, and Malleability,” *Sci. Rep.*, vol. 3, p. 1455, Mar. 2013.

[13] Y. Shi, B. Yang, and P. K. Liaw, “Corrosion-Resistant High-Entropy Alloys: A Review,” *Metals (Basel).*, vol. 7, no. 2, 2017.

[14] Y. Qiu, M. A. Gibson, H. L. Fraser, and N. Birbilis, “Corrosion characteristics of high entropy alloys,” *Mater. Sci. Technol.*, vol. 31, no. 10, pp. 1235–1243, 2015.

[15] S. John Mary, R. Nagalakshmi, S. Rajendran, and R. Epshipha, “High entropy alloys and corrosion resistance. A bird’s eye view,” *Eur. Chem. Bull.*, vol.

3, no. 12, pp. 1031–1035, 2014.

[16] D. B. Miracle, J. D. Miller, O. N. Senkov, C. Woodward, M. D. Uchic, and J. Tiley, “Exploration and Development of High Entropy Alloys for Structural Applications,” *Entropy*, vol. 16, no. 1, pp. 494–525, 2014.

[17] D. B. Miracle, “Critical Assessment 14: High entropy alloys and their development as structural materials,” *Mater. Sci. Technol.*, vol. 31, no. 10, pp. 1142–1147, 2015.

[18] Y. Zhang *et al.*, “Microstructures and properties of high-entropy alloys,” *Prog. Mater. Sci.*, vol. 61, pp. 1–93, 2014.

[19] B. Gludovatz, A. Hohenwarter, D. Catoor, E. H. Chang, E. P. George, and R. O. Ritchie, “A fracture-resistant high-entropy alloy for cryogenic applications,” *Science (80-.).*, vol. 345, no. 6201, pp. 1153–1158, 2014.

[20] H. Y. Diao, R. Feng, K. A. Dahmen, and P. K. Liaw, “Fundamental deformation behavior in high-entropy alloys: An overview,” *Curr. Opin. Solid State Mater. Sci.*, vol. 21, no. 5, pp. 252–266, Oct. 2017.

[21] W. Li, P. K. Liaw, and Y. Gao, “Fracture resistance of high entropy alloys: A review,” *Intermetallics*, vol. 99, pp. 69–83, 2018.

[22] B. S. Murty, J. W. Yeh, and S. Ranganathan, *High-Entropy Alloys*. Elsevier Science, 2014.

[23] M. C. Gao, J.-W. Yeh, P. K. Liaw, and Y. Zhang, Eds., *High-Entropy Alloys*. Cham: Springer International Publishing, 2016.

[24] S. Varalakshmi, M. Kamaraj, and B. S. Murty, “Synthesis and characterization of nanocrystalline AlFeTiCrZnCu high entropy solid solution by mechanical alloying,” *J. Alloys Compd.*, vol. 460, no. 1, pp. 253–257, 2008.

[25] K. B. Zhang *et al.*, “Nanocrystalline CoCrFeNiCuAl high-entropy solid solution synthesized by mechanical alloying,” *Journal of Alloys and Compounds*, vol. 485, no. 1. pp. L31–L34, 2009.

[26] Y.-L. Chen *et al.*, “Alloying behavior of binary to octonary alloys based on Cu–Ni–Al–Co–Cr–Fe–Ti–Mo during mechanical alloying,” *J. Alloys Compd.*, vol. 477, no. 1–2, pp. 696–705, May 2009.

[27] C. C. Koch, “Nanocrystalline high-entropy alloys,” *J. Mater. Res.*, vol. 32, no. 18, pp. 3435–3444, 2017.

[28] A. Kumar and M. Gupta, “An Insight into Evolution of Light Weight High Entropy Alloys: A Review,” *Metals (Basel).*, vol. 6, no. 9, 2016.

[29] O. N. Senkov, G. B. Wilks, D. B. Miracle, C. P. Chuang, and P. K. Liaw, “Refractory high-entropy alloys,” *Intermetallics*, vol. 18, no. 9, pp. 1758–1765, Sep. 2010.

[30] J.-W. Yeh, “Alloy Design Strategies and Future Trends in High-Entropy Alloys,” *JOM*, vol. 65, no. 12, pp. 1759–1771, 2013.

[31] G. W. Milligan and M. C. Cooper, “A Study of the Comparability of External Criteria for Hierarchical Cluster Analysis,” *Multivariate Behav. Res.*, vol. 21, no. 4, pp. 441–458, 1986.

[32] X.-W. Qiu, “Microstructure and properties of AlCrFeNiCoCu high entropy alloy prepared by powder metallurgy,” *J. Alloys Compd.*, vol. 555, pp. 246–249, Apr. 2013.

[33] F. Yuhu, Z. Yunpeng, G. Hongyan, S. Huimin, and H. Li, “AlNiCrFexMo0.2CoCu High Entropy Alloys Prepared by Powder Metallurgy,” *Rare Met. Mater. Eng.*, vol. 42, no. 6, pp. 1127–1129, Jun. 2013.

[34] S. Fang, W. Chen, and Z. Fu, “Microstructure and mechanical properties of twinned Al0.5CrFeNiCo0.3C0.2 high entropy alloy processed by mechanical alloying and spark plasma sintering,” *Mater. Des.*, vol. 54, pp. 973–979, 2014.

[35] C. S. babu, K. Sivaprasad, V. Muthupandi, and J. A. Szpunar, “Characterization of Nanocrystalline AlCoCrCuNiFeZn High Entropy Alloy Produced by Mechanical Alloying,” *Procedia Mater. Sci.*, vol. 5, pp. 1020–1026, Jan. 2014.

[36] Z. Fu, W. Chen, Z. Chen, H. Wen, and E. J. Lavernia, “Influence of Ti addition and sintering method on microstructure and mechanical behavior of a medium-entropy Al0.6CoNiFe alloy,” *Mater. Sci. Eng. A*, vol. 619, pp. 137–145, Dec. 2014.

[37] H. Zhang, Y. Pan, Y. He, and H. Jiao, “Microstructure and properties of 6FeNiCoSiCrAlTi high-entropy alloy coating prepared by laser cladding,” *Appl. Surf. Sci.*, vol. 257, no. 6, pp. 2259–2263, 2011.

[38] Y. Shaofeng, Z. Yan, C. Jialin, Z. Chen, and C. Weiping, “Microstructure and Properties of Al0.4FeCrNiCo1.5Ti0.3 High Entropy Alloy Prepared by MA-HP Technique,” *Rare Met. Mater. Eng.*, vol. 43, no. 12, pp. 2948–2952, Dec. 2014.

[39] W. Ji *et al.*, “Mechanical alloying synthesis and spark plasma sintering consolidation of CoCrFeNiAl high-entropy alloy,” *J. Alloys Compd.*, vol. 589, pp. 61–66, 2014.

[40] G. Zhu, Y. Liu, and J. Ye, “Fabrication and properties of Ti(C,N)-based cermets with multi-component AlCoCrFeNi high-entropy alloys binder,” *Mater. Lett.*, vol. 113, pp. 80–82, Dec. 2013.

[41] Z. Chen, W. Chen, B. Wu, X. Cao, L. Liu, and Z. Fu, “Effects of Co and Ti on microstructure and mechanical behavior of Al0.75FeNiCrCo high entropy alloy prepared by mechanical alloying and spark plasma sintering,” *Mater. Sci. Eng. A*, vol. 648, pp. 217–224, 2015.

[42] Y.-L. Chen, Y.-H. Hu, C.-W. Tsai, J.-W. Yeh, S.-K. Chen, and S.-Y. Chang, “Structural evolution during mechanical milling and subsequent annealing of

Cu–Ni–Al–Co–Cr–Fe–Ti alloys," *Mater. Chem. Phys.*, vol. 118, no. 2–3, pp. 354–361, Dec. 2009.

[43] F. J. Baldenebro-Lopez, J. M. Herrera-Ramírez, S. P. Arredondo-Rea, C. D. Gómez-Esparza, and R. Martínez-Sánchez, "Simultaneous effect of mechanical alloying and arc-melting processes in the microstructure and hardness of an AlCoFeMoNiTi high-entropy alloy," *J. Alloys Compd.*, vol. 643, pp. S250–S255, 2015.

[44] R. Sriharitha, B. S. Murty, and R. S. Kottada, "Phase formation in mechanically alloyed AlxCoCrCuFeNi (x = 0.45, 1, 2.5, 5 mol) high entropy alloys," *Intermetallics*, vol. 32, pp. 119–126, 2013.

[45] Z. Fu, W. Chen, H. Wen, Z. Chen, and E. J. Lavernia, "Effects of Co and sintering method on microstructure and mechanical behavior of a high-entropy Al0.6NiFeCrCo alloy prepared by powder metallurgy," *J. Alloys Compd.*, vol. 646, pp. 175–182, Oct. 2015.

[46] W. Chen, Z. Fu, S. Fang, Y. Wang, H. Xiao, and D. Zhu, "Processing, microstructure and properties of Al0.6CoNiFeTi0.4 high entropy alloy with nanoscale twins," *Mater. Sci. Eng. A*, vol. 565, pp. 439–444, Mar. 2013.

[47] G. Zhu, Y. Liu, and J. Ye, "Early high-temperature oxidation behavior of Ti(C,N)-based cermets with multi-component AlCoCrFeNi high-entropy alloy binder," *Int. J. Refract. Met. Hard Mater.*, vol. 44, pp. 35–41, 2014.

[48] W. Ji *et al.*, "Fabrication and properties of TiB2-based cermets by spark plasma sintering with CoCrFeNiTiAl high-entropy alloy as sintering aid," *J. Eur. Ceram. Soc.*, vol. 35, no. 3, pp. 879–886, Mar. 2015.

[49] P. Veronesi, R. Rosa, E. Colombini, and C. Leonelli, "Microwave-Assisted Preparation of High Entropy Alloys," *Technologies*, vol. 3, no. 4, pp. 182–197, Oct. 2015.

[50] Z. Fu *et al.*, "Microstructure and strengthening mechanisms in an FCC structured single-phase nanocrystalline Co25Ni25Fe25Al7.5Cu17.5 high-entropy alloy," *Acta Mater.*, vol. 107, pp. 59–71, Apr. 2016.

[51] H. Shiratori *et al.*, "Relationship between the microstructure and mechanical properties of an equiatomic AlCoCrFeNi high-entropy alloy fabricated by selective electron beam melting," *Mater. Sci. Eng. A*, vol. 656, pp. 39–46, 2016.

[52] X. Qiu, C. Huang, M. Wu, C. Liu, and Y. Zhang, "Structure and properties of AlCrFeNiCuTi six principal elements equimolar alloy," *J. Alloys Compd.*, vol. 658, pp. 1–5, Feb. 2016.

[53] K. B. Zhang *et al.*, "Microstructure and mechanical properties of CoCrFeNiTiAlx high-entropy alloys," *Mater. Sci. Eng. A*, vol. 508, no. 1–2, pp. 214–219, May 2009.

[54] A. Raphel, S. Kumaran, K. V. Kumar, and L. Varghese, “Oxidation and Corrosion resistance of AlCoCrFeTiHigh Entropy Alloy,” *Mater. Today Proc.*, vol. 4, no. 2, pp. 195–202, Jan. 2017.

[55] P. Wang, X. Cheng, H. Cai, Y. Xue, and Y. Zhang, “Influence of increasing Al concentration on phase, microstructure and mechanical behaviors of Ni1.5CoFeCu1−xAlxV0.5 high entropy alloys,” *Mater. Sci. Eng. A*, vol. 708, pp. 523–536, Dec. 2017.

[56] H. Prasad, S. Singh, and B. B. Panigrahi, “Mechanical activated synthesis of alumina dispersed FeNiCoCrAlMn high entropy alloy,” *J. Alloys Compd.*, vol. 692, pp. 720–726, 2017.

[57] J. Li, W. Craeghs, C. Jing, S. Gong, and F. Shan, “Microstructure and physical performance of laser-induction nanocrystals modified high-entropy alloy composites on titanium alloy,” *Mater. Des.*, vol. 117, pp. 363–370, Mar. 2017.

[58] S. Mohanty *et al.*, “Powder metallurgical processing of equiatomic AlCoCrFeNi high entropy alloy: Microstructure and mechanical properties,” *Mater. Sci. Eng. A*, vol. 679, pp. 299–313, Jan. 2017.

[59] C.-C. Yang, J. L. Hang Chau, C.-J. Weng, C.-S. Chen, and Y.-H. Chou, “Preparation of high-entropy AlCoCrCuFeNiSi alloy powders by gas atomization process,” *Mater. Chem. Phys.*, vol. 202, pp. 151–158, Dec. 2017.

[60] R. S. Ganji, P. Sai Karthik, K. Bhanu Sankara Rao, and K. V. Rajulapati, “Strengthening mechanisms in equiatomic ultrafine grained AlCoCrCuFeNi high-entropy alloy studied by micro- and nanoindentation methods,” *Acta Mater.*, vol. 125, pp. 58–68, Feb. 2017.

[61] S. Riva, A. Tudball, S. Mehraban, N. P. Lavery, S. G. R. Brown, and K. V. Yusenko, “A novel High-Entropy Alloy-based composite material,” *J. Alloys Compd.*, vol. 730, pp. 544–551, Jan. 2018.

[62] S. Yang, J. Pi, W. Yang, H. Zhou, and D. Zhu, “Deformation twinning structure and interface in a FCC-based Al0.3FeNiCo1.2CrCu high-entropy alloy matrix composites,” *Mater. Lett.*, vol. 214, pp. 50–52, Mar. 2018.

[63] S. Yang, X. Yan, K. Yang, and Z. Fu, “Effect of the addition of nano-Al2O3 on the microstructure and mechanical properties of twinned Al0.4FeCrCoNi1.2Ti0.3 alloys,” *Vacuum*, vol. 131, pp. 69–72, Sep. 2016.

[64] K. B. Zhang, Z. Y. Fu, J. Y. Zhang, W. M. Wang, S. W. Lee, and K. Niihara, “Characterization of nanocrystalline CoCrFeNiTiAl high-entropy solid solution processed by mechanical alloying,” *J. Alloys Compd.*, vol. 495, no. 1, pp. 33–38, 2010.

[65] J. Joseph, P. Hodgson, T. Jarvis, X. Wu, N. Stanford, and D. M. Fabijanic, “Effect of hot isostatic pressing on the microstructure and mechanical properties of additive manufactured AlxCoCrFeNi high entropy alloys,” *Mater. Sci. Eng. A*, vol. 733, pp. 59–70, Aug. 2018.

[66] W. Luo, Y. Liu, Y. Luo, and M. Wu, “Fabrication and characterization of WC-AlCoCrCuFeNi high-entropy alloy composites by spark plasma sintering,” *J. Alloys Compd.*, vol. 754, pp. 163–170, Jul. 2018.

[67] A. Erdogan, T. Yener, and S. Zeytin, “Fast production of high entropy alloys (CoCrFeNiAlxTiy) by electric current activated sintering system,” *Vacuum*, vol. 155, pp. 64–72, Sep. 2018.

[68] P. L. Zhou, D. H. Xiao, P. F. Zhou, and T. C. Yuan, “Microstructure and properties of ultrafine grained AlCrFeCoNi/WC cemented carbides,” *Ceram. Int.*, Jun. 2018.

[69] E. Colombini, R. Rosa, L. Trombi, M. Zadra, A. Casagrande, and P. Veronesi, “High entropy alloys obtained by field assisted powder metallurgy route: SPS and microwave heating,” *Mater. Chem. Phys.*, vol. 210, pp. 78–86, May 2018.

[70] K. V. Yusenko *et al.*, “High-pressure high-temperature tailoring of High Entropy Alloys for extreme environments,” *J. Alloys Compd.*, vol. 738, pp. 491–500, Mar. 2018.

[71] C. Wang, W. Ji, and Z. Fu, “Mechanical alloying and spark plasma sintering of CoCrFeNiMnAl high-entropy alloy,” *Adv. Powder Technol.*, vol. 25, no. 4, pp. 1334–1338, 2014.

[72] R. Sriharitha, B. S. Murty, and R. S. Kottada, “Alloying, thermal stability and strengthening in spark plasma sintered AlxCoCrCuFeNi high entropy alloys,” *J. Alloys Compd.*, vol. 583, pp. 419–426, 2014.

[73] I. Kunce, M. Polanski, K. Karczewski, T. Plocinski, and K. J. Kurzydlowski, “Microstructural characterisation of high-entropy alloy AlCoCrFeNi fabricated by laser engineered net shaping,” *J. Alloys Compd.*, vol. 648, pp. 751–758, Nov. 2015.

[74] C. D. Gómez-Esparza *et al.*, “Series of Nanocrystalline NiCoAlFe(Cr, Cu, Mo, Ti) High-Entropy Alloys produced by Mechanical Alloying,” *Mater. Res.*, vol. 19, no. suppl 1, pp. 39–46, Aug. 2016.

[75] C. D. Gómez-Esparza *et al.*, “Microstructure of NiCoAlFeCuCr multi-component systems synthesized by mechanical alloying,” *J. Alloys Compd.*, vol. 509, pp. S279–S283, Jun. 2011.

[76] J. Chen *et al.*, “Fabrication and mechanical properties of AlCoNiCrFe high-entropy alloy particle reinforced Cu matrix composites,” *J. Alloys Compd.*, vol. 649, pp. 630–634, 2015.

[77] Y. Brif, M. Thomas, and I. Todd, “The use of high-entropy alloys in additive manufacturing,” *Scr. Mater.*, vol. 99, pp. 93–96, Apr. 2015.

[78] T. Fujieda *et al.*, “First demonstration of promising selective electron beam melting method for utilizing high-entropy alloys as engineering

materials," *Mater. Lett.*, vol. 159, pp. 12–15, 2015.

[79] J. Joseph, T. Jarvis, X. Wu, N. Stanford, P. Hodgson, and D. M. Fabijanic, "Comparative study of the microstructures and mechanical properties of direct laser fabricated and arc-melted AlxCoCrFeNi high entropy alloys," *Mater. Sci. Eng. A*, vol. 633, pp. 184–193, 2015.

[80] A. Zhang, J. Han, J. Meng, B. Su, and P. Li, "Rapid preparation of AlCoCrFeNi high entropy alloy by spark plasma sintering from elemental powder mixture," 2016.

[81] Z. Tan, L. Wang, Y. Xue, P. Zhang, T. Cao, and X. Cheng, "High-entropy alloy particle reinforced Al-based amorphous alloy composite with ultrahigh strength prepared by spark plasma sintering," *Mater. Des.*, vol. 109, pp. 219–226, Nov. 2016.

[82] J. Joseph, N. Stanford, P. Hodgson, and D. M. Fabijanic, "Tension/compression asymmetry in additive manufactured face centered cubic high entropy alloy," *Scr. Mater.*, vol. 129, pp. 30–34, Mar. 2017.

[83] P. Veronesi, E. Colombini, R. Rosa, C. Leonelli, and M. Garuti, "Microwave processing of high entropy alloys: A powder metallurgy approach," *Chem. Eng. Process. Process Intensif.*, vol. 122, pp. 397–403, Dec. 2017.

[84] R. Wang, K. Zhang, C. Davies, and X. Wu, "Evolution of microstructure, mechanical and corrosion properties of AlCoCrFeNi high-entropy alloy prepared by direct laser fabrication," *J. Alloys Compd.*, vol. 694, pp. 971–981, 2017.

[85] S. Nam, M. J. Kim, J. Y. Hwang, and H. Choi, "Strengthening of Al0.15CoCrCuFeNiTix–C (x = 0, 1, 2) high-entropy alloys by grain refinement and using nanoscale carbides via powder metallurgical route," *J. Alloys Compd.*, vol. 762, pp. 29–37, Sep. 2018.

[86] S. Praveen, B. S. Murty, and R. S. Kottada, "Alloying behavior in multi-component AlCoCrCuFe and NiCoCrCuFe high entropy alloys," *Mater. Sci. Eng. A*, vol. 534, pp. 83–89, 2012.

[87] T. Lu *et al.*, "The influence of nanocrystalline CoNiFeAl0.4Ti0.6Cr0.5 high-entropy alloy particles addition on microstructure and mechanical properties of SiCp/7075Al composites," *Mater. Sci. Eng. A*, vol. 726, pp. 126–136, 2018.

[88] R. M. Pohan *et al.*, "Microstructures and mechanical properties of mechanically alloyed and spark plasma sintered Al0.3CoCrFeMnNi high entropy alloy," *Mater. Chem. Phys.*, vol. 210, pp. 62–70, May 2018.

[89] K. Kuwabara, H. Shiratori, T. Fujieda, K. Yamanaka, Y. Koizumi, and A. Chiba, "Mechanical and Corrosion Properties of AlCoCrFeNi High-Entropy Alloy Fabricated with Selective Electron Beam Melting," *Addit. Manuf.*, Jun. 2018.

[90] Z. Fu *et al.*, "Influence of Cr removal on the microstructure and mechanical behaviour of a high-entropy Al0.8Ti0.2CoNiFeCr alloy fabricated by

powder metallurgy," *Powder Metall.*, vol. 61, no. 2, pp. 106–114, 2018.

[91] E. Colombini *et al.*, "SPS-assisted Synthesis of SICp reinforced high entropy alloys: reactivity of SIC and effects of pre-mechanical alloying and post-annealing treatment," *Powder Metall.*, vol. 61, no. 1, pp. 64–72, 2018.

[92] S. Varalakshmi, M. Kamaraj, and B. S. Murty, "Processing and properties of nanocrystalline CuNiCoZnAlTi high entropy alloys by mechanical alloying," *Mater. Sci. Eng. A*, vol. 527, no. 4, pp. 1027–1030, Feb. 2010.

[93] Y.-L. Chen, Y.-H. Hu, C.-A. Hsieh, J.-W. Yeh, and S.-K. Chen, "Competition between elements during mechanical alloying in an octonary multi-principal-element alloy system," *J. Alloys Compd.*, vol. 481, no. 1–2, pp. 768–775, Jul. 2009.

[94] S. Varalakshmi, M. Kamaraj, and B. S. Murty, "Formation and Stability of Equiatomic and Nonequiatomic Nanocrystalline CuNiCoZnAlTi High-Entropy Alloys by Mechanical Alloying," *Metall. Mater. Trans. A*, vol. 41, no. 10, pp. 2703–2709, Oct. 2010.

[95] Z. Fu *et al.*, "Microstructure and mechanical behavior of a novel Co20Ni20Fe20Al20Ti20 alloy fabricated by mechanical alloying and spark plasma sintering," *Mater. Sci. Eng. A*, vol. 644, pp. 10–16, 2015.

[96] P. Wang, H. Cai, and X. Cheng, "Effect of Ni/Cr ratio on phase, microstructure and mechanical properties of NixCoCuFeCr2−x (x = 1.0, 1.2, 1.5, 1.8 mol) high entropy alloys," *J. Alloys Compd.*, vol. 662, pp. 20–31, Mar. 2016.

[97] N. H. Tariq, M. Naeem, B. A. Hasan, J. I. Akhter, and M. Siddique, "Effect of W and Zr on structural, thermal and magnetic properties of AlCoCrCuFeNi high entropy alloy," *J. Alloys Compd.*, vol. 556, pp. 79–85, Apr. 2013.

[98] S. Yang, Y. Zhang, X. Yan, H. Zhou, J. Pi, and D. Zhu, "Deformation twins and interface characteristics of nano-Al2O3 reinforced Al0.4FeCrCo1.5NiTi0.3 high entropy alloy composites," *Mater. Chem. Phys.*, vol. 210, pp. 240–244, May 2018.

[99] W. Chen, Z. Fu, S. Fang, H. Xiao, and D. Zhu, "Alloying behavior, microstructure and mechanical properties in a FeNiCrCo0.3Al0.7 high entropy alloy," *Mater. Des.*, vol. 51, pp. 854–860, Oct. 2013.

[100] Z. Fu, W. Chen, S. Fang, D. Zhang, H. Xiao, and D. Zhu, "Alloying behavior and deformation twinning in a CoNiFeCrAl0.6Ti0.4 high entropy alloy processed by spark plasma sintering," *J. Alloys Compd.*, vol. 553, pp. 316–323, Mar. 2013.

[101] S. Varalakshmi, G. Appa Rao, M. Kamaraj, and B. S. Murty, "Hot consolidation and mechanical properties of nanocrystalline equiatomic AlFeTiCrZnCu high entropy alloy after mechanical alloying," *J. Mater. Sci.*, vol. 45, no. 19, pp. 5158–5163, Oct. 2010.

[102] W. Ge *et al.*, "Characterization and properties of CuZrAlTiNi high entropy alloy coating obtained by mechanical alloying and vacuum hot pressing

sintering," *Adv. Powder Technol.*, vol. 28, no. 10, pp. 2556–2563, Oct. 2017.

[103] S. Mohanty, N. P. Gurao, and K. Biswas, "Sinter ageing of equiatomic Al20Co20Cu20Zn20Ni20 high entropy alloy via mechanical alloying," *Mater. Sci. Eng. A*, vol. 617, pp. 211–218, 2014.

[104] W. Ge, Y. Wang, C. Shang, Z. Zhang, and Y. Wang, "Microstructures and properties of equiatomic CuZr and CuZrAlTiNi bulk alloys fabricated by mechanical alloying and spark plasma sintering," *J. Mater. Sci.*, vol. 52, no. 10, pp. 5726–5737, May 2017.

[105] W. Ji *et al.*, "Alloying behavior and novel properties of CoCrFeNiMn high-entropy alloy fabricated by mechanical alloying and spark plasma sintering," *Intermetallics*, vol. 56, pp. 24–27, Jan. 2015.

[106] P. F. Yu *et al.*, "The high-entropy alloys with high hardness and soft magnetic property prepared by mechanical alloying and high-pressure sintering," *Intermetallics*, vol. 70, pp. 82–87, 2016.

[107] B. Wang *et al.*, "Mechanical Properties and Microstructure of the CoCrFeMnNi High Entropy Alloy Under High Strain Rate Compression," *J. Mater. Eng. Perform.*, vol. 25, no. 7, pp. 2985–2992, Jul. 2016.

[108] B. Liu *et al.*, "Microstructure and mechanical properties of equimolar FeCoCrNi high entropy alloy prepared via powder extrusion," *Intermetallics*, vol. 75, pp. 25–30, 2016.

[109] J. Wang *et al.*, "Flow behavior and microstructures of powder metallurgical CrFeCoNiMo0.2 high entropy alloy during high temperature deformation," *Mater. Sci. Eng. A*, vol. 689, pp. 233–242, Mar. 2017.

[110] Ł. Rogal, D. Kalita, and L. Litynska-Dobrzynska, "CoCrFeMnNi high entropy alloy matrix nanocomposite with addition of Al2O3," *Intermetallics*, vol. 86, pp. 104–109, 2017.

[111] N. Eißmann, B. Klöden, T. Weißgärber, and B. Kieback, "High-entropy alloy CoCrFeMnNi produced by powder metallurgy," *Powder Metall.*, vol. 60, no. 3, pp. 184–197, 2017.

[112] C. Shang *et al.*, "CoCrFeNi(W1−xMox) high-entropy alloy coatings with excellent mechanical properties and corrosion resistance prepared by mechanical alloying and hot pressing sintering," *Mater. Des.*, vol. 117, pp. 193–202, Mar. 2017.

[113] C. Haase, F. Tang, M. B. Wilms, A. Weisheit, and B. Hallstedt, "Combining thermodynamic modeling and 3D printing of elemental powder blends for high-throughput investigation of high-entropy alloys – Towards rapid alloy screening and design," *Mater. Sci. Eng. A*, vol. 688, pp. 180–189, 2017.

[114] D. Yim *et al.*, "Shock wave compaction and sintering of mechanically alloyed CoCrFeMnNi high-entropy alloy powders," *Mater. Sci. Eng. A*, vol. 708,

pp. 291–300, Dec. 2017.

[115] H. Hadraba *et al.*, “Oxide dispersion strengthened CoCrFeNiMn high-entropy alloy,” *Mater. Sci. Eng. A*, vol. 689, pp. 252–256, Mar. 2017.

[116] Ł. Rogal, D. Kalita, A. Tarasek, P. Bobrowski, and F. Czerwinski, “Effect of SiC nano-particles on microstructure and mechanical properties of the CoCrFeMnNi high entropy alloy,” *J. Alloys Compd.*, vol. 708, pp. 344–352, 2017.

[117] Y. Liu, J. Wang, Q. Fang, B. Liu, Y. Wu, and S. Chen, “Preparation of superfine-grained high entropy alloy by spark plasma sintering gas atomized powder,” *Intermetallics*, vol. 68, pp. 16–22, 2016.

[118] P. Sathiyamoorthi, J. Basu, S. Kashyap, K. G. Pradeep, and R. S. Kottada, “Thermal stability and grain boundary strengthening in ultrafine-grained CoCrFeNi high entropy alloy composite,” *Mater. Des.*, vol. 134, pp. 426–433, Nov. 2017.

[119] C. Sun, P. Li, S. Xi, Y. Zhou, S. Li, and X. Yang, “A new type of high entropy alloy composite Fe18Ni23Co25Cr21Mo8WNb3C2 prepared by mechanical alloying and hot pressing sintering,” *Mater. Sci. Eng. A*, vol. 728, pp. 144–150, 2018.

[120] A. Zhang, J. Han, B. Su, and J. Meng, “A promising new high temperature self-lubricating material: CoCrFeNiS0.5 high entropy alloy,” *Mater. Sci. Eng. A*, vol. 731, pp. 36–43, 2018.

[121] D. Yim *et al.*, “Compaction behavior of water-atomized CoCrFeMnNi high-entropy alloy powders,” *Mater. Chem. Phys.*, vol. 210, pp. 95–102, May 2018.

[122] S. Praveen, J. Basu, S. Kashyap, and R. S. Kottada, “Exceptional resistance to grain growth in nanocrystalline CoCrFeNi high entropy alloy at high homologous temperatures,” *J. Alloys Compd.*, vol. 662, pp. 361–367, Mar. 2016.

[123] F. Dobeš, H. Hadraba, Z. Chlup, A. Dlouhý, M. Vilémová, and J. Matějíček, “Compressive creep behavior of an oxide-dispersion-strengthened CoCrFeMnNi high-entropy alloy,” *Mater. Sci. Eng. A*, vol. 732, pp. 99–104, 2018.

[124] R. B. Mane and B. B. Panigrahi, “Effect of alloying order on non-isothermal sintering kinetics of mechanically alloyed high entropy alloy powders,” *Mater. Lett.*, vol. 217, pp. 131–134, Apr. 2018.

[125] H. Cheng, W. Chen, X. Liu, Q. Tang, Y. Xie, and P. Dai, “Effect of Ti and C additions on the microstructure and mechanical properties of the FeCoCrNiMn high-entropy alloy,” *Mater. Sci. Eng. A*, vol. 719, pp. 192–198, Mar. 2018.

[126] M. D. Alcalá, C. Real, I. Fombella, I. Trigo, and J. M. Córdoba, “Effects of milling time, sintering temperature, Al content on the chemical nature, microhardness and microstructure of mechanochemically synthesized FeCoNiCrMn high entropy alloy,” *J. Alloys Compd.*, vol. 749, pp. 834–843, 2018.

[127] Y. Xie, H. Cheng, Q. Tang, W. Chen, W. Chen, and P. Dai, “Effects of N addition on microstructure and mechanical properties of CoCrFeNiMn high entropy alloy produced by mechanical alloying and vacuum hot pressing sintering,” *Intermetallics*, vol. 93, pp. 228–234, Feb. 2018.

[128] A. Zhang, J. Han, B. Su, P. Li, and J. Meng, “Microstructure, mechanical properties and tribological performance of CoCrFeNi high entropy alloy matrix self-lubricating composite,” *Mater. Des.*, vol. 114, pp. 253–263, 2017.

[129] I. L. Velo, F. J. Gotor, M. D. Alcalá, C. Real, and J. M. Córdoba, “Fabrication and characterization of WC-HEA cemented carbide based on the CoCrFeNiMn high entropy alloy,” *J. Alloys Compd.*, vol. 746, pp. 1–8, 2018.

[130] Z. G. Zhu *et al.*, “Hierarchical microstructure and strengthening mechanisms of a CoCrFeNiMn high entropy alloy additively manufactured by selective laser melting,” *Scr. Mater.*, vol. 154, pp. 20–24, Sep. 2018.

[131] R. Zhou, G. Chen, B. Liu, J. Wang, L. Han, and Y. Liu, “Microstructures and wear behaviour of (FeCoCrNi)1-x(WC)x high entropy alloy composites,” *Int. J. Refract. Met. Hard Mater.*, vol. 75, pp. 56–62, Sep. 2018.

[132] Z. Szklarz, J. Lekki, P. Bobrowski, M. B. Szklarz, and Ł. Rogal, “The effect of SiC nanoparticles addition on the electrochemical response of mechanically alloyed CoCrFeMnNi high entropy alloy,” *Mater. Chem. Phys.*, vol. 215, pp. 385–392, Aug. 2018.

[133] B. Wang, X. Huang, A. Fu, Y. Liu, and B. Liu, “Serration behavior and microstructure of high entropy alloy CoCrFeMnNi prepared by powder metallurgy,” *Mater. Sci. Eng. A*, vol. 726, pp. 37–44, May 2018.

[134] R. Zhou *et al.*, “Microstructures and mechanical properties of C-containing FeCoCrNi high-entropy alloy fabricated by selective laser melting,” *Intermetallics*, vol. 94, pp. 165–171, 2018.

[135] R. Li, P. Niu, T. Yuan, P. Cao, C. Chen, and K. Zhou, “Selective laser melting of an equiatomic CoCrFeMnNi high-entropy alloy: Processability, non-equilibrium microstructure and mechanical property,” *J. Alloys Compd.*, vol. 746, pp. 125–134, 2018.

[136] J. Guo, M. Goh, Z. Zhu, X. Lee, M. L. S. Nai, and J. Wei, “On the machining of selective laser melting CoCrFeMnNi high-entropy alloy,” *Mater. Des.*, vol. 153, pp. 211–220, 2018.

[137] A. Piglione, B. Dovgyy, C. Liu, C. M. Gourlay, P. A. Hooper, and M. S. Pham, “Printability and microstructure of the CoCrFeMnNi high-entropy alloy fabricated by laser powder bed fusion,” *Mater. Lett.*, vol. 224, pp. 22–25, Aug. 2018.

[138] M. Zhang, W. Zhang, Y. Liu, B. Liu, and J. Wang, “FeCoCrNiMo high-entropy alloys prepared by powder metallurgy processing for diamond tool applications,” *Powder Metall.*, vol. 61, no. 2, pp. 123–130, 2018.

[139] S.-H. Joo *et al.*, “Structure and properties of ultrafine-grained CoCrFeMnNi high-entropy alloys produced by mechanical alloying and spark plasma sintering,” *J. Alloys Compd.*, vol. 698, pp. 591–604, Mar. 2017.

[140] Q. Yang, Y. Tang, Y. Wen, Q. Zhang, D. Deng, and X. Nai, “Microstructures and properties of CoCrCuFeNiMox high-entropy alloys fabricated by mechanical alloying and spark plasma sintering,” *Powder Metall.*, vol. 61, no. 2, pp. 115–122, 2018.

[141] R. B. Mane, R. Y., and B. B. Panigrahi, “Sintering mechanism of CoCrFeMnNi high-entropy alloy powders,” *Powder Metall.*, vol. 61, no. 2, pp. 131–138, 2018.

[142] S. Praveen, B. S. Murty, and R. S. Kottada, “Phase Evolution and Densification Behavior of Nanocrystalline Multicomponent High Entropy Alloys During Spark Plasma Sintering,” *JOM*, vol. 65, no. 12, pp. 1797–1804, 2013.

[143] Z.-W. He, M.-Z. Wang, X.-L. Hao, Q. Zou, and Y.-C. Zhao, “Novel cemented carbide produced with TiN0.3 and high-entropy alloys,” *Rare Met.*, vol. 36, no. 6, pp. 494–500, Jun. 2017.

[144] S. Praveen, A. Anupam, R. Tilak, and R. S. Kottada, “Phase evolution and thermal stability of AlCoCrFe high entropy alloy with carbon as unsolicited addition from milling media,” *Mater. Chem. Phys.*, vol. 210, pp. 57–61, 2018.

[145] Z. Qiu, C. Yao, K. Feng, Z. Li, and P. K. Chu, “Cryogenic deformation mechanism of CrMnFeCoNi high-entropy alloy fabricated by laser additive manufacturing process,” *Int. J. Light. Mater. Manuf.*, vol. 1, no. 1, pp. 33–39, Mar. 2018.

[146] A. G. de la Obra, M. A. Avilés, Y. Torres, E. Chicardi, and F. J. Gotor, “A new family of cermets: Chemically complex but microstructurally simple,” *Int. J. Refract. Met. Hard Mater.*, vol. 63, pp. 17–25, Feb. 2017.

[147] W. H. Liu *et al.*, “Ductile CoCrFeNiMox high entropy alloys strengthened by hard intermetallic phases,” *Acta Mater.*, vol. 116, pp. 332–342, Sep. 2016.

[148] B. Wu, W. Chen, Z. Jiang, Z. Chen, and Z. Fu, “Influence of Ti addition on microstructure and mechanical behavior of a FCC-based Fe30Ni30Co30Mn10 alloy,” *Mater. Sci. Eng. A*, vol. 676, pp. 492–500, Oct. 2016.

[149] Z. Fu, W. Chen, H. Xiao, L. Zhou, D. Zhu, and S. Yang, “Fabrication and properties of nanocrystalline Co0.5FeNiCrTi0.5 high entropy alloy by MA–SPS technique,” *Mater. Des.*, vol. 44, pp. 535–539, Feb. 2013.

[150] C.-M. Lin, C.-W. Tsai, S.-M. Huang, C.-C. Yang, and J.-W. Yeh, “New TiC/Co1.5CrFeNi1.5Ti0.5 Cermet with Slow TiC Coarsening During Sintering,” *JOM*, vol. 66, no. 10, pp. 2050–2056, Oct. 2014.

[151] I. Kunce, M. Polanski, and J. Bystrzycki, “Structure and hydrogen storage properties of a high entropy ZrTiVCrFeNi alloy synthesized using Laser

Engineered Net Shaping (LENS)," *Int. J. Hydrogen Energy*, vol. 38, no. 27, pp. 12180–12189, 2013.

[152] I. Moravcik *et al.*, "Microstructure and mechanical properties of Ni1,5Co1,5CrFeTi0,5 high entropy alloy fabricated by mechanical alloying and spark plasma sintering," *Mater. Des.*, vol. 119, pp. 141–150, Apr. 2017.

[153] Z. Cai, G. Jin, X. Cui, Y. Li, Y. Fan, and J. Song, "Experimental and simulated data about microstructure and phase composition of a NiCrCoTiV high-entropy alloy prepared by vacuum hot-pressing sintering," *Vacuum*, vol. 124, pp. 5–10, Feb. 2016.

[154] B. Liu, J. Wang, J. Chen, Q. Fang, and Y. Liu, "Ultra-High Strength TiC/Refractory High-Entropy-Alloy Composite Prepared by Powder Metallurgy," *JOM*, vol. 69, no. 4, pp. 651–656, Apr. 2017.

[155] G. Zepon *et al.*, "Hydrogen-induced phase transition of MgZrTiFe0.5Co0.5Ni0.5 high entropy alloy," *Int. J. Hydrogen Energy*, vol. 43, no. 3, pp. 1702–1708, Jan. 2018.

[156] Z. Fu *et al.*, "Fcc nanostructured TiFeCoNi alloy with multi-scale grains and enhanced plasticity," *Scr. Mater.*, vol. 143, pp. 108–112, Jan. 2018.

[157] E. Holmström *et al.*, "High entropy alloys: Substituting for cobalt in cutting edge technology," *Appl. Mater. Today*, vol. 12, pp. 322–329, Sep. 2018.

[158] Z. Cai, X. Cui, Z. Liu, Y. Li, M. Dong, and G. Jin, "Microstructure and wear resistance of laser cladded Ni-Cr-Co-Ti-V high-entropy alloy coating after laser remelting processing," *Opt. Laser Technol.*, vol. 99, pp. 276–281, 2018.

[159] S. Varalakshmi, M. Kamaraj, and B. S. Murty, "Synthesis and characterization of nanocrystalline AlFeTiCrZnCu high entropy solid solution by mechanical alloying," *J. Alloys Compd.*, vol. 460, no. 1–2, pp. 253–257, Jul. 2008.

[160] E. Prieto *et al.*, "Processing of a new high entropy alloy: AlCrFeMoNiTi," *Powder Metall.*, vol. 61, no. 3, pp. 258–265, 2018.

[161] N. T. B. N. Koundinya, C. Sajith Babu, K. Sivaprasad, P. Susila, N. Kishore Babu, and J. Baburao, "Phase Evolution and Thermal Analysis of Nanocrystalline AlCrCuFeNiZn High Entropy Alloy Produced by Mechanical Alloying," *J. Mater. Eng. Perform.*, vol. 22, no. 10, pp. 3077–3084, Oct. 2013.

[162] O. Maulik, D. Kumar, S. Kumar, D. M. Fabijanic, and V. Kumar, "Structural evolution of spark plasma sintered AlFeCuCrMgx (x = 0, 0.5, 1, 1.7) high entropy alloys," *Intermetallics*, vol. 77, pp. 46–56, 2016.

[163] S. Mridha, S. Samal, P. Y. Khan, K. Biswas, and Govind, "Processing and Consolidation of Nanocrystalline Cu-Zn-Ti-Fe-Cr High-Entropy Alloys via Mechanical Alloying," *Metall. Mater. Trans. A*, vol. 44, no. 10, pp. 4532–4541, Oct. 2013.

[164] A. S. Sharma, S. Yadav, K. Biswas, and B. Basu, “High-entropy alloys and metallic nanocomposites: Processing challenges, microstructure development and property enhancement,” *Mater. Sci. Eng. R Reports*, vol. 131, pp. 1–42, Sep. 2018.

[165] S. Yadav, A. Kumar, and K. Biswas, “Wear behavior of high entropy alloys containing soft dispersoids (Pb, Bi),” *Mater. Chem. Phys.*, vol. 210, pp. 222–232, May 2018.

[166] S. Yadav, S. Sarkar, A. Aggarwal, A. Kumar, and K. Biswas, “Wear and mechanical properties of novel (CuCrFeTiZn)100-xPbx high entropy alloy composite via mechanical alloying and spark plasma sintering,” *Wear*, vol. 410, pp. 93–109, 2018.

[167] D. Kumar, O. Maulik, S. Kumar, Y. V. S. S. Prasad, and V. Kumar, “Phase and thermal study of equiatomic AlCuCrFeMnW high entropy alloy processed via spark plasma sintering,” *Mater. Chem. Phys.*, vol. 210, pp. 71–77, 2018.

[168] M. Murali, S. P. K. Babu, J. Majhi, A. Vallimanalan, and R. Mahendran, “Processing and characterisation of nano crystalline AlCoCrCuFeTix high-entropy alloy,” *Powder Metall.*, vol. 61, no. 2, pp. 139–148, 2018.

[169] H. Dobbelstein, M. Thiele, E. L. Gurevich, E. P. George, and A. Ostendorf, “Direct Metal Deposition of Refractory High Entropy Alloy MoNbTaW,” *Phys. Procedia*, vol. 83, pp. 624–633, Jan. 2016.

[170] B. Kang, J. Lee, H. J. Ryu, and S. H. Hong, “Ultra-high strength WNbMoTaV high-entropy alloys with fine grain structure fabricated by powder metallurgical process,” *Mater. Sci. Eng. A*, vol. 712, pp. 616–624, 2018.

[171] P. Wang, H. Cai, S. Zhou, and L. Xu, “Processing, microstructure and properties of Ni1.5CoCuFeCr0.5−xVx high entropy alloys with carbon introduced from process control agent,” *J. Alloys Compd.*, vol. 695, pp. 462–475, Feb. 2017.

[172] O. A. Waseem, J. Lee, H. M. Lee, and H. J. Ryu, “The effect of Ti on the sintering and mechanical properties of refractory high-entropy alloy TixWTaVCr fabricated via spark plasma sintering for fusion plasma-facing materials,” *Mater. Chem. Phys.*, vol. 210, pp. 87–94, 2018.

[173] O. A. Waseem and H. J. Ryu, “Powder Metallurgy Processing of a WxTaTiVCr High-Entropy Alloy and Its Derivative Alloys for Fusion Material Applications,” *Sci. Rep.*, vol. 7, no. 1, p. 1926, 2017.

[174] D. Linder, E. Holmström, and S. Norgren, “High entropy alloy binders in gradient sintered hardmetal,” *Int. J. Refract. Met. Hard Mater.*, vol. 71, pp. 217–220, Feb. 2018.

[175] Y. Cao, Y. Liu, B. Liu, and W. Zhang, “Precipitation behavior during hot deformation of powder metallurgy Ti-Nb-Ta-Zr-Al high entropy alloys,” *Intermetallics*, vol. 100, pp. 95–103, Sep. 2018.

[176] I. Kunce, M. Polanski, and J. Bystrzycki, “Microstructure and hydrogen storage properties of a TiZrNbMoV high entropy alloy synthesized using Laser Engineered Net Shaping (LENS),” *Int. J. Hydrogen Energy*, vol. 39, no. 18, pp. 9904–9910, Jun. 2014.

[177] A. Raza, B. Kang, J. Lee, H. J. Ryu, and S. H. Hong, “Transition in microstructural and mechanical behavior by reduction of sigma-forming element content in a novel high entropy alloy,” *Mater. Des.*, vol. 145, pp. 11–19, May 2018.

[178] R. Song, L. Wei, C. Yang, and S. Wu, “Phase formation and strengthening mechanisms in a dual-phase nanocrystalline CrMnFeVTi high-entropy alloy with ultrahigh hardness,” *J. Alloys Compd.*, vol. 744, pp. 552–560, May 2018.

[179] O. Senkov, D. Isheim, D. Seidman, and A. Pilchak, “Development of a Refractory High Entropy Superalloy,” *Entropy*, vol. 18, no. 3, p. 102, Mar. 2016.

[180] Y. Zhang, Y. J. Zhou, J. P. Lin, G. L. Chen, and P. K. Liaw, “Solid-Solution Phase Formation Rules for Multi-component Alloys,” *Adv. Eng. Mater.*, vol. 10, no. 6, pp. 534–538, 2008.

[181] S. GUO and C. T. LIU, “Phase stability in high entropy alloys: Formation of solid-solution phase or amorphous phase,” *Prog. Nat. Sci. Mater. Int.*, vol. 21, no. 6, pp. 433–446, Dec. 2011.

[182] F. Tian, L. K. Varga, N. Chen, J. Shen, and L. Vitos, “Empirical design of single phase high-entropy alloys with high hardness,” *Intermetallics*, vol. 58, pp. 1–6, 2015.

[183] S. Guo, Q. Hu, C. Ng, and C. T. Liu, “More than entropy in high-entropy alloys: Forming solid solutions or amorphous phase,” *Intermetallics*, vol. 41, pp. 96–103, Oct. 2013.

[184] S. Guo, C. Ng, J. Lu, and C. T. Liu, “Effect of valence electron concentration on stability of fcc or bcc phase in high entropy alloys,” *J. Appl. Phys.*, vol. 109, no. 10, p. 103505, May 2011.

[185] M.-H. Tsai, K.-Y. Tsai, C.-W. Tsai, C. Lee, C.-C. Juan, and J.-W. Yeh, “Criterion for Sigma Phase Formation in Cr- and V-Containing High-Entropy Alloys,” *Mater. Res. Lett.*, vol. 1, no. 4, pp. 207–212, 2013.

[186] K. Górecki, J. Zýka, J. Malek, J. Horvát, J. Čapek, and P. Bała, “Sintering and heat treatment of $Al_{15}Ti_{5}Co_{35}Ni_{25}Fe_{20}$ high-entropy alloy,” *IOP Conf. Ser. Mater. Sci. Eng.*, vol. 179, p. 012027, Feb. 2017.

[187] X.-W. Qiu, Y.-P. Zhang, L. He, and C. Liu, “Microstructure and corrosion resistance of AlCrFeCuCo high entropy alloy,” *J. Alloys Compd.*, vol. 549, pp. 195–199, 2013.

[188] K. Eymann *et al.*, “Consolidation of mechanically alloyed nanocrystalline Cu–Nb–ZrO2 powder by spark plasma sintering,” *J. Alloys Compd.*, vol. 535,

pp. 62–69, 2012.

[189] X.-W. Qiu and C.-G. Liu, “Microstructure and properties of Al2CrFeCoCuTiNix high-entropy alloys prepared by laser cladding,” *J. Alloys Compd.*, vol. 553, pp. 216–220, Mar. 2013.

[190] Z. A. Munir, U. Anselmi-Tamburini, and M. Ohyanagi, “The effect of electric field and pressure on the synthesis and consolidation of materials: A review of the spark plasma sintering method,” *J. Mater. Sci.*, vol. 41, no. 3, pp. 763–777, Feb. 2006.

[191] A. Gali and E. P. George, “Tensile properties of high- and medium-entropy alloys,” *Intermetallics*, vol. 39, pp. 74–78, Aug. 2013.

[192] S. Curtze and V.-T. Kuokkala, “Dependence of tensile deformation behavior of TWIP steels on stacking fault energy, temperature and strain rate,” *Acta Mater.*, vol. 58, no. 15, pp. 5129–5141, Sep. 2010.

[193] E. C. Santos, M. Shiomi, K. Osakada, and T. Laoui, “Rapid manufacturing of metal components by laser forming,” *Int. J. Mach. Tools Manuf.*, vol. 46, no. 12–13, pp. 1459–1468, Oct. 2006.

[194] D. D. Gu, W. Meiners, K. Wissenbach, and R. Poprawe, “Laser additive manufacturing of metallic components: materials, processes and mechanisms,” *Int. Mater. Rev.*, vol. 57, no. 3, pp. 133–164, 2012.

[195] W. E. Frazier, “Metal Additive Manufacturing: A Review,” *J. Mater. Eng. Perform.*, vol. 23, no. 6, pp. 1917–1928, Jun. 2014.

[196] S. Gorsse, C. Hutchinson, M. Gouné, and R. Banerjee, “Additive manufacturing of metals: a brief review of the characteristic microstructures and properties of steels, Ti-6Al-4V and high-entropy alloys,” *Sci. Technol. Adv. Mater.*, vol. 18, no. 1, pp. 584–610, 2017.

[197] Q. He and Y. Yang, “On Lattice Distortion in High Entropy Alloys,” *Front. Mater.*, vol. 5, p. 42, 2018.

[198] F. Otto, A. Dlouhý, C. Somsen, H. Bei, G. Eggeler, and E. P. George, “The influences of temperature and microstructure on the tensile properties of a CoCrFeMnNi high-entropy alloy,” *Acta Mater.*, vol. 61, no. 15, pp. 5743–5755, Sep. 2013.

[199] B. Cai *et al.*, “Deformation mechanisms of Mo alloyed FeCoCrNi high entropy alloy: In situ neutron diffraction,” *Acta Mater.*, vol. 127, pp. 471–480, Apr. 2017.

[200] S. K. C. Ch.-W. Tsai, Y.-L. Chen, M.-H. Tsai, J.W. Yeh, T.T. Shun, “Deformation and annealing behaviors of high-entropy alloy Al0.5CoCrCuFeNi,” *J. Alloys Compd.*, vol. 486, no. 1–2, pp. 427–435, Nov. 2009.

[201] E. El-Danaf, S. R. Kalidindi, and R. D. Doherty, “Influence of grain size and stacking-fault energy on deformation twinning in fcc metals,” *Metall. Mater.*

Trans. A, vol. 30, no. 5, pp. 1223–1233, May 1999.

[202] K. L. Y. Zhang, N.R. Tao, "Effect of stacking-fault energy on deformation twin thickness in Cu–Al alloys," *Scr. Mater.*, vol. 60, no. 4, pp. 211–213, Feb. 2009.

[203] E. Ma, "Eight routes to improve the tensile ductility of bulk nanostructured metals and alloys," *JOM*, vol. 58, no. 4, pp. 49–53, 2006.

[204] S. Praveen and H. S. Kim, "High-Entropy Alloys: Potential Candidates for High-Temperature Applications – An Overview," *Adv. Eng. Mater.*, vol. 20, no. 1, p. 1700645.

[205] Y. Lu *et al.*, "A Promising New Class of High-Temperature Alloys: Eutectic High-Entropy Alloys," *Sci. Rep.*, vol. 4, p. 6200, Aug. 2014.

[206] A. Chauhan, D. Litvinov, and J. Aktaa, "High temperature tensile properties and fracture characteristics of bimodal 12Cr-ODS steel," *J. Nucl. Mater.*, vol. 468, pp. 1–8, Jan. 2016.

[207] Y. J. Zhou, Y. Zhang, Y. L. Wang, and G. L. Chen, "Solid solution alloys of AlCoCrFeNiTix with excellent room-temperature mechanical properties," *Appl. Phys. Lett.*, vol. 90, no. 18, p. 181904, Apr. 2007.

[208] Y. Dong, K. Zhou, Y. Lu, X. Gao, T. Wang, and T. Li, "Effect of vanadium addition on the microstructure and properties of AlCoCrFeNi high entropy alloy," *Mater. Des.*, vol. 57, pp. 67–72, May 2014.

[209] G. A. Salishchev *et al.*, "Effect of Mn and V on structure and mechanical properties of high-entropy alloys based on CoCrFeNi system," *J. Alloys Compd.*, vol. 591, pp. 11–21, Apr. 2014.

[210] N. D. Stepanov, D. G. Shaysultanov, G. A. Salishchev, and M. A. Tikhonovsky, "Structure and mechanical properties of a light-weight AlNbTiV high entropy alloy," *Mater. Lett.*, vol. 142, pp. 153–155, Mar. 2015.

[211] Y. J. Zhou, Y. Zhang, Y. L. Wang, and G. L. Chen, "Microstructure and compressive properties of multicomponent Alx(TiVCrMnFeCoNiCu)100−x high-entropy alloys," *Mater. Sci. Eng. A*, vol. 454–455, pp. 260–265, Apr. 2007.

[212] X. F. Wang, Y. Zhang, Y. Qiao, and G. L. Chen, "Novel microstructure and properties of multicomponent CoCrCuFeNiTix alloys," *Intermetallics*, vol. 15, no. 3, pp. 357–362, Mar. 2007.

[213] Y. P. Wang, B. S. Li, M. X. Ren, C. Yang, and H. Z. Fu, "Microstructure and compressive properties of AlCrFeCoNi high entropy alloy," *Mater. Sci. Eng. A*, vol. 491, no. 1–2, pp. 154–158, Sep. 2008.

[214] B. S. Li, Y. P. Wang, M. X. Ren, C. Yang, and H. Z. Fu, “Effects of Mn, Ti and V on the microstructure and properties of AlCrFeCoNiCu high entropy alloy,” *Mater. Sci. Eng. A*, vol. 498, no. 1–2, pp. 482–486, Dec. 2008.

[215] O. N. Senkov, G. B. Wilks, J. M. Scott, and D. B. Miracle, “Mechanical properties of Nb25Mo25Ta25W25 and V20Nb20Mo20Ta20W20 refractory high entropy alloys,” *Intermetallics*, vol. 19, no. 5, pp. 698–706, May 2011.

[216] S. G. Ma and Y. Zhang, “Effect of Nb addition on the microstructure and properties of AlCoCrFeNi high-entropy alloy,” *Mater. Sci. Eng. A*, vol. 532, pp. 480–486, Jan. 2012.

[217] Y. Dong, Y. Lu, J. Kong, J. Zhang, and T. Li, “Microstructure and mechanical properties of multi-component AlCrFeNiMox high-entropy alloys,” *J. Alloys Compd.*, vol. 573, pp. 96–101, Oct. 2013.

[218] O. N. Senkov, C. Woodward, and D. B. Miracle, “Microstructure and Properties of Aluminum-Containing Refractory High-Entropy Alloys,” *JOM*, vol. 66, no. 10, pp. 2030–2042, Oct. 2014.

[219] M. J. Yao, K. G. Pradeep, C. C. Tasan, and D. Raabe, “A novel, single phase, non-equiatomic FeMnNiCoCr high-entropy alloy with exceptional phase stability and tensile ductility,” *Scr. Mater.*, vol. 72–73, pp. 5–8, Feb. 2014.

[220] A. V. Kuznetsov, D. G. Shaysultanov, N. D. Stepanov, G. A. Salishchev, and O. N. Senkov, “Tensile properties of an AlCrCuNiFeCo high-entropy alloy in as-cast and wrought conditions,” *Mater. Sci. Eng. A*, vol. 533, pp. 107–118, Jan. 2012.

[221] Z. Tang *et al.*, “Tensile ductility of an AlCoCrFeNi multi-phase high-entropy alloy through hot isostatic pressing (HIP) and homogenization,” *Mater. Sci. Eng. A*, vol. 647, pp. 229–240, Oct. 2015.

[222] I. S. Wani *et al.*, “Ultrafine-Grained AlCoCrFeNi2.1 Eutectic High-Entropy Alloy,” *Mater. Res. Lett.*, vol. 4, no. 3, pp. 174–179, 2016.

[223] Y. Dong, X. Gao, Y. Lu, T. Wang, and T. Li, “A multi-component AlCrFe2Ni2 alloy with excellent mechanical properties,” *Mater. Lett.*, vol. 169, pp. 62–64, Apr. 2016.

[224] W. H. Liu *et al.*, “Ductile CoCrFeNiMox high entropy alloys strengthened by hard intermetallic phases,” *Acta Mater.*, vol. 116, pp. 332–342, Sep. 2016.

[225] W. H. Liu, J. Y. He, H. L. Huang, H. Wang, Z. P. Lu, and C. T. Liu, “Effects of Nb additions on the microstructure and mechanical property of CoCrFeNi high-entropy alloys,” *Intermetallics*, vol. 60, pp. 1–8, May 2015.

[226] S. G. Ma *et al.*, “Superior high tensile elongation of a single-crystal CoCrFeNiAl0.3 high-entropy alloy by Bridgman solidification,” *Intermetallics*, vol. 54, pp. 104–109, Nov. 2014.

[227] J. Y. He *et al.*, “Effects of Al addition on structural evolution and tensile properties of the FeCoNiCrMn high-entropy alloy system,” *Acta Mater.*, vol. 62, pp. 105–113, Jan. 2014.

[228] T.-T. Shun and Y.-C. Du, “Microstructure and tensile behaviors of FCC Al0.3CoCrFeNi high entropy alloy,” *J. Alloys Compd.*, vol. 479, no. 1–2, pp. 157–160, Jun. 2009.

[229] T. Zuo, S. Ren, P. K. Liaw, and Y. Zhang, “Processing effects on the magnetic and mechanical properties of FeCoNiAl0.2Si0.2 high entropy alloy,” *Int. J. Miner. Metall. Mater.*, vol. 20, no. 6, pp. 549–555, Jun. 2013.

[230] Y. D. Wu *et al.*, “A refractory Hf25Nb25Ti25Zr25 high-entropy alloy with excellent structural stability and tensile properties,” *Mater. Lett.*, vol. 130, pp. 277–280, Sep. 2014.

[231] C.-W. Tsai, M.-H. Tsai, K.-Y. Tsai, S.-Y. Chang, J.-W. Yeh, and A.-C. Yeh, “Microstructure and tensile properties of Al0.5CoCrCuFeNi alloys produced by simple rolling and annealing,” *Mater. Sci. Technol.*, vol. 31, no. 10, pp. 1178–1183, 2015.

[232] Y. Deng, C. C. Tasan, K. G. Pradeep, H. Springer, A. Kostka, and D. Raabe, “Design of a twinning-induced plasticity high entropy alloy,” *Acta Mater.*, vol. 94, pp. 124–133, Aug. 2015.

[233] C.-W. Tsai, M.-H. Tsai, J.-W. Yeh, and C.-C. Yang, “Effect of temperature on mechanical properties of Al0.5CoCrCuFeNi wrought alloy,” *J. Alloys Compd.*, vol. 490, no. 1–2, pp. 160–165, Feb. 2010.

[234] M. Niinomi, “Mechanical properties of biomedical titanium alloys,” *Mater. Sci. Eng. A*, vol. 243, no. 1–2, pp. 231–236, Mar. 1998.

[235] J. W. Lu *et al.*, “Microstructure and mechanical properties of new high strength beta-titanium alloy Ti-1300,” *Mater. Sci. Eng. A*, vol. 621, pp. 182–189, Jan. 2015.

[236] J. Chen and B. Young, “Stress–strain curves for stainless steel at elevated temperatures,” *Eng. Struct.*, vol. 28, no. 2, pp. 229–239, Jan. 2006.

[237] V. Venkatesh and H. J. Rack, “Elevated temperature hardening of INCONEL 690,” *Mech. Mater.*, vol. 30, no. 1, pp. 69–81, Sep. 1998.

[238] R. Schaeublin, T. Leguey, P. Spätig, N. Baluc, and M. Victoria, “Microstructure and mechanical properties of two ODS ferritic/martensitic steels,” *J. Nucl. Mater.*, vol. 307–311, pp. 778–782, Dec. 2002.

[239] R. S. Sundar and S. C. Deevi, “High-temperature strength and creep resistance of FeAl,” *Mater. Sci. Eng. A*, vol. 357, no. 1–2, pp. 124–133, Sep. 2003.

[240] K. B. Zhang *et al.*, “Annealing on the structure and properties evolution of the CoCrFeNiCuAl high-entropy alloy,” *J. Alloys Compd.*, vol. 502, no. 2, pp.

295–299, Jul. 2010.

[241] S. R. Shinde *et al.*, “Co-occurrence of Superparamagnetism and Anomalous Hall Effect in Highly Reduced Cobalt-Doped Rutile ${\mathrm{TiO}}_{2\ensuremath{-}\ensuremath{\delta}}$ Films,” *Phys. Rev. Lett.*, vol. 92, no. 16, p. 166601, 2004.

[242] M. Aoki, T. Noritake, A. Ito, M. Ishikiriyama, and S. Towata, “Improvement of cyclic durability of Ti–Cr–V alloy by Fe substitution,” *Int. J. Hydrogen Energy*, vol. 36, no. 19, pp. 12329–12332, Sep. 2011.

[243] V. S. R.K. Prabakaran, A.N. Sait, “Synthesis and characteristization of high entropy alloy (CrMnFeNiCu) reinforced AA6061 aluminium matrix composite,” *Mech. Mech. Eng.*, vol. 21, no. 2, pp. 415–424, 2017.

[244] G. M. Karthik, S. Panikar, G. D. J. Ram, and R. S. Kottada, “Additive manufacturing of an aluminum matrix composite reinforced with nanocrystalline high-entropy alloy particles,” *Mater. Sci. Eng. A*, vol. 679, pp. 193–203, 2017.

[245] C.-S. Chen, C.-C. Yang, H.-Y. Chai, J.-W. Yeh, and J. L. H. Chau, “Novel cermet material of WC/multi-element alloy,” *Int. J. Refract. Met. Hard Mater.*, vol. 43, pp. 200–204, Mar. 2014.

[246] T. T. Shen *et al.*, “Effects of LaB6 addition on the microstructure and mechanical properties of ultrafine grained WC–10Co alloys,” *J. Alloys Compd.*, vol. 509, no. 4, pp. 1236–1243, Jan. 2011.

[247] P.-F. Zhou, D.-H. Xiao, and T.-C. Yuan, “Comparison between ultrafine-grained WC–Co and WC–HEA-cemented carbides,” *Powder Metall.*, vol. 60, no. 1, pp. 1–6, 2017.

[248] M. S. El-Eskandarany, A. A. Mahday, H. . Ahmed, and A. . Amer, “Synthesis and characterizations of ball-milled nanocrystalline WC and nanocomposite WC–Co powders and subsequent consolidations,” *J. Alloys Compd.*, vol. 312, no. 1–2, pp. 315–325, Nov. 2000.

[249] L. SUN, C. JIA, C. LIN, and R. CAO, “VC Addition Prepared Ultrafine WC-11Co Composites by Spark Plasma Sintering,” *J. Iron Steel Res. Int.*, vol. 14, no. 5, pp. 85–89, Sep. 2007.

[250] S. I. Cha, S. H. Hong, and B. K. Kim, “Spark plasma sintering behavior of nanocrystalline WC–10Co cemented carbide powders,” *Mater. Sci. Eng. A*, vol. 351, no. 1–2, pp. 31–38, Jun. 2003.

[251] H.-C. Kim, I.-J. Shon, I.-K. Jeong, I.-Y. Ko, J.-K. Yoon, and J.-M. Doh, “Rapid sintering of ultra fine WC and WC-Co hard materials by high-frequency induction heated sintering and their mechanical properties,” *Met. Mater. Int.*, vol. 13, no. 1, pp. 39–45, Feb. 2007.

[252] A. Michalski and D. Siemiaszko, “Nanocrystalline cemented carbides sintered by the pulse plasma method,” *Int. J. Refract. Met. Hard Mater.*, vol. 25,

no. 2, pp. 153–158, Mar. 2007.

[253] C. Lin, E. Kny, G. Yuan, and B. Djuricic, “Microstructure and properties of ultrafine WC–0.6VC–10Co hardmetals densified by pressure-assisted critical liquid phase sintering,” *J. Alloys Compd.*, vol. 383, no. 1–2, pp. 98–102, Nov. 2004.

[254] D. Sivaprahasam, S. B. Chandrasekar, and R. Sundaresan, “Microstructure and mechanical properties of nanocrystalline WC–12Co consolidated by spark plasma sintering,” *Int. J. Refract. Met. Hard Mater.*, vol. 25, no. 2, pp. 144–152, Mar. 2007.

[255] L. H. Zhu, Q. W. Huang, and H. F. Zhao, “Preparation of nanocrystalline WC-10Co-0.8VC by spark plasma sintering,” *J. Mater. Sci. Lett.*, vol. 22, pp. 1631–1633, 2003.

[256] Z. Z. Fang, X. Wang, T. Ryu, K. S. Hwang, and H. Y. Sohn, “Synthesis, sintering, and mechanical properties of nanocrystalline cemented tungsten carbide – A review,” *Int. J. Refract. Met. Hard Mater.*, vol. 27, no. 2, pp. 288–299, 2009.

[257] I. Moravcik *et al.*, “Synergic strengthening by oxide and coherent precipitate dispersions in high-entropy alloy prepared by powder metallurgy,” *Scr. Mater.*, vol. 157, pp. 24–29, 2018.

[258] J.-O. Andersson, T. Helander, L. Höglund, P. Shi, and B. Sundman, “Thermo-Calc & DICTRA, computational tools for materials science,” *Calphad*, vol. 26, no. 2, pp. 273–312, Jun. 2002.

[259] N. Saunders, U. K. Z. Guo, X. Li, A. P. Miodownik, and J.-P. Schillé, “Using JMatPro to model materials properties and behavior,” *JOM*, vol. 55, no. 12, pp. 60–65, 2003.

[260] H. R. Sistla, J. W. Newkirk, and F. Frank Liou, “Effect of Al/Ni ratio, heat treatment on phase transformations and microstructure of AlxFeCoCrNi2−x (x = 0.3, 1) high entropy alloys,” *Mater. Des.*, vol. 81, pp. 113–121, Sep. 2015.

[261] B. Cai *et al.*, “Deformation mechanisms of Mo alloyed FeCoCrNi high entropy alloy: In situ neutron diffraction,” *Acta Mater.*, vol. 127, pp. 471–480, Apr. 2017.

[262] A. Kilmametov *et al.*, “High-pressure torsion driven mechanical alloying of CoCrFeMnNi high entropy alloy,” *Scr. Mater.*, vol. 158, pp. 29–33, 2019.

[263] G. Zhu, Y. Liu, and J. Ye, “Fabrication and properties of Ti(C,N)-based cermets with multi-component AlCoCrFeNi high-entropy alloys binder,” 2013.

[264] I. Moravcik, J. Cizek, P. Gavendova, S. Sheikh, S. Guo, and I. Dlouhy, “Effect of heat treatment on microstructure and mechanical properties of spark plasma sintered AlCoCrFeNiTi0.5 high entropy alloy,” 2016.

[265] X. Qiu, “Microstructure, hardness and corrosion resistance of Al<inf>2</inf>CoCrCuFeNiTi<inf>x</inf>high-entropy alloy coatings prepared by rapid solidification,” *J. Alloys Compd.*, vol. 735, pp. 359–364, 2018.

[266] T. Fujieda *et al.*, “CoCrFeNiTi-based high-entropy alloy with superior tensile strength and corrosion resistance achieved by a combination of additive manufacturing using selective electron beam melting and solution treatment,” *Mater. Lett.*, vol. 189, pp. 148–151, Feb. 2017.

[267] G. A. Salishchev *et al.*, “Effect of Mn and V on structure and mechanical properties of high-entropy alloys based on CoCrFeNi system,” *J. Alloys Compd.*, vol. 591, pp. 11–21, Apr. 2014.

[268] Z. Tang *et al.*, “Tensile ductility of an AlCoCrFeNi multi-phase high-entropy alloy through hot isostatic pressing (HIP) and homogenization,” *Mater. Sci. Eng. A*, vol. 647, pp. 229–240, Oct. 2015.

[269] W.-F. Ho, “A comparison of tensile properties and corrosion behavior of cast Ti–7.5Mo with c.p. Ti, Ti–15Mo and Ti–6Al–4V alloys,” *J. Alloys Compd.*, vol. 464, no. 1–2, pp. 580–583, Sep. 2008.

[270] Z. Fu, W. Chen, S. Fang, and X. Li, “Effect of Cr addition on the alloying behavior, microstructure and mechanical properties of twinned CoFeNiAl0.5Ti0.5 alloy,” *Mater. Sci. Eng. A*, vol. 597, pp. 204–211, Mar. 2014.

[271] N. N. Guo *et al.*, “Microstructure and mechanical properties of in-situ MC-carbide particulates-reinforced refractory high-entropy Mo0.5NbHf0.5ZrTi matrix alloy composite,” *Intermetallics*, vol. 69, pp. 74–77, Feb. 2016.

[272] F. Zhang, J. Shen, and J. Sun, “The effect of phosphorus additions on densification, grain growth and properties of nanocrystalline WC–Co composites,” *J. Alloys Compd.*, vol. 385, no. 1–2, pp. 96–103, Dec. 2004.